Politecnico di Torino

Politecnico di Torino

DEPARTMENT OF MECHANICAL AND AEROSPACE ENGINEERING

Master of Science programme Aerospace engineering
Graduation session July 2021

LTO noise prediction methodology for SST aircraft conceptual design

Thesis advisor:
Prof. Nicole Viola

Research supervisors:
Ing. Luigi Federico
Prof. Roberta Fusaro

Candidate:
Grazia Piccirillo

ID number s265939

Academic year 2020/2021

Alla mia famiglia, per aver sempre creduto in me.
A Lorenzo, per essere stato costantemente al mio fianco.

Abstract

The new emerging generation of SuperSonic Transport (SST) aircraft demands an enhanced approach for the consideration and analysis of its impact on environment, with the subsequent delivery of relevant Standards and Recommended Practices (SARPs) to make the certification of a supersonic aeroplane possible in the 2020-2025 timeframe. Focusing on noise generated during Landing and Take-Off (LTO) cycle, the presented activities address the development of a methodology aimig at predicting noise levels in the early stages of SST aircraft design process, accounting for noise requirements as a design constraint and supporting a design-to-noise approach. The methodology includes a supersonic aircraft noise model in which overall aircraft noise is predicted as an assembly of major noise sources, each modelled with an individual semi-empirical noise source model based on the equations reported in "Aircraft Noise Prediction Program – Theoretical Manual" published by NASA. Following the aeroacoustics modelling applied in Aircraft NOise Prediction Program (ANOPP), the major LTO noise sources of an SST aircraft have been selected and in addition the noise attenuation due to the propagation in the atmosphere has been considered in accordance with SAE ARP 866 B. The integration of the noise model within the overall methodology framework leads to the prediction of the aircraft noise level. The accuracy of the method in predicting the overall aircraft noise level has been estimated through a dedicated validation with experimental data provided by the Aircraft Noise and Performance (ANP) database for flyover trajectories at different altitudes and thrust ratings. Considering that the goal of the methodology is to predict noise levels for future supersonic aircraft, the only available supersonic aircraft of the ANP, i.e. the Concorde, has been selected as case study. The matching with Noise Power Distance (NPD) curves has been evaluated for maximum A-weighting sound pressure level (LAmax) and Sound Exposure Level (SEL). Ranging from an altitude of about 200 m to 3000 m, the results have showed that the prediction error falls within ± 1.5 dBA. Considering that the accuracy is acceptable for applications at a conceptual design level, the overall methodology has been applied to predict noise level at the three certification measuring points (sideline, flyover and approach) defined by ICAO. The results have been reported for each noise source contribution and overall aircraft noise, identifying jet noise as the dominant LTO noise source. The outcome of this research activity demonstrates the capability of the developed methodology in introducing noise evaluations since the early stages of aircraft design. With appropriate improvements in noise source and engine modelling, the methodology can be useful to provide guidelines for the design of future low-noise SST together with operational procedures able to mitigate the LTO noise.

Ringraziamenti

Giunta al termine di questo percorso, desidero innanzitutto ringraziare la professoressa Nicole Viola e la professoressa Roberta Fusaro, per avermi offerto l'opportunità di affrontare tematiche innovative all'interno della tesi e per avermi accompagnato costantemente e con estrema disponibilità in questo sfidante lavoro, incoraggiorandomi e fornendomi tutto il supporto necessario, nonostante le difficoltà del periodo storico che stiamo vivendo. Un ringraziamento speciale va all'Ing. Luigi Federico, ricercatore presso il Centro Italiano Ricerche Aerospaziali (CIRA), per aver riposto grande fiducia in me e aver messo a mia disposizione le sue elevate competenze, supervisionando operosamente le diverse attività svolte. Sono sinceramente onorata di aver collaborato con Voi e farò certamente tesoro di tutto ciò che mi avete dato modo di apprendere per la mia futura carriera. Dal punto di vista personale, mi è doveroso ringraziare la mia famiglia: mio padre, mia madre, mio fratello e mia Zia Assunta. Sono infinitamente grata a loro per avermi concesso di vivere questo grande sogno e per aver preso parte ad ogni mio successo o delusione, riuscendo sempre pienamente a comprendermi e sostenermi, nonostante le peculiarità dei miei studi. Ringrazio poi, tutti i miei colleghi, tra cui vecchie e nuove amicizie. Vi ringrazio per tutto ciò che, forse inconsapevolmente, mi avete insegnato, ma anche per l'empatia, il conforto e i sorrisi condivisi insieme e che, anche a chilometri di distanza da casa, non mi hanno fatto mai sentire sola. Non posso fare a meno di ringraziare le mie amiche di sempre, Fefi e Nancy, che rappresentano per me il sostegno più prezioso. Grazie per aver sempre creduto in me, per essere state sempre presenti con piccoli e grandi gesti, per avermi capita e essermi venute incontro, nonostante le nostre diversità, la distanza e gli impegni. Ancora, ringrazio la mia coinquilina Martina, la mia vera complice durante tutta questa esperienza e la scoperta più sensazionale che potessi fare. Non basterebbero tutte le pagine di questa tesi per elencare i motivi per cui debba ringraziarti; abbiamo riso, abbiamo pianto, abbiamo vissuto mille emozioni insieme e ti ringrazio per essere stata sempre al mio fianco, proprio come farebbe una sorella. *Last but not least*, ringrazio il mio fidanzato Lorenzo e la sua famiglia, per avermi sempre sostenuta e incoraggiata, facendo dissolvere le mie ansie e dandomi sicurezza. In particolare, ringrazio Lorenzo, per quella lungimiranza di cui mi sono fidata e che mi ha dato il coraggio di uscire dalla mia *comfort zone* e provare sempre più a superare i miei limiti: se oggi sono una persona migliore è soprattutto grazie a te.

Contents

List of Tables

List of Figures

Chapter 1

Introduction

Recent rise in environmental concern and renewed interest in supersonic flight involved an intense scientific activity aimed to realize a new generation of sustainable supersonic aircraft. Hereby, the motivation of this thesis is the investigation of the noise requirements implications on the design of future generation of SuperSonic Transport (SST) aircraft, focusing on the evaluation of Landing and Take-Off (LTO) noise resulting from SST aircraft design and operational procedure. After a brief overview of the status of the commercial aviation sector, the aim and the roadmap pursued in this work are presented.

1.1 The environmental concern

The outbreak of Covid-19 pandemic has spread new uncertainties over the commercial aviation sector and has slow down the worldwide air transport growth. Nevertheless, a long-term increase in air traffic is expected. According to IATA outlook update to April 2021 [1], once travel restriction are lowered, a strong rebound of travel should be expected, leading to an increase in air traffic, even though at a slower pace than expected before 2019 (Fig. 1.1). Furthermore, an optimpistic perspective provided by Boeing suggests a greater confidence in the resilience of commercial aviation and expects a significant increase in replacement as share of new deliveries (Fig. 1.2), focused on a renew of airline fleets to provide future network flexibility, maximizing capability while minimizing risk, and improving efficiency and sustainability [2]. Therefore, the future increasing air traffic and the need for innovation in the aviation industry have put greater emphasis on several aspects, such as operations, RAMS (Reliability, Availability, Maintenance and Safety) and economic and environmental sustainability, leading to the introduction of new constraints in the aircraft design process.

Among these, the rise in public awareness has made the environmental requirements the most pressing issues hampering commercial aviation growth today. As stated by Violeta Bulc, the European commissioner for transport, in the European Aviation Environmental Report [3], the demand from EU citizens for air travel is expected to growth, “but growth for the sake of growth cannot be an objective in itself”, since

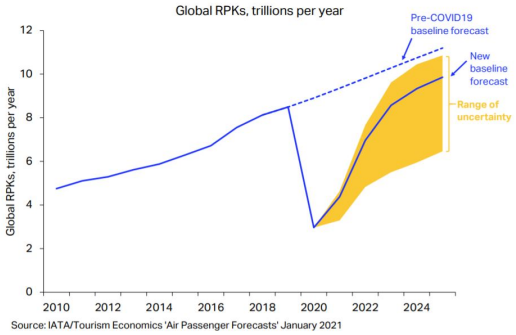

Figure 1.1: Global RPKs per years.[1]

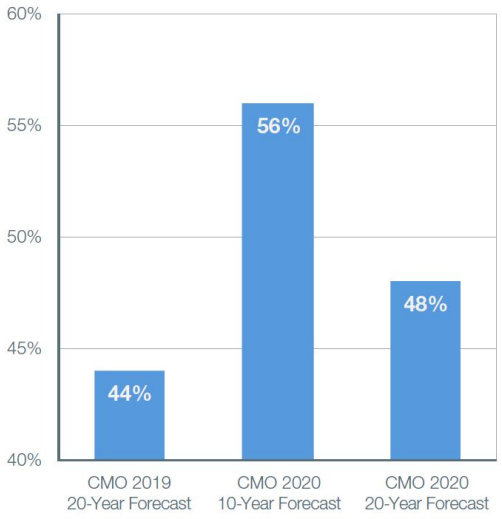

Figure 1.2: Replacement as a share of new deliveries. [2]

environmental matters can not be overlooked for the aviation industry to maintain the European leadership position in the air transport sector, and "this is why the European Commission considers it a priority that the future growth of aviation goes hand in hand with sustainability policies".

Currently, many efforts are undertaken to make aviation more sustainable, researching new and innovative technologies, including aircraft designing, improving operational efficiency, air traffic control and monitoring. The new, quickly emerging aviation technologies and innovations demand an enhanced approach for the consideration and analysis of their impact on environment, with the subsequent delivery of relevant Standards and Recommended Practices (SARPs). This aim is pursued by ICAO, which cooperates with the new governmental and non-governmental organizations, industry bodies and research institutes to support all international aviation stakeholders reduce their environmental footprint in the air and on the ground.

Precisely, ICAO Council established its technical Committee on Aviation Environmental Protection (CAEP) 38 years ago, superseding the Committee on Aircraft Noise (CAN) and the Committee on Aircraft Engine Emissions (CAEE). The role of CAEP has been crucial in assisting the ICAO Council in formulating new policies and adopting new international Standards and Recommended Practices (SARPs) relating to aircraft noise and emissions. The most significant and demanding deliverables from CAEP (Fig. 1.4) are reflected in the International Standards and Recommended Practices (SARPs) contained in Annex 16 to the Convention on International Civil Aviation. These encompass:

- Aircraft noise - Annex 16, Volume I
- Aircraft engine emissions - Annex 16, Volume II

- Aeroplane CO_2 emissions - Annex 16, Volume III
- Carbon Offsetting and Reduction Scheme for International Aviation (CORSIA) - Annex 16, Volume IV

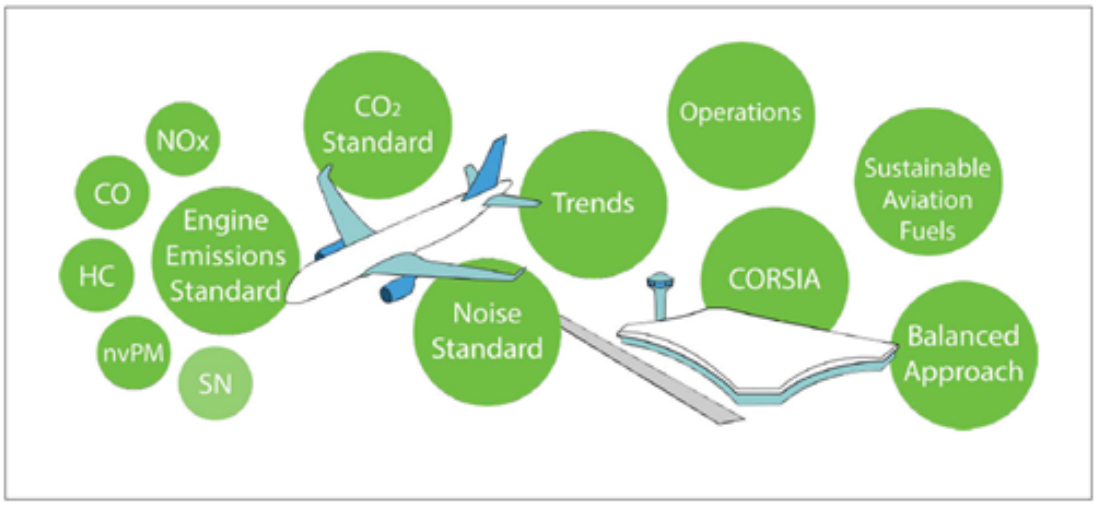

Figure 1.3: CAEP deliverables. [4]

CAEP also developed various guidance materials that support States' initiatives towards the environmental goals defined by the ICAO Assembly [4].

The activities of CAEP also provide for continuous monitoring and assessment of aviation environmental matters, keeping its publications up to date, ensuring that the latest environmental technologies are incorporated into new aircraft designs, and the environmental impact of international civil aviation is limited and reduced. Hence, despite the current downturn, the highly dynamic context of the air transport sector is driving the aviation industry to attain ever rising economic, environmental, and social standards in the coming years. The achievement of these long-term objectives is supported by national and international agencies with the formulation of new SARPs and guidelines, that will involve the adoption of innovative air vehicle designs and systematic changes to the manufacture and operation of aircraft, including the type of fuel used, engine performance, weight metrics, air traffic management strategies and advances in safety.

1.2 Sustainable supersonic flight

Recent years have seen a revival of interest in supersonic aircraft and today there are many projects under development that try to overcome the technological limits of a few decades ago to bring commercial supersonic civil transport flight back to reality. But why supersonic flight?

As already mentioned, current market requirement is to have more efficient aircraft. Supersonic flight allows us to reduce the flight time and to reach increasingly longer point-to-point routes, with no need for stopovers. However, it was over two decade ago when the last civil supersonic aircraft could be seen airborne. Since then, not only no passenger supersonic airplane has taken off, but also the development of almost all supersonic airliners has been terminated. After the pioneering era of the first supersonic aircraft generation, such as Concorde and the Tupolev (Tu-144), aircraft manufacturers have mostly abandoned the idea of supersonic travelling, due to a broad range of issues related to supersonic transport. Concorde was certainly a technological accomplishment for its time, reaching a maximum cruising speed of 2179 km/h per hour with Mach 2.04, allowing the aircraft to reduce the flight time between London and New York to about three hours. Despite of this, its environmental and operational limitations hindered the achievement of the success its creators had hoped for. Beyond the high production cost, the problems of the Concorde consisted in the high consumption (about 13 litres/100 km per seat) and noise emissions, associated with take-off and sonic boom. Sonic boom occurred when Concorde flew faster than the speed of sound and the thunderous sound was caused by series of shock waves coming from the aircraft's nose, wings and engines. It rattled and broke windows and also frightened both humans and animals. That is why Concorde planes were never permitted to fly at full and supersonic speeds over land, as they were restricted to subsonic speeds on land. On July 25 in 2000, a Concorde en route from Paris to New York City suffered engine failure shortly after take-off, when debris from a burst tire caused a fuel tank to rupture and burst into flames. The aircraft crashed into a small hotel and restaurant. All 109 persons on board, including 100 passengers and 9 crew members, died; 4 people on the ground were also killed. Considering the economic failure, on October 24 in 2003 the Concorde was definitively retired and any supersonic passenger aircraft projects were shut down. Clearly, the possibility of future development of SuperSonic Transport (SST) is closely connected with solving related environmental problems.

After a few decades, aviation technology has considerably advanced and the aviation industry is ready to face the challenges of supersonic flight and overcome them, welcoming a new generation of SST aircraft. The National Aeronautics and Space Administration (NASA) in partnership with Lockheed Martin is currently working on the development of a low-boom flight demonstrator known as X-59 Quiet SuperSonic Technology (QueSST)(Fig. 1.4). X-59 QueSST is an experimental supersonic aircraft which preliminary design started in February 2016, with the scheduled for delivery in late 2021 for flight tests from 2022. It is expected to cruise at Mach 1.42, creating a low 75 Perceived Level decibel (PLdB) thump to evaluate supersonic transport acceptability. The demonstrator aims to fly in the 2020 timeframe and the data gathered may open the future to commercial supersonic flight over land.

Figure 1.4: Low-boom flight demonstrator X-59 QueSST.

A further step forward has been done by Denver-based aerospace company Boom Technology, with the development of XB-1, a 1/3 scale demonstrator, and Overture (Fig. 1.5), a 55-passenger sustainable supersonic airliner with 8300 Km of range, that aims to fly at Mach 1.7, optimized to run on 100% sustainable aviation fuel (SAF) with net-zero carbon emissions. Since 3rd June 2021, the United Airlines have announced a commercial agreement with Boom Supersonic to add 15 aircraft to its global fleet. Under the terms of the agreement, United will purchase 15 Overture airliners, once Overture meets United's demanding safety, operating and sustainability requirements, with an option for an additional 35 aircraft. Overture is slated to roll out in 2025, fly in 2026 and expected to carry passengers by 2029 [5].

Figure 1.5: Future supersonic airliner Overture.

Meanwhile, Boston-based Spike aerospace is focusing on the development of Spike S-512 (Fig. 1.6), a supersonic business jet flying at Mach 1.6 and intended for private use.

Figure 1.6: Future supersonic business jet Spike S-512.

These technological advances suggest that a new era of enduring supersonic flight is close. However, the lack of agreed-upon international standards or agreements is likely to hinder production as well as operations [6]. Since 1973 United States and other countries have banned supersonic flight over land, except in limited circumstances, because the annoyance due to sonic boom exposure was considered unacceptable for the public. Consequently, such restriction has severely limited the viability of supersonic flight and has compromised its economic competitiveness, increasing operating costs and flight times. At present, sonic boom reduction measures have been included in the designs of the new SST aircraft, but no change has been introduced in the regulation from the times of Concorde. For this reason, an investigation about the acceptable levels of sonic boom and the establishment of a univocal and homogeneous regulation are the indispensable premise for the new SST aircraft to fly and go faster than sound.

1.2.1 Noise acceptability and regulation

The main regulatory issues related to supersonic flight arise from limitations imposed by community noise levels acceptability. Noise annoyance in the vicinity of airport is a problem concern both subsonic and supersonic aircraft. Since 1960s aircraft noise was recognized as a serious environmental pollutant. The growth of jet-powered fleet and the increasing air traffic revealed the necessity to set local mandatory noise limits around the airport, thus the government started to introduce the concept of noise certification, whose requirements were made much more stringent and were more widely applied during the following years [7]. Such a tightening has been due to an increasing

public awareness and a significant transnational political attention about the magnitude of the environmental problem and the effects of pollution on human beings, as air traffic has increased more and more. The findings collected from social surveys and research activities draw attention to noise adverse effects on the health of exposed individuals: exposure to aircraft noise and the health indicators claiming that subjects who have been chronically exposed to high aircraft noise level are more likely to report stress, sleep disturbance and hypertension compared with those not exposed to aircraft noise [8],[9],[10].

During the years, health-based guidelines on community noise have driven the formulation of noise standards within a framework of noise management to safeguard the health of airport neighbours through appropriate regulation of LTO noise levels. However, the incoming supersonic fligh presents regulatory authorities with a new challenge. A supersonic aircraft taking-off significantly exceeds noise levels of subsonic passenger aircraft, as the greater jet speed of supersonic engine has a large influence on noise generation. Looking at the Figure 1.7, the Concorde represents a good example of the additional noise associated with supersonic aircraft compared to subsonic aircraft. Among the noise levels produced by the aircraft enetered into service between 1955 and 1990, it can be observed that the average noise levels of more recent subsonic aircraft decreased considerably (by more than 20 EPNdB), but Concorde produced more noise than the loudest jet aircraft. These differences can only be explained by the large difference in design requirements between supersonic and subsonic aircraft [11].

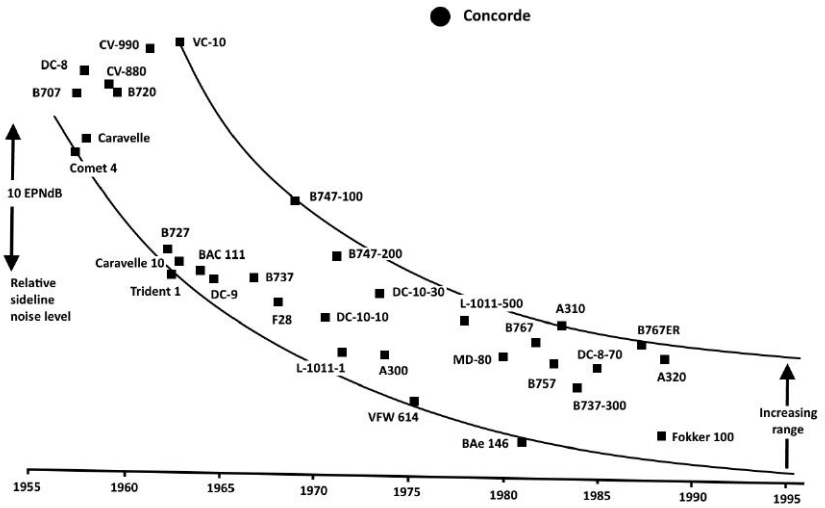

Figure 1.7: Jet aircraft noise levels at entry into service until 1990. [11]

For this reason, a more specific understanding of airport noise impacts resulting from the introduction of SST aircraft is needed. Current noise provisions defined in ICAO Annex 16, Vol.I [12] recommended to take SARPs defined for subsonic jet airplanes as guidelines for Landing and Take-Off (LTO) noise requirements of the new generation SST aircraft. As previously said, aircraft noise standards have become much stricter

since the Concorde entered service. The introduction of Turbofan engines with high by-pass ratio and further noise reduction technologies incorporated into engine and airframe designs led to incremental improvements in aircraft noise performance and increasingly stringent noise standards, that currently are reported in Chapter 14 of Annex 16, Vol I (1.8).

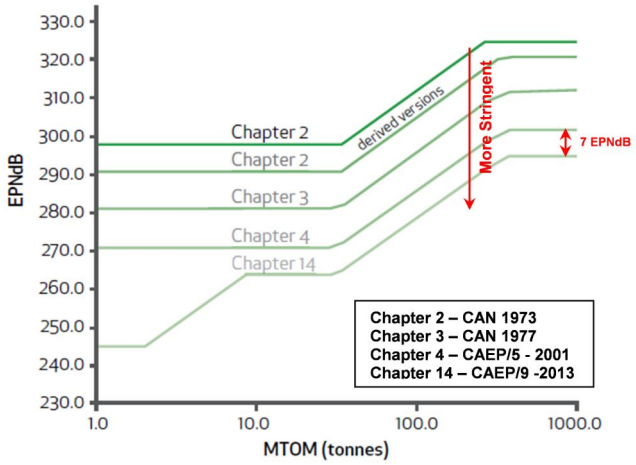

Figure 1.8: The progression of the ICAO LTO noise Standards for aeroplanes – Cumulative noise limits vs. Maximum Take-Off Mass (MTOM). [13]

Aircraft noise limits for LTO cycle are defined by ICAO as Effective Perceived Noise Levels (EPNL). The EPNL is a noise evaluator for the noisiness due to an aircraft pass-by, accounting for effects on human beings and consisting of an integration over noise duration of the Perceived Noise Level (PNL), normalized to a reference duration of 10 seconds. The noise levels for certification are associated with three different operating conditions of the engines, each of which corresponds to the definition of a ground reference measurement point:

- *Lateral full-power reference noise measurement point (maximum power condition)*: the measurement point is along the line parallel to the axis of runaway centre line at a distance of 450 m, where the noise level is maximum during take-off.
- *Flyover reference noise measurement point (intermediate power condition)*: the measurement point is along the extended runaway centre line at a distance of 6500 m from the start to roll.
- *Approach reference noise measurement point (low power condition)*: the measurement point on the ground it is along the extended runaway centre line at 2000 m from the threshold. This corresponds to a position 120 m vertically below the 3° descent path originating from a point 300 m beyond the threshold.

The reference measurement points are respectively lateral (or sideline), flyover (or cutback) and approach reference point, as represented in Figure (1.9).

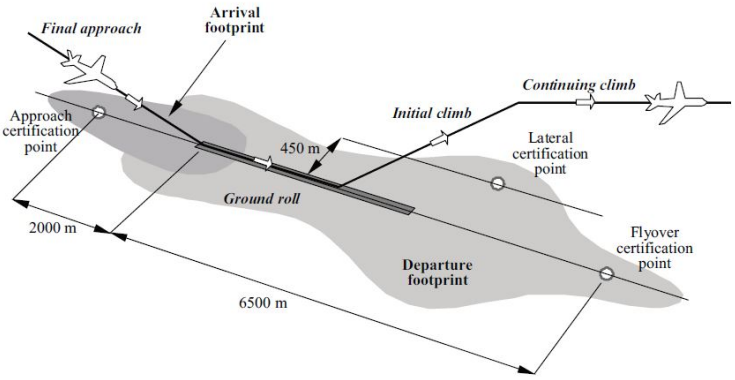

Figure 1.9: Aircraft noise certification reference measurement points. [20]

Noise is recorded continuously at these locations during take-off and landing. The total time-integrated noise, i.e. the EPNL, must not exceed a set limit, established according to MTOW and number of engines, as specified in Attachment A of ICAO Annex 16, Vol.I. Within Annex 16, Vol. I Chapter 3 (Chapter 14 refers to this chapter), in addition to the definition of the three noise measurement points based on the engine power levels, the noise certification reference procedures are also reported. These define the mass, thrust levels, speeds and configuration that the aircraft must have for take-off and approach, respectively for the noise measurement at the sideline and cutback reference measurement point and approach reference measurement point.

Another noise concern of supersonic aircraft is the sonic boom generated during supersonic cruise. When an aircrfat flies faster than sound, it creates a series of pressure waves that travel at the speed of sound and, as the aircraft speed increases, the waves are compressed together. At very large distances from the body, the wave system tends to distort and steepen, ultimately coalescing into a bow and a tail wave. The Figure 1.10 shows a schematic diagram representing the typical far-field wave patterns. At the bow wave a compression occurs in which the local pressure p rises to a value Δp above atmospheric pressure. Then, a slow expansion occurs until some value below atmospheric pressure is reached, after which there is a sudden recompression at the tail wave. This nominal sonic boom signature is called an N-wave. It moves with the aircraft and is associated with continuous supersonic flight, not just with "breaking the sound barrier." One speaks of a sonic boom "carpet", whose width depends on flight and atmospheric conditions, swept out under the full length of a supersonic flight. Receivers within the carpet detect the sonic boom, that is the N-wave once as the aircraft passes. If these waves were sweeping by an observer on the ground, the ear's aural response would be as shown schematically in the sketch at the bottom of the Figure 1.10. Since the duration of this wave signal usually is less than 0.1 second, the pressure rises are heard as a single bang.

In a future scenario, where SST aircraft will be able to fly, this thunderous noise

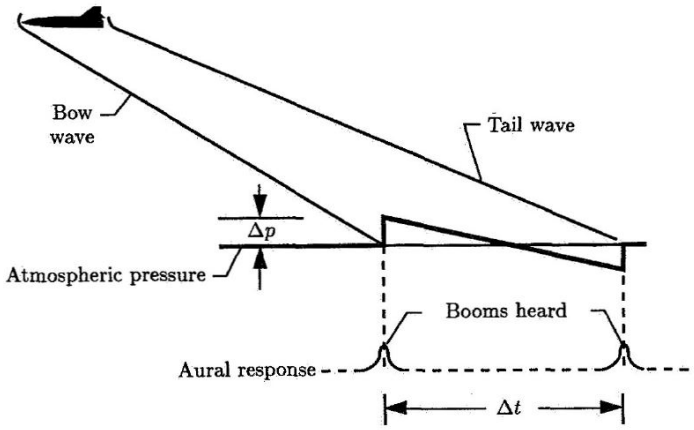

Figure 1.10: Sonic boom pressure far-field wave patterns.[15]

level needs to be regulated. However, whereas supersonic LTO noise standard has defined in accordance with subsonic ones, no regulations have yet been established for regulating sonic boom levels during supersonic flight. The latest ICAO resolution about limitations of enroute flight of the SST aircraft dates back to 1998 and aims at ensuring that no unacceptable situation for the public is created by sonic boom from supersonic aircraft in commercial service. In the following years, the work on civil supersonic development programs and research initiatives has led ICAO to intensify its efforts towards creating a comprehensive regulatory framework for future supersonic aircraft, identifying certification measurement locations and noise metrics for assessing sonic boom noise on the ground and evaluating the benefits of using sonic boom predictions in supersonic noise certification in addition to physical measurements. A set of exploratory studies and research programs are supporting ICAO activities to make the certification of a supersonic aeroplane possible in the 2020-2025 timeframe. A relevant example is RUMBLE (RegUlation and norM for low sonic Boom LEvels), a three-year program sponsored by the European Commission and the Russian Federation, that seeks to address both technical and regulatory aspects of sonic booms. The main actions of the project are:

- Development and assessment of sonic boom prediction tools.
- Study of the human response to sonic boom.
- Validation of the findings using wind-tunnel experiments and actual flight tests

RUMBLE activities are dedicated to the production of the scientific evidence requested by national, European and international regulation authorities to determine the acceptable level of overland sonic booms and the appropriate ways to comply with it [14]. Ultimatly, work is ongoing in civil aviation authorities, industries and research institutes to achieve greater awareness of the environmental impact of future supersonic aircraft and develop a specific regulation that overcomes the current lack, allowing the certification of supersonic aircraft as soon as possible.

1.3 Research goal

Noise levels restrictions imposed in the vicinity of airport and over populated areas constitute the main regulatory issue surrounding civil supersonic flight. Therefore, focusing on LTO noise, the presented work addresses the development of a methodology aimed at including noise requirements as a design constraint in the early stages of SST aircraft. Such purpose is placed in the scenario of the "Balanced approach", proposed by CAEP in the field of aircraft noise management. Such approach consists of identifying the noise problem at an airport and analysing the various measures available to reduce noise through the exploration of four principal elements, namely *reduction at source*, *land-use planning and management*, *abatement operational procedure and operating restrinctions*, with the goal of addressing noise in the most cost-effective manner [15].

In this context, the developed methodology could be able to gain a better understanding of noise requirements on the aircraft design process and support the *reduction of noise at source*, through the analysis of the relationship between noise and aircraft design and operational parameter and the identification of guidelines to include noise reduction measures into aircraft design, promoting a *design-to-noise* approach.

The main objectives of the presented activities are:

- To demonstrate the feasibility of introducing noise emission estimation at conceptual design level and identify design and performance parameters which might be impacted by noise requirements.
- To validate the developed methodology with experimental data and assess its accuracy in noise prediction.
- To show an application to departure and approach procedures, testing the ability of the methodology in the evaluation of the noise levels at the three certification noise measurement points.

The progression followed in order to achieve these objectives is summed up in the roadmap in the Figure 1.11. The activities performed can be considered as split into two parts. Firstly, an in-depth research activity about methods for modelling and predicting aircraft noise has been conducted in order to classify the different methodologies currently adopted for aircraft noise prediction purposes and to achieve an understanding of the general requirements of avaiable state of art tools. After that, a semi-empirical approach has been selected as the most appropriate for applications at a conceptual design level. Hence, an SST aircraft noise model based on Aircraft NOise Prediction Program (ANOPP) equations has been developed and employed through a set of Matlab routines. At least, the noise model has been integrated within the overall methodology framework, that encompasses other routines involving engine operation modelling, flight path simulation, atmospheric absorption effect and calculation of noise metrics. Chapter 2 and Chapter 3 of the thesis cover these arguments.

Secondly, once the methodology has been developed, it was used to assess SST aircraft noise levels and the results were discussed. Chapter 4 and Chapter 5 deals

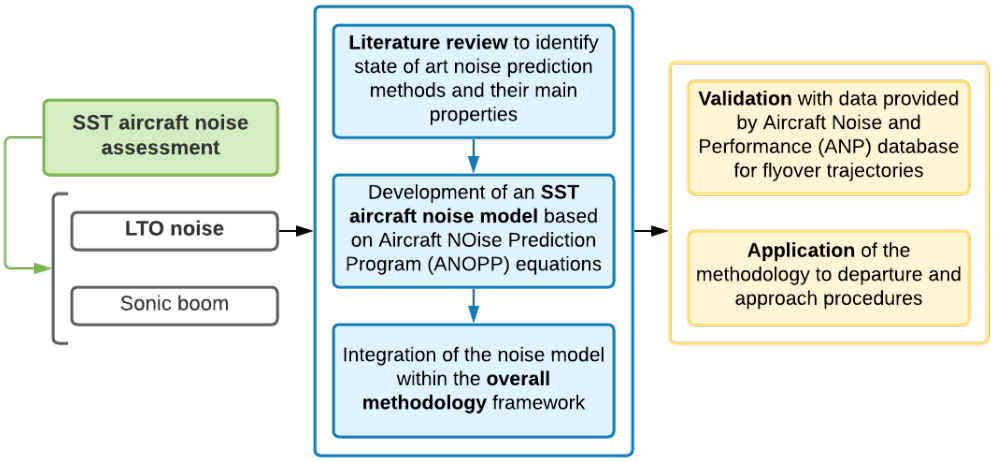

Figure 1.11: Roadmap of the activities performed in the thesis.

with its application and give an example of its noise prediction capabilities integrated within conceptual design. The Matlab program has been run for flyover trajectories at different thrust ratings and altitudes to perform a dedicated validation with experimental data provided by Aircraft Noise and Performance (ANP) database, considering both instantaneous and integrated noise metrics. The only available SST aircraft of the ANP, i.e. the Concorde, has been selected as case study. The results obtained have shown an acceptable level of accuracy for applications at a conceptual design level, leaving options open to gain a higher fidelity-level with further improvements and correction in noise prediction and engine modelling. Furhtermore, fixed-point data provided by ANP have been employed to simulate trajectories for departure and approach procedures to predict noise level at the certification points during LTO cycle. The outcome of the work demonstrated the capability of the developed methodology to be applied for evaluating the noise requirements since the early stages of aircraft design and providing useful guidelines for the design of future low-noise SST together with operational procedures able to mitigate the LTO noise.

A synthesis of the objectives achieved is reported in the concluding Chapter, with considerations regarding possible improvements and future developments.

Chapter 2

Noise source modelling

The Chapter addresses the noise source modelling starting from an assessment of state of art in aircraft noise prediction. Hence, a literature review on current methods and tools availables to model and predict aircraft noise is presented, focusing on the most relevant under the scope of this thesis, i.e. Aircraft NOise Prediction Program developed by NASA. After that, the SST aircraft LTO noise model employed is described, providing the noise sources breakdown and the relative equations to each sub-components of overall noise. Lastly, the model has been implemented in different Matlab routines and results obtained have been reported.

2.1 Literature review

Currently, many tools and methods are available to account for environmental sustainability requirements as project constraints in the early design of the aircraft and mission, aiming at reducing the environmental impact and/or operating costs. A number of optimization studies towards different objectives can be found in the literature, e.g. [17], [18], [19]. Such activities usually include the application of a noise prediction software, in order to assess the environmental impact of an overall aircraft system. In the sphere of the overall aircraft noise prediction, several computer programs are widely used, according to the application background. An exaustive classification about the state of art in aircraft noise prediction is presented in [20], [21], [22]. Possible methos adopted to model and predict aircraft noise are listed below:

- *Fully analytical*: both the fluid mechanic and acoustic results used in the analysis are obtained analytically. Despite the high efficiency of these methods, they are suitable only for simple models and basic research. Modelling aircraft noise sources with a fully analytical approach is not recommended, as the problem has multidisciplinary implications and involves an advanced knowledge of fluid dynamics, acoustic and mathematics.

- *CFD combined with acoustic analogy*: these methods involve turbulent simulation in the near field, determining the acoustic propagation from aerodynamic flow calculation. The main shortcoming of the analytical methos is partially overcome, as CFD are able to model more complex sources. However, these methods, especially fully CFD, often require high computational time.

- *Scientific*: typically based on some empirical data and on an adeguate physical model for noise generation mechanism, these methods provide a parametric source definition that allows to account for the impact of operational settings and airframe/engine geometry on noise generation. Their strength relies on the reliability of the results obtained in a certain field of validity, without excluding the possibility to extend the prediction also outside it and explore the noise evaluation of unconventional aircraft.

- *Best practice*: they rely almost exclusively on ground measurements of a specific aircraft. Then, the measured noise immission related to overall aircraft noise is corrected accounting for propagation effect to determine the originating emission noise level of the aircraft. Best pratice methods allows a faster and more pratical approach. However, their fidelity is restricted to the aircraft considered and the predicted overall noise cannot be categorized into individual sub-components.

Scientific and best pratice are the most common methods used to predict overall aircraft noise. In the next paragraphs some examples of state of art tools relying on these methods are given.

Scientific methods Namely also semi-empirical, componential or parametric, these methods are the most widely used for noise evaluation at a conceptual design level, as they are able to predict noise immission from both conventional and unconventional aircraft. Scientific noise prediction is furthermore characterized by a parametric modelling of each individual noise source. Such a parametric formulations enable the prediction of the various effects on noise radiation caused by the variations of aircraft configuration and operating conditions throughout simulated flight operations. Such models capture the major physical effects and correlations yet allow for a fast noise prediction. Thus, many efforts have been undertaken for the development of noise prediction methodologies based on a semi-emprical approach The most relevat example of this kind of tools is Aircraft NOise Prediction Program (ANOPP), the first computer program with noise prediction capabilities developed by NASA Langley Research Center in the early 1970s. One of the first major applications of ANOPP was to support the Supersonic Cruise Research (SCR) project at Langley, while next application was in conjunction with the Federal Aviation Administration (FAA) study to determine economically reasonable and technologically feasible noise limits for future supersonic transports [23]. NASA has been continuing its activity in this area, and have announced a new release of the program with ANOPP2, whose purpose has been extended to noise evaluation for unconventional aircraft configurations [24].

In recent years, also the German Aerospace Center (DLR) has developed another noise prediction tool, the Parametric Aircraft Noise Analysis Module (PANAM). The current version of PANAM is applicable to the noise evaluation of conventional aircraft configurations along arbitrary threedimensional flight trajectories. The PANAM framework allows for a straight forward integration of additional or updated noise source models reflecting progress in modeling the physics of noise source mechanisms and their parametrical dependencies. The modular setup allows for either self-contained operation or for direct integration in a multidisciplinary design code such as the code preliminary aircraft design and optimization developed at the Technical University of Braunschweig, Germany. The PRADO integration allows for fully automated low noise optimization of aircraft configurations in the preliminary design process [25], [30].

Meanwhile, the University of Manchester has been developing FLIGHT, a program with the aim of creating a reliable software framework for the current generation of commercial aircraft powered by gas turbine engines. Yet, unlike other computer models, this program does not address any issue of conceptual design. Indeed, it uses the framework, composed by different modules (geometry, aerodynamics, propulsion, airframe-engine integration, flight mechanics, trajectory optimisation, thermo-structural performance, static stability, parametric analysis and aircraft noise), to generate reliable models of the aircraft systems by using a composite method that relies on a large data base with the aim of obtain a basis for model and noise validation. Also for this tool, the aircraft noise is modeled on the basis of the method of components, with some consideration for interference factors between the sources [26].

Best pratice methods Tools that can be assigned to this category provide an evaluation of medium to long term average noise levels around airports rather than for prediction of single flyover events and qualify for application in air traffic management and legislation processes. Typically best practice methods rely on Noise Power Distance (NPD) experimental data for an individual aircraft. NPD relationships are obtained as a function of observer distance via spherical spreading through a standard atmosphere and represents the standard technique for evaluating noise from flight procedures, accounting for modifications to flight path, runway/airport layout, and fleet mix on overall ground noise through the introduction of corrective factors. The first example of best practice tool is the Integrated Noise Model (INM) developed by FAA. In this case, noise prediction procedure is based on NPD data normalization to a specific straight horizontal flight segments with constant operational and configurational setting. In this way, noise immission along a selected flight path is predicted assembling the corresponding trajectory from these straight flight segments [27]. The fixed-wing aircraft portion of the INM database is harmonized with ICAO's Aircraft Noise and Performance (ANP) database, which accompanies ECAC's Doc 29 [28].

Another example of this tools, that may be defined as an hybrid approach, is SIMUL, another tool developed by DLR. The concept of SIMUL is a description of the aircraft as a sound source by a set of partial sound sources. This separation process is based on the way the source mechanisms are influenced by the aircraft speed. The actual version of the model describes the following separate mechanisms: jet nois is influenced

by the aircraft speed as well as the jet speed. The remaining sources of engine noise are influenced by aircraft speed only. SIMUL database is derived from measurements and manufacturer information for engine model, wheareas is based on PANAM results for airframe noise. As a result, SIMUL represents a compromise between a pure empirical model and a pure analytical model [29].

2.1.1 ANOPP

As already mentioned, ANOPP was the first computer program applicable to the preliminary design of the aircraft to elaborate and indicate where further theoretical and experimental research on noise prediction is needed. NASA initiated the development of ANOPP approximately 50 years ago to support high-speed transport research programs sponsored by U.S. goverament. The purpose of ANOPP first code was to predict noise from an aircraft by accounting for the effects of its engines, its operations, the atmosphere including ground effects, and other characteristics which may influence the noise it generates. The prediction methodologies implemented within the code were empirical or semiempirical and relied on a widly available experimental data sets and acoustic prediction methods. Following a componential approach, overall aircraft noise was computed as an assembly of each major noise sources. Indeed, an intensive research has been conducted during the years about noise prediction models for airframe and engine contributions (that are considered the most dominant aircraft noise sources) that underlie the overall noise prediction. However, the core of the program, that was the noise source model, interfaced with several other modules, in order to obtain a comprehensive model for noise prediction. Precisely, "comprehensive" means that various aspects of the aircraft are modelled in the code, such as main sub-systems and their mutual integration, in order to offer a realistic simulation tool of the aircraft without the need of too much detail on each system, which would be unavailable anyway [26]. Hence, ANOPP embedded models for sound propagation from near the aircraft towards the observer on the ground, including the effects of the atmosphere and terrain, and installation effect, including scattering and shielding, and is integrated with other performance modules for flight dynamics and engine operations.

In ANOPP first version any of the prediction methods work well for conventional aircraft configurations,but lack capability and fidelity required for non conventional configurations. As a conquence, in 2011 NASA released the new version ANOPP2, including the tools of the older ANOPP version for engine and airframe noise and introduces new tools with a higher level of fidelity for source noise component prediction, installation effects, and propagation to the far-field in order to predict noise for unconventional designs [24]. However, ANOPP2 incorporates the same fundamental concepts of the first version, with improvements in terms of reliability, accuracy and validity of the results. Therefore, it is possible to say that starting from the first version of the program, ANOPP constitutes a guideline in the development of comprhensive methodologies for the prediction of noise, differing essentially only for the models employed. To understand the program concept, a description of noise evaluation problem is necessary (Fig. 2.1).

Once aircraft noise emission has been predicted in terms of Sound Pressure Level (SPL) for a given instant of time and in a single point of the trajectory, the integration with aircraft flight dynamics lead to the extension of noise prediction along the flight path. The estimation obtained is not yet the noise that the observer on ground receive, as propagation effects from atmosphere and ground have to be accounted for. It is clear that aircraft noise evaluation alog a trajectory involves different parameters related to aircraft operation and configuration and ambient condition.

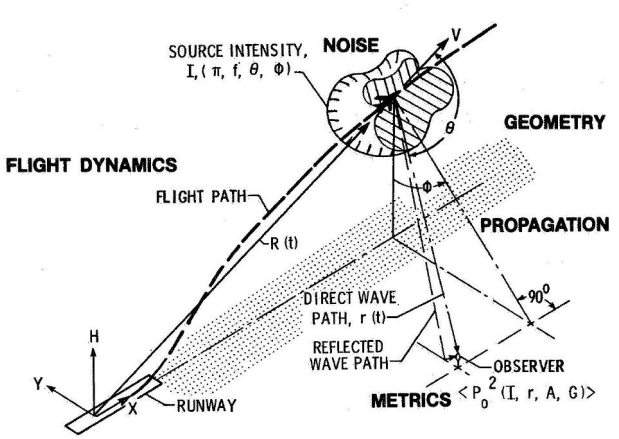

Figure 2.1: Aircraft noise prediction problem [23].

The ANOPP System is divided into two parts: the executive system and the functional module library. The executive system controls execution of the program , whereas the functional module library contains all of the research functional modules. Each functional module is an independent group of subprograms which performs noise prediction functions. A flow chart of the ANOPP system functional module is shown in Fig. 2.2. The procedure begins by defining an atmosphere using the Atmosphere Module (ATM), followed by the atmospheric absorption module (ABS). The steady flyover module (SFO) is used for the approach measurement point, and the jet takeoff module (JTO)for sideline and takeoff measurement points. The geometry module (GEO) computes the range and directivity angles from the observer to the noise source. At this point, the various noise sources modules are run: Heidmann's18 for fan noise (HDNFAN), Stone's19 for coaxial jet noise (STNJET) and Fink's20 for airframe noise (FNKAFM). Once data has been generated by the noise source modules, the propagation module (PRO) applies corrections to the noise data in the source frame of reference to transfer it to the observer frame of reference. Atmospheric absorption effects are applied at this point. The noise levels module (LEV) computes the tonecorrected Perceived Noise (PNLdB),and the effective noise level module (EFF)is run next to compute the EPNdB levels used as noise metrics in this research [24].

ANOPP has also been extended to a high-speed research program with the Aircraft Noise Prediction Program's High Speed Research prediction system (ANOPP-HSR), including modules to serve particular prediction requirements relative to high-speed

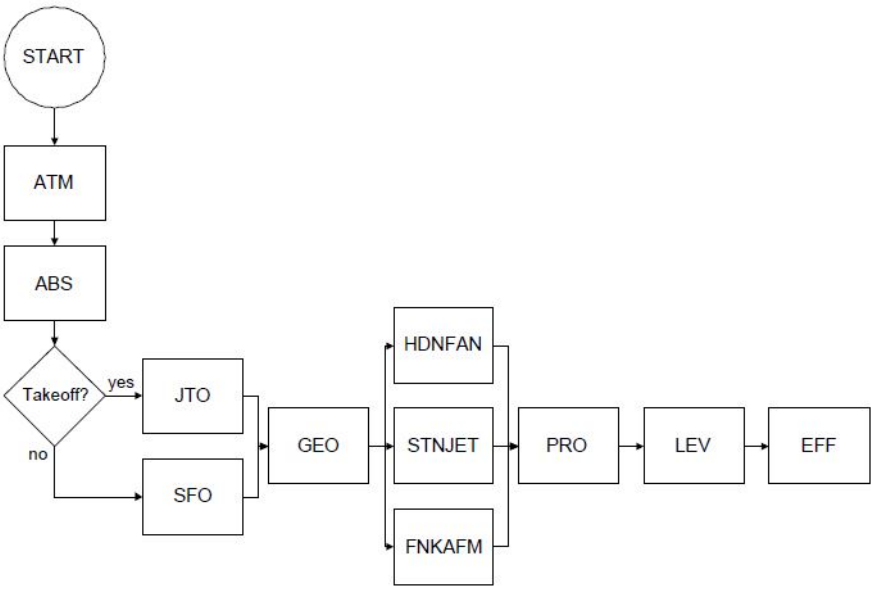

Figure 2.2: Flow chart of ANOPP functional modules.[24].

aircraft [31]. Hence, under the scope of this work, ANOPP has been taken as a reference, since it is considered an example of a comprehensive methodology for aircraft noise prediction, suitable also for SST aircraft.

2.2 SST aircraft LTO noise model

The method of components has become the prevalent method for predicting aircraft noise. Such method relies on the typical distiction of aircraft noise in propulsive and non propulsive (airframe) sources. In turn, these two contributions are broken down into other sub-components depending on design and operational parameters. In order to identify the noise sub-components for a supersonic aircraft leading to the generation of noise during take-off and landing, a comparison between subsonic and supersonic aircraft has been considered. In general, neglecting interaction and installation effects, aircraft components listed and described in Tables A.1 and A.2 (Appendix A) can be considered the main noise sources for a subsonic aircraft.

The main differences between subsonic and supersonic aircraft are exhaustively described in [11] and are summed below:

- The wing shape: even thought this is the most visible physical difference between subsonic and supersonic aircraft, it has not much influence on the total noise generated. Clean wing noise is mainly due to the turbolence generation at trailing egde, thus the most influential parameters are velocity, wing span and boundarylayer thickness.

- The high-lift devices: for a subsonic aircraft the slat noise is one of the most dominant noise source [34]. Since supersonic aircraft control system typically does not provided with secondary control devices the additional turbulence and increased boundary layer thickness generated by the slats will not be present and therefore reduce the noise production.

- The landing gear: supersonic aircrafts are usually equipped with longer landing gear compared to subsonic ones, as it allows an increased ground clearance when rotating for takeoff or during landing, that is needed because the larger angle of attack during takeoff or landing. This noise component influences enough airframe noise and might impact on noise generation with a significant difference.

- The engine: current subsonic engines can have By-Pass Ratio (BPR) of up to 12.5, whereas supersonic engines are optimized for supersonic flight, so they must have a limited engine front area. Since the exhaust flow speed greatly influence noise generation, higher BPR have a beneficial effect on aircraft noise. As a consequence, the main issue for supersonic aircraft noise is the highly exhasut jet speed.

- Operations: a supersonic aircraft has lower aerodynamic performance during take-off and landing and requires higher thrust to control the aircraft and counter the increased drag. Furthermore, this requires an higher approach speed, since wings optimised for supersonic flight likely have a higher stall speed. Noise depends on the fifth power of flight speed, hence this may be the most important factor in both approach and departure noise compared to subsonic aircraft.

Accounting for this differences, it is conceivable to consider SST aircraft noise sources related to take-off and landing likewise to subsonic ones. As previously noted, a distinction emerges between aircraft and engine noise, each characterized in turn by other different sub-components. On this basis, the noise sources were specialized in the case of an SST aircraft, considering the Concorde design as the reference aircraft. Lokking at the Figure 2.3, there were not considered in the model the contributions of flaps, slats, spoilers, speed brakes and leading edge devices to airframe noise, as well as the horizontal tail. Secondly, noise generation due to shock cells noise, that occurs when the exhaust flow speed becomes supersonic, has to be considered.

Each of this sub-components has been modelled with the equations provided by "Aircraft Noise Prediction Program – Theoretical Manual" [32]. Thus, the mean-square acoustic pressure has been computed for each component as a function of 1/3 octave center frequency, polar directivity angle and azimuthal directivity. Precisely, polar directivity angle is the angle between aircraft longitudinal axis and observer on ground, whereas azimuthal directivity angle is the one between aircraft lateral axis and the observer on ground. At least, the total noise has been computed as assembly of each mean-square acoutic pressure contributions. Aircraft design and operational parameters that might be impacted by noise generation have been identified and different Matlab routines have been employed to evaluate the output of the equations.

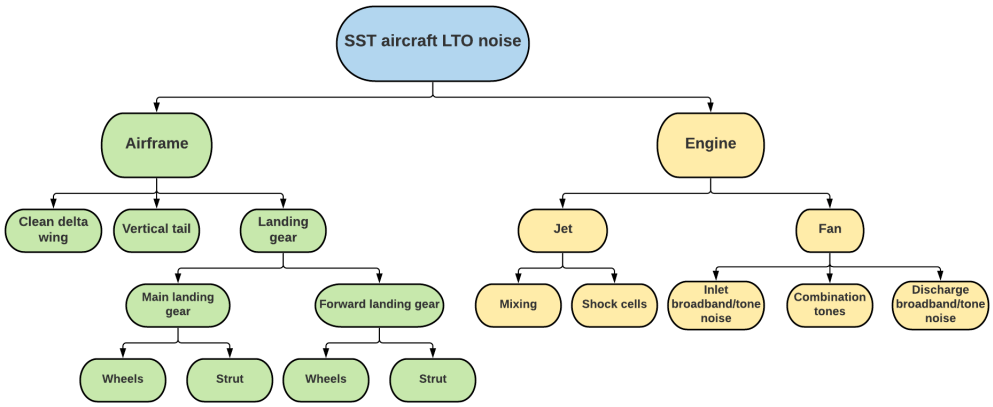

Figure 2.3: SST aircraft LTO noise sources breakdown.

Assumptions In order to develop a noise prediction model suitable to conceptual design evaluations several approximations have been made:

- Each noise source is assumed to be independent, hence interaction and installation effects are neglected.
- Noise scattering, reflection and shielding effects are not considered.
- The aircraft is assumed to be a lumped mass and all the acoustic sources are concentrated on the airplane's centre of gravity.
- Flap and slat noise are not present due to supersonic aircraft design considered.
- Turbomachinery and combustion noise are neglected.

2.2.1 Airframe noise

A review of several airframe noise prediction schemes is reported in [**?**], but that due to Fink is the one most widely accepted as correct in its combination of a wide range of full-scale and model data. Accordingly, this work presents the main points of Fink's proposals following mathematical formalism implemented in ANOPP. Considering a generic subsonic aircraft, in Fink's component method applied in [35] the overall airframe noise is assembled as a combination of these individual models:

- Clean wing and tail surfaces noise
- Landing gear noise
- Trailing edge flap noise
- Leading edge slat and flap noise

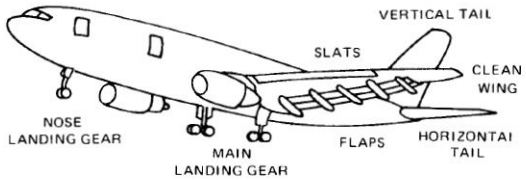

Figure 2.4: Individual noise-radiating airframe components.[35]

Noise radiation from clean airframe, with all gear and high-lift devices retracted, is assumed to be entirely associated with turbolent boundary layer flow over the trailing edges of the wing and tail surfaces. Hence, noise generation due to clean wing and tail surfaces is modeled as trailing edge noise, that is in general a consequence of the interaction between unsteadiness in the flow and the sharp corner formed by the trailing edge of a lifting surface. Leading edge is ignored, and this approximation is realistic as long as the airfoil chord remains large compared to the acoustic wavelength of the sound produced. To the trailing edge noise predictions for the clean wing and horizontal and vertical tails Fink's noise component method adds predictions for the noise of forward and main landing gear and of wing flaps and leading-edge slats. With the exception of the leading-edge slats, for which very few data are available, no interactions are included between these fields.

Noise contributions from the forward landing gear and main landing gear are calculated separately, because generally each has a different size, and therefore a different peak frequency. Noise from the trailing edge flaps is calculated independent of whether the landing gear are extended or retracted.

Neglecting this type of interaction noise is a strong approximation. Yet, the machanism for noise generation due to landing-gear extension is complex and dependent on the particular landing-gear design being considered. The process has been simplified with the assumption, based on the experimental comparisons, showing that noise generated by the strut and wheel appears to dominate other potential sources. Separate predictions are made for the strut and wheel noise which are added together to yield the total landing-gear noise. An empirical approach was used for noise from extended landing gear and deflected flaps and slats. As previously specified, for an SST aircraft the contributions of flap and slat will be excluded.

Secondly, the prediction of broadband noise for the dominant component of the airframe is computed by the method applied in [32]. This one employs empirical and assumed functions to produce sound spectra as function of frequency, polar directivity angle and azimuthal directivity angle. Each spectrum is the sum of all the airframe component spectra produced by the wing, vertical tail and landing gear. This method is intended to capture the source and the convective effects by means of simple geometric relationships and a number of coefficients which are determined from curve-fitting

of empirical data. In spite of the theoretical shortcomings, specifically the misunderstanding that most of the noise was generated at the trailing edge, this method remains widely used and (until recently) seldom criticised [22].

The general approach for each contribution is the same and is based on the following equation for the calculation of the far-field acoustic mean-square pressure:

$$< p^2 >^* = \frac{\Pi^*}{4\pi(r_s^*)} \frac{D(\theta,\phi)F(S)}{(1 - M_\infty \cos\theta)^4} \tag{2.1}$$

Where:

- $< p^2 >^*$: dimensionless mean-square acoustic pressure, re $\rho_\infty^2 c_\infty^4$
- Π^*: dimensionless overall acoustic power, re $\rho_\infty c_\infty^3 b_w^2$
- $D(\theta,\phi)$: directivity function
- $F(S)$: spectrum function
- S: Strouhal number
- r_s^*: dimensionless distance from source to observer, re b_w
- $(1 - M_\infty \cos\theta)^4$: Doppler factor, that accounts the forward velocity effect
- θ: polar directivity angle, deg
- ϕ: azimuthal directivity angle, deg

With ρ_∞ ambient density in $[Kg/m^3]$, c_∞ ambient speed of sound in [m/s] and M_∞ aircraft Mach number; $4\pi(r_s^*)$ is a spherical propagation factor. The Strouhal number S is defined as:

$$S = \frac{fL}{M_\infty c_\infty}(1 - M_\infty \cos\theta) \tag{2.2}$$

Where L is some length scale characteristic of the particular airframe noise source being computed. The acoustic power for the airframe Π^* can be expressed as:

$$\Pi^* = K(M_\infty)^a G \tag{2.3}$$

Where:

- K and a are constants determined from empirical data.
- G is a geometry function different for each airframe component and incorporated all geometry effects on the acoustic power.

Source	K	a	G
Clean wing (aerodinamically clean)	$7.075 \cdot 10^{-6}$	5	δ^*_w
Vertical tail (aerodinamically clean)	$7.075 \cdot 10^{-6}$	5	$\delta^*_v(\frac{b_v}{b_w})^2$
1-and-2 wheel landing gear wheel noise	$4.349 \cdot 10^{-4}$	6	$n(\frac{d}{b_w})^2$
4 wheel landing gear wheel noise	$3.414 \cdot 10^{-4}$	6	$n(\frac{d}{b_w})^2$
Landing gear strut noise	$2.753 \cdot 10^{-4}$	6	$(\frac{d}{b_w})^2(\frac{l}{d})$

Table 2.1: K, a and G for each airframe noise component for SST aircraft. [32]

The values of K, a and G for this case study are reported in the Table 2.4 for each airframe noise component.

Clear wing and vertical tail are considered as *aerodinamically clean*, such as a sailplane or a jet aircraft with simple trailing edge flap mechanism. Moreover, for landing gear, n, d and l are respectively the number of wheels per landing gear, the tire diameter and the struct length. The parameter δ^* is the dimensionless turbolent boundary-layer thickness, computed from the standard flat-plate turbolent boundary-layer model, defined as:

$$\delta^* = 0.37\frac{A}{b^2}(\frac{\rho_\infty M_\infty c_\infty A}{\mu_\infty b})^{-0.2} \tag{2.4}$$

Where A and b are the wing surface and the wing span, chosen appropriately for the wing or tail surface, wheares μ_∞ is the ambient dynamic viscosity. Each airframe noise source has its own directivity function and spectrum function, listed in the table 2.5; in the table 2.6 Strouhal number for each contribuition is reported.

Using these functions and the acoustic power, the mean-square acoustic pressure can be computed as a function of frequency, polar directivity angle and azimuthal directivity angle for a given set of input parameters.

Source	Directivity	Spectrum function
Clean delta wing	$4\cos^2\phi\cos^2\frac{\theta}{2}$	$0.485(10S)^4[(10S)^{1.35}+0.5]^{-4}$
Vertical tail	$4\sin^2\phi\cos^2\frac{\theta}{2}$	$0.613(10S)^4[(10S)^{1.5}+0.5]^{-4}$
1-and-2-wheel landing gear wheel	$\frac{3}{2}\sin^2\theta$	$13.59S^2(12.5+S^2)^{-2.25}$
1-and-2-wheel landing gear strut	$\frac{3}{2}\sin^2\theta\sin^2\phi$	$5.32S^2(30+S^8)^{-1}$
4 wheel landing gear wheel	$\frac{3}{2}\sin^2\theta$	$0.0577S^2(1+0.25S^2)^{-1.5}$
4 wheel landing gear strut	$\frac{3}{2}\sin^2\theta\sin^2\phi$	$1.280S^3(1.06+S^2)^{-3}$

Table 2.2: Directivity function D and Spectrum function $F(S)$ for each airframe noise component for SST aircraft [32]

Source	Strouhal number S
Clean delta wing	$\frac{f\delta_w^* b_w}{M_\infty c_\infty}(1-M_\infty\cos\theta)$
Vertical tail	$\frac{f\delta_v^* b_v}{M_\infty c_\infty}(1-M_\infty\cos\theta)$
1-and-2-wheel landing gear wheel	$\frac{fd}{M_\infty c_\infty}(1-M_\infty\cos\theta)$
1-and-2-wheel landing gear strut	$\frac{fd}{M_\infty c_\infty}(1-M_\infty\cos\theta)$
4 wheel landing gear wheel	$\frac{fd}{M_\infty c_\infty}(1-M_\infty\cos\theta)$
4 wheel landing gear strut	$\frac{fd}{M_\infty c_\infty}(1-M_\infty\cos\theta)$

Table 2.3: Strouhal number S for each airframe noise component for SST aircraft [32]

2.2.2 Engine noise

Noise generated by engine consists of several contributions, which in literature are generally classified into: fan noise, jet noise and engine core noise (compressor stages, combustor, turbine stages), as depicted in Figure 2.5.

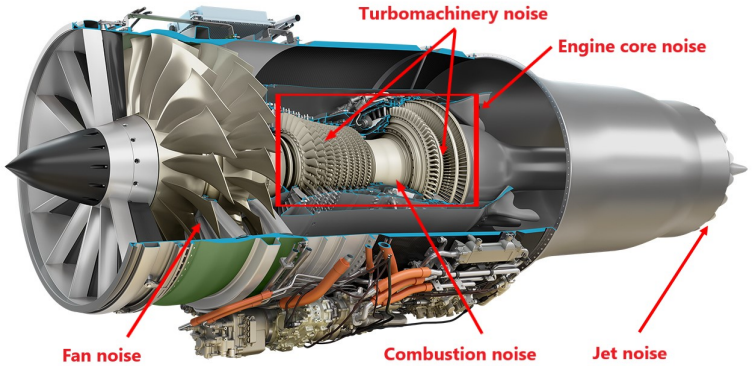

Figure 2.5: Summary of engine noise sources (General Electric Affinity by GE Aviation - Turbofan for supersonic transport)

ANOPP provides different modules capable to predict each contribution:

- Fan noise: predicts the broadband noise and pure tones for an axial flow compressor or fan. The method is based on the method developed by M. F. Heidman.
- Combustion noise: predicts the noise from conventional combustors installed in gas turbine engines. The method is based on that one proposed by SAE ARP 876.
- Turbine noise: predicts the broadband noise and pure tones for an axial flow turbine. The method is based on a method developed by the General Electric Company.
- Single stream circular jet noise: predicts the single stream jet mixing noise from shock-free circular nozzles, on the basis of SA ARP 876.
- Circular jet shock cell: predicts the broadband shock-associated noise from a single convergent nozzle operating at supercritical pressure ratios, on the basis of method proposed by SAE ARP 876.
- Stone jet noise: predicts the far-field mean-square acoustic pressure for single stream and coaxial circular jets. Included in the prediction are both jet mixing noise and shock-turbulence interaction noise, on the basis of Stone method. For coaxial nozzles, the method is limitedto jets whose core jet velocity is greater than the secondary jet velocity. Further, only the core jet velocity may be supersonic.

- Dual stream coannular jet noise: predicts the noise characteristics of a coannular jet exhaust nozzle with an inverted velocity profile.

Yet, considering the large amount of data required to compute each contribution, at a conceptual design level it is conceivable to account only for the two most predominant noise sources, which are fan and jet noise. Furthermore, a distinction must be made among the different types of engine that could propel a supersonic aircraft. For turbojet engines jet noise is modelled as single stream jet, whereas for turbofan it is modelled as dual coaxial stream jet. Secondly, fan noise for turbojet engines can be associated with noise generated by the first stage of compressor.

Jet noise Jet noise is the most widely studied among the aircraft noise sources, firstly to allow the use of the jet engine as a power plant for civil aircraft and not only for military one [**?**]. Jet noise as a study in aerodynamic noise had its foundations in the work of Lighthill on "Sound generated aerodynamically". The most relevant finding of that work was the *Lighthill's eighth power law*, that states that power of the sound created by a turbulent motion, far from the turbulence, is proportional to eighth power of the characteristic turbulent velocity. Approches to jet noise reduction have been also widly investigated, focusing on particular and complex nozzle design.

At present, the most comprehensive method for coaxial and single strem jet is that of Stone, which has been validated over the year 171 and extended to include details such as chevron and various geometrical details of the nozzle and the plug [36], [37]. Therefore, in this work jet noise is predicted using Stone method. The total far-field jet noise is typically computed as the sum of the jet mixing noise and shock noise, that occurs when $\sqrt{(M_1^2 - 1)})$ is greater than zero, with M_1 the primary stream Mach number (Fig. 2.6).

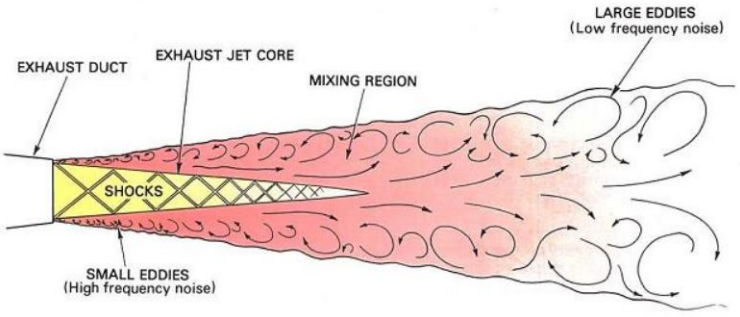

Figure 2.6: Jet flow exhaust mixing and shock structure.

The method uses empirically functions to provide the directivity and the spectral content of the field with the computed overall mean-square acoustic pressure at $\theta = 90°$, that is $< p^2(\sqrt{A_e}, 90°) >^*$, used to fix the amplitude throughout the field. The equation

used to calculate the jet mixing noise at a distance r_s from the nozzle exit is:

$$< p^2(r_s^*, \theta) >^* = \frac{< p^2(\sqrt{A_e}, 90°) >^*}{(r_s^*)^2} \left[\frac{1 + (0.124 V_1^*)^2}{(1 + 0.62 V_1^* \cos\theta)^2 + (0.124 V_1^*)^2} \right]^{\frac{3}{2}} \cdot D_m(\theta') F_m(S_m, \theta') H_m(M_\infty, \theta, V_1^*, \rho_1^*, T_1^*) G_c G_p \tag{2.5}$$

$$< p^2(r_s^*, \theta) >^* = \frac{< p^2(\sqrt{A_e}, 90°) >^*}{(r_s^*)^2} \left[\frac{1 + (0.124 V_1^*)^2}{(1 + 0.62 V_1^* \cos\theta)^2 + (0.124 V_1^*)^2} \right]^{\frac{3}{2}} \cdot D_m(\theta') F_m(S_m, \theta') H_m(M_\infty, \theta, V_1^*, \rho_1^*, T_1^*) G_c G_p \tag{2.6}$$

Where $< p^2(\sqrt{A_e}, 90°) >^*$ is the mean-square acoustic pressure for a stationary jet calculated at the reference distance $\sqrt{A_e}$ from the nozzle exit at $\theta = 90°$, and is defined as:

$$< p^2(\sqrt{A_e}, 90°) >^* = \frac{2.502 \cdot 10^{-6} A_{j,1}^* (\rho_1^*)^{\omega_\circ} (V_1^*)^{7.5}}{[1 + (0.124 V_1^*)^2]^{\frac{3}{2}}} \tag{2.7}$$

The density exponent $\omega_\circ$ is an empirically determined function of V_1^* given by:

$$\omega_\circ = \frac{2(V_1^*)^{3.5} - 0.6}{(V_1^*)^{3.5} + 0.6} \tag{2.8}$$

While the other parameters are:

- r_s^*: dimensionless distance from the nozzle exit r_s, referred to $\sqrt{A_e}$.
- $A_{j,1}^*, \rho_1^*, V_1^*$ and T_1^* : fully expanded jet area, density, velocity and total temperature respectively, with all three quantities evaluated for the primary stream, and nondimensionalized by A_e, ρ_∞, c_∞ and T_∞.
- θ': modified directivity angle, $\theta' = \theta (V_1^*)^{0.1}$.
- $D_m(\theta')$: directivity function.
- $F_m(S_m, \theta')$: spectral distribution function.
- $H_m(M_\infty, \theta, V_1^*, \rho_1^*, T_1^*)$: forward flight effects factor.
- G_c and G_p: configuration factors.
- S_m: jet mixing noise Strouhal number.

The jet mixing noise Strouhal number S_m is calculated as:

$$S_m = \frac{f^* d_{j,1}^* [1 - M_\infty \cos(\theta - \delta)] (T_1^*)^{0.4(1+\cos\theta')}}{V_1^* (1 - \frac{M_\infty}{V_1^*})} \cdot \left\{ \frac{[1 + 0.62(V_1^* - M_\infty)\cos\theta]^2 + [1 + (0.124(V_1^* - M_\infty)]^2}{(1 + 0.62 V_1^* \cos\theta)^2 (0.124 V_1^*)^2} \right\}^{\frac{1}{2}} g_c g_p \tag{2.9}$$

Where g_c and g_p are configuration factors and f^* is the Helmhotz number, given as:

$$f^* = \frac{f\sqrt{A_e}}{c_\infty} \tag{2.10}$$

While $d^*_{j,1}$ is the jet diameter, given as:

$$d^*_{j,1} = \sqrt{\frac{4A^*_{j,1}}{\pi}} \tag{2.11}$$

The forward velocity effects factor $H_m(M_\infty, \theta, V_1^*, \rho_1^*, T_1^*)$ is given by:

$$\begin{aligned} H_m(M_\infty, \theta, V_1^*, \rho_1^*, T_1^*) = & \left\{ \frac{(1 + 0.62V_1^* \cos\theta)^2 + (0.124(V_1^*)^2}{[1 + 0.62(V_1^* - M_\infty)\cos\theta]^2 + [1 + (0.124(V_1^* - M_\infty)]^2} \right\}^{\frac{3}{2}} \\ & \cdot \frac{1 - (\frac{M_\infty}{V_1})^5 (\rho_1^*)^{\omega - \omega_\circ}}{1 - M_\infty \cos(\theta - \delta)} \end{aligned} \tag{2.12}$$

Where δ is the angle between the flight vector and the engine inlet axis in degrees and $\omega - \omega_\circ$ is:

$$\omega - \omega_\circ = \frac{1.8\{[V_1^*(1 - \frac{M_\infty}{V_1^*})^{\frac{2}{3}}]^{3.5} - (V_1^*)^{3.5}\}}{\{0.6 + [V_1^*(1 - \frac{M_\infty}{V_1^*})^{\frac{2}{3}}]^{3.5}\}[0.6 + (V_1^*)^{3.5}]} \tag{2.13}$$

Finally, the configuration factors G_p and G_c take the mean-square acoustic pressure predicted for a single stream circular nozzle and adjust it to predict the mean-square acoustic pressure for plug and single nozzles, respectively. The factor G_p is given by:

$$G_p = \begin{cases} \left(0.10 + \frac{2R_d^2}{1+R_d^2}\right)^{0.3} & \text{Nozzle with plug} \\ 1 & \text{Nozzle without plug} \end{cases} \tag{2.14}$$

With:

$$R_d = \frac{d^*_{h,1}}{d^*_{e,1}} \tag{2.15}$$

With $d^*_{h,1}$, the plug nozzle hydraulic diameter, given by:

$$d^*_{h,1} = \sqrt{d^*_{e,1} + (d^*_p)^2} - d^*_p \tag{2.16}$$

With d^*_p the plug diameter, referred to $\sqrt{A_e}$, and $d^*_{e,1} = d^*_{j,1}$ nozzle equivalent diameter.

The factor G_c is given by:

$$G_c = \begin{cases} \left(\frac{T_1^*}{T_2^*}\right)^{\frac{1}{2}} \left\{ (1 - \frac{V_2^*}{V_1^*})^m + \frac{1.2\left[1+\frac{A_{j,2}^*(V_2^*)^2}{A_{j,1}^*(V_1^*)^2}\right]^4}{\left(1+\frac{A_{j,2}^*}{A_{j,1}^*}\right)^3} \right\} & \text{Coaxial nozzle} \\ 1 & \text{Single nozzle} \end{cases} \tag{2.17}$$

Where the exponent m is given by:

$$m = \begin{cases} 1.1\sqrt{\frac{A_{j,2}^*}{A_{j,1}^*}} & \frac{A_{j,2}^*}{A_{j,1}^*} < 29.7 \\ 6 & \frac{A_{j,2}^*}{A_{j,1}^*} \geq 29.7 \end{cases} \tag{2.18}$$

Finally, the factors g_P and g_c adjusts the Strouhal number S_m for a single stream circular jet to that for a plug nozzle or a single nozzle respectively. These factors are given by:

$$g_p = \begin{cases} (R_d)^{0.4} & \text{Nozzle with plug} \\ 1 & \text{Nozzle without plug} \end{cases} \tag{2.19}$$

$$g_c = \begin{cases} \left(1 - \frac{T_2^* f_s}{T_1^*}\right)^{-1} & \text{Coaxial nozzle} \\ 1 & \text{Single nozzle} \end{cases} \tag{2.20}$$

With f_s empirically determined function of the area ratio parameter $1+\frac{A_{j,2}^*}{A_{j,1}^*}$ and the velocity ratio $\frac{V_2^*}{V_1^*}$. Shock jet noise is generated by the interaction of the downstream convecting coherent structures of the jet flow with the shock cells in the jet plume, that occurs when a convergent-divergent nozzle is operated at off-design Mach numbers and when a convergent nozzle is operated at super-critical nozzle pressure ratios. The intensity of shock-associated noise is dependent on the degree of mismatch between the design Mach number M_d and the fully expanded jet Mach number M_j.

The 1/3 octave band mean square acoustic pressure due to shock turbolence interaction noise is calculated through use of the following equation:

$$< p^2 >^* = \frac{(3.15 \cdot 10^{-4}) A_{j,1}^*}{(r_s^*)^2} \frac{\beta^4}{1-\beta^4} \frac{F_s(S_s) D_s(\theta, M_1) G_c}{1 - M_\infty \cos(\theta - \delta)} \tag{2.21}$$

With β pressure ratio parameter, equal to $\beta = \sqrt{(M_1^2 - 1)}$, which must be greater than zero for shock cell noise to occur. The function $D_s(\theta, M_1)$ provides the dependence of the shock cell noise, for a stationary jet, on the directivity angle θ and the fully expanded primary stream Mach number M_1. This function is given by:

$$D_s(\theta, M_1) = \begin{cases} 1 & \theta \leq \theta_m \\ 1.189 & \theta > \theta_m \end{cases} \tag{2.22}$$

Where θ_m is the Mach angle defined by: $\theta_m = \arcsin \frac{1}{M_1}$.

The spectral content of the shock noise is provided through the function $F_s(S_s)$ which depends on the Strouhal number S_s:

$$S_s = \frac{f^* d^*_{j,1}}{0.70 V_1^*} \beta [1 - M_\infty \cos(\theta - \delta)][1 + 0.7 V_1^* \cos\theta)^2 + (0.14 V_1^*)^2]^{\frac{1}{2}} \tag{2.23}$$

The total far-field jet noise will be the sum of the shock noise and the jet mixing noise.

Fan noise Fan noise dominates most flight conditions and can be higher than jet noise. Efforts have been made in fan noise reduction and methods are available to make a first-order estimate of the acoustic pressures arising from a fan specified by a limited number of design parameters: diameter, tip chord, number of blades, rotational speed, fan-stator distance, pressure ratio, mass flow ratio, temperature rise across the fan. The method proposed by Heidman in the mid 1970s has come to dominate the arena of empirical fan and single-stage compressor noise prediction [22]. Heidmann prediction method is applicable to turbojet compressors and to single-and-two-stage turbofans with and without inlet guide vanes. The total noise levels are obtainen by spectrally summing the predicted levels of broadband, discrete-tone and combination-tone noise components [40]. Precisely, the predicted free-field radiation patterns consist of composite of the following separately predicted noise components (Fig. 2.7):

- Noise emitted from the fan or compressor inlet duct (broadband noise, direcrete-tone noise, combination-tone noise);
- Noise emitted from the fan discharge duct (broadband noise, direcrete-tone noise)

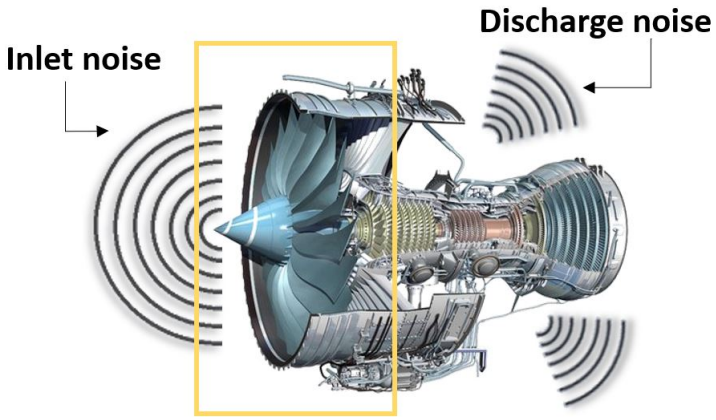

Figure 2.7: Fan inlet and discharge noise.

In this work, the total fan noise is predicted by summing the noise from six separate components:

- Inlet broadband noise
- Inlet rotor-stator interaction tones
- Inlet flow distortion tones
- Combination tone noise
- Discharge broadband noise
- Discharge rotor-stator interaction tones

All noise sources are combined into single 1/3-octave-band spectrum for each directivity angle. The general approach is the same for each noise component and is based on the following equation for the computation of far-field mean-square acoustic pressure:

$$< p^2 >^* = \frac{A^* \Pi^*}{4\pi (r_s^*)} \frac{D(\theta) S(\eta)}{(1 - M_\infty \cos\theta)^4} \tag{2.24}$$

Where:

- $< p^2 >^*$: dimensionless root mean-square acoustic pressure, re $\rho_\infty^2 c_\infty^4$
- Π^*: dimensionless overall acoustic power, re $\rho_\infty c_\infty^3 b_w^2$
- $D(\theta, \phi)$: directivity function
- $S(\eta)$: spectrum function
- r_s^*: dimensionless distance from source to observer, re $\sqrt{A_e}$
- $(1 - M_\infty \cos\theta)^4$: Doppler factor, that accounts the forward velocity effect
- θ: polar directivity angle, deg

The frequency parameter η is defined as:

$$\eta = (1 - M_\infty \cos\theta) \frac{f}{f_b} \tag{2.25}$$

Where the blade passing frequency f_b is:

$$f_b = \frac{N^* B c_\infty}{d^* \sqrt{A_e}} \tag{2.26}$$

With B number of rotor blades. The acoustic power Π^* for the fan is expressed as:

$$\Pi^* = KG(i,j)(s^*)^{-a(k,l)} M_m^b (\frac{\dot{m}^*}{A^*})(\Delta T^*)^2 F(M_r, M_m) \tag{2.27}$$

The equation contains several empirical constants and the empirical function F. The constant K is different for each noise component. The constant G depends on the noise component and the indices i and j, defined as:

$$i = \begin{cases} 1 & \text{Fan with no inlet guide vanes} \\ 2 & \text{Fan with inlet guide vanes} \end{cases} \tag{2.28}$$

$$j = \begin{cases} 1 & \delta > 1.05 \\ 2 & \delta \leq 1.05 \end{cases} \tag{2.29}$$

With δ fundamental tone cut-off factor, defined as

$$\delta = \frac{M_t}{|1 - \frac{V}{B}|} \tag{2.30}$$

Where the fan rotor tip Mach number M_t is

$$M_t = \pi N^* \tag{2.31}$$

If $M_t > 1.05$, then $\delta = M_t$. The fundamental cut-off occurs when the value of δ is less than 1.05. The cut-off factor determines the range of the tip Mach number where the fundamental blade passing frequency dominates. The rotor-spacing exponent $a(k, l)$ depends on the noise component and the indices k and l defined as:

$$k = \begin{cases} 1 & s^* \leq 1 \\ 2 & s^* > 1 \end{cases} \tag{2.32}$$

$$l = \begin{cases} 1 & \text{No inlet flow distortion} \\ 2 & \text{Inlet flow distortion} \end{cases} \tag{2.33}$$

Inlet flow distortion tends to reduce rotor-stator spacing effects. Inlet flow distortion is assumed to occur during static and ground roll operations. The design point Mach number index M_m is defined as:

$$M_m = max(1, M_d) \tag{2.34}$$

Where M_d is the design value of the relative tip Mach number. The exponent b in the equation (21) gives the effect of M_m on each fan noise component.

The final empirical quantity in the equation (21) is the power function F. The power function depends on the fan noise source and is, in general, a function of the relative tip Mach number M_r and the design point Mach number index. The relative tip Mach number is defined as:

$$M_r = (M_t^2 - M_x^2)^{\frac{1}{2}} \tag{2.35}$$

Where M_x is the axial flow Mach number, equal to $\frac{\dot{m}}{A^*}$ since the inlet static density and speed of sound can be assumed equal to the ambient values.

Equation (24) must be specialized for each noise component to compute the overall acoustic power:

- Inlet broadband noise

$$\Pi^* = (1.552 \cdot 10^{-4})(s^*)^{-a(k,l)} M_m^2 (\frac{\dot{m}^*}{A^*})(\Delta T^*)^2 F(M_r) \tag{2.36}$$

- Inlet rotor-stator interaction tones

$$\Pi^* = (2.683 \cdot 10^{-4}) G(i,j)(s^*)^{-a(k,l)} M_m^{4.31} (\frac{\dot{m}^*}{A^*})(\Delta T^*)^2 F(M_r, M_m) \tag{2.37}$$

- Inlet flow distortion tones

$$\Pi^* = (1.488 \cdot 10^{-4}) G(i,j)(s^*)^{-a(k,l)} M_m^{4.31} (\frac{\dot{m}^*}{A^*})(\Delta T^*)^2 F(M_r, M_m) \tag{2.38}$$

- Combination tone noise

$$\Pi^* = K G(i,j)(s^*)^{-a(k,l)} M_m^b (\frac{\dot{m}^*}{A^*})(\Delta T^*)^2 F(M_r, M_m) \tag{2.39}$$

  With $K = 6.225 \cdot 10^{-4}$ for 1/8 fundamental combination tone, $K = 2.030 \cdot 10^{-3}$ for 1/4 fundamental combination tone and $K = 2.525 \cdot 10^{-3}$ for 1/2 fundamental combination tone.

- Discharge broadband noise

$$\Pi^* = (3.206 \cdot 10^{-4}) G(i,j)(s^*)^{-a(k,l)} M_m^2 (\frac{\dot{m}^*}{A^*})(\Delta T^*)^2 F(M_r) \tag{2.40}$$

- Discharge rotor-stator interaction tones

$$\Pi^* = (2.643 \cdot 10^{-4}) G(i,j)(s^*)^{-a(k,l)} M_m^2 (\frac{\dot{m}^*}{A^*})(\Delta T^*)^2 F(M_r) \tag{2.41}$$

The values of empirical constants and function $F(M_r, M_m)$ are reported in [32] for each fan noise component.

2.2.3 Output

Once the distance between the noise source and the observer on ground has been fixed, the semi-empirical equations previously presented allow the computation of the mean-square acoustic pressure for each desired value of frequency, polar directivity angle, and azimuthal directivity angle. Hence, they have been employed in different Matlab routines to compute the mean-square acoustic pressure of each sub-component of LTO noise generated by an SST aircraft. After that, the relative Sound Pressure Level (SPL) has been calulated as:

$$SPL = 10log_{10} < p^2 >^* + 20log_{10}\frac{\rho_\infty c_\infty^2}{p_{ref}} \tag{2.42}$$

Where p_{ref} is the lowest sound pressure possible to hear to human ear, that is approximately 20^{-5} Pa. The final output consists in the Sound Pressure Level (SPL) as a function of frequency for each aircarft noise component. Aircraft position data for noise prediction and ambient conditions has been fixed to consider a single overflight point at the values reported in the Table 2.4. Input data required for each routine are respectively specified in the following paragraphs.

Noise prediction input data	
Distance r	300 m
Polar directivity θ	90°
Azimuthal directivity ϕ	0°
Ambient density ρ_∞	1.225 kg/m^3
Ambient temperature T_∞	288 K
Speed of sound a_∞	340 m/s
Mach M_∞	0.23

Table 2.4: Flight path and ambient conditions data.

Airframe noise Directivity functions are provided in Appedix B. Design parameters that affect noise generation are reported in the Table 2.5. The results obtained shows that landing gear noise is the most dominant airframe noise source. The clean delta wing does not influence noise generation, whereas vertical tail contribution does not compare, since for $\theta = 90°$ its directivity function goes to zero. Ultimatly, looking at reached noise levels, it can be deduced that airframe noise due to supersonic aircraft is comparable to subsonic airframe noise, and that likely it will not be the most relevant noise source.

Airframe noise parameters	
Wing span b_w	25.6 m
Wing surface S_w	358.25 m^2
Wing span (vertical tail) b_v	11.32 m
Wing surface (vertical tail) S_v	33.91 m^2
N struct main landing-gear n_{strut_m}	2
N wheels main landing-gear n_{wheels_m}	4
Tyre diameter main landing-gear d_{tyre_m}	1.2 m
Length strut main landing-gear l_{strut_m}	2.5 m
N struct forward landing-gear n_{strut_f}	1
N wheels forward landing-gear n_{wheels_f}	2
Tyre diameter forward landing-gear d_{tyre_f}	0.787 m
Length strut forward landing-gear l_{strut_f}	3 m

Table 2.5: Airframe noise parameters for noise prediction.

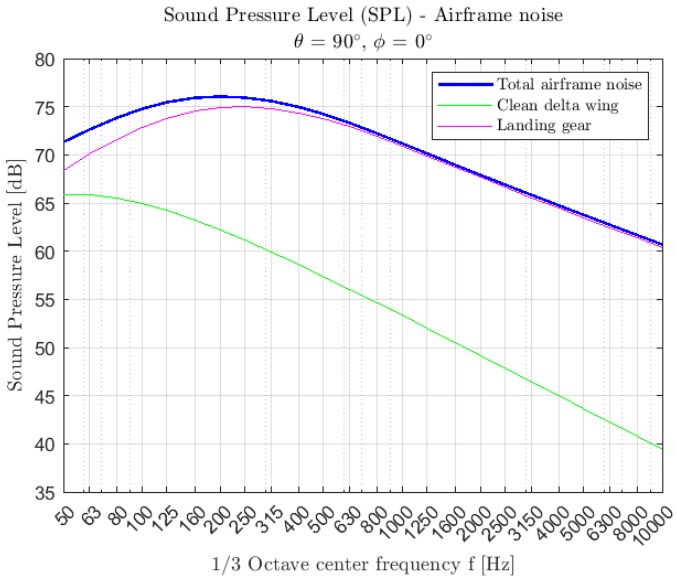

Figure 2.8: Airframe noise SPL ($\theta = 90°$,$\phi = 0°$).

Jet noise Jet mixing noise directivity function is provided in Appedix C. The parameters that affect noise generation are reported in the Table 2.6. Considering a slightly supersonic jet, the results obtained shows that when shock cells noise occurs, it is the prevalent jet noise source. The main parameters that influence jet noise generation are the exhaust jet speed V_j and the jet Mach number M_j. Hence, jet mixing noise variation versus V_j and shock cells noise variation versus M_j are reported below. It can be observed that these contributions icrease with jet exhaust speed and Mach number.

Jet noise parameters	
Number of engines N_e	4
Engine reference area A_e	1.15 m^2
Fully expanded jet area A_j	1.15 m^2
Fully expanded jet density ρ_j	1.225 kg/m^3
Jet speed V_j	500 m/s
Fully expanded jet total temprature T_j	288 K
Fully expanded jet pressure p_j	101325 Pa
Mach M_j	1.05
Angle between flight vector and engine inlet axis δ	0°

Table 2.6: Jet noise parameters for noise prediction.

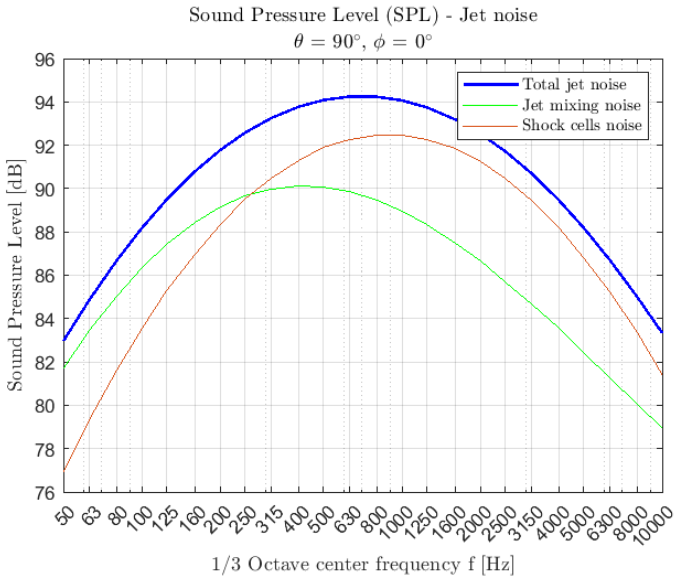

Figure 2.9: Jet noise SPL ($\theta = 90°$,$\phi = 0°$).

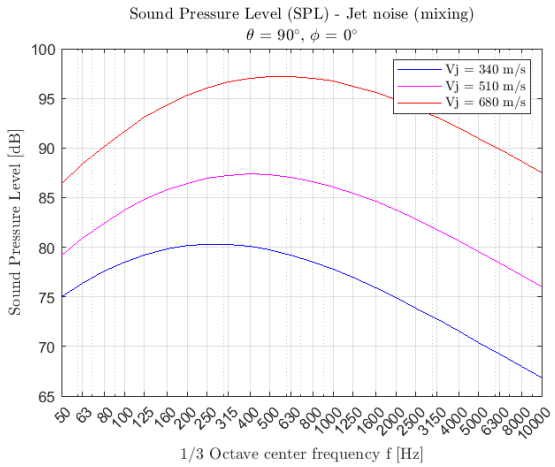

Figure 2.10: Jet mixing noise SPL versus V_j.

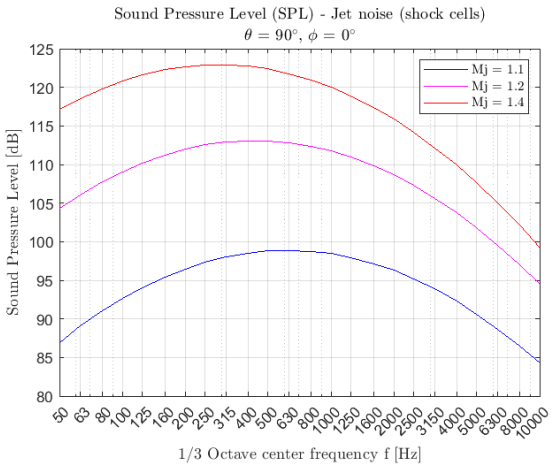

Figure 2.11: Shock cells noise SPL versus M_j.

Fan noise Fan noise directivity function are provided in Appedix C. The parameters that affect noise generation are reported in the Table 2.7. Observing the Figure 2.11, the main broadband noise contribution is the discharge noise, whereas combination tone noise causes some peaks in the SPL that depends on the blade passing prequency f_b. The main parameters that influence fan noise generation are the air mass flow $\dot{m}$, the rotational speed N and the rise of temperature across fan ΔT. Hence, fan noise variation versus $\dot{m}$, N and ΔT are reported below. It can be deduced that and increase in $\dot{m}$ and ΔT produces an increment of SPL, whereas N shifts peak values to lower frequencies, as it increase.

Fan noise parameters	
Number of engines N_e	4
Engine reference area A_e	1.15 m^2
Fan rotor diameter d_{rot}	1.21 m
Fan reference area A_{fan}	1.15 m^2
Number of stator vanes nV	32
Number of blades B	19
Mean rotor blade chord C	0.22 m
Rotor-stator spacing s	0.22 m
Fan rotor relative tip Mach number at design point M_d	1
Air mass flow $\dot{m}$	186 kg/s
Fan rotational speed N	108 Hz
Temperature rise across fan ΔT	57.6 K
Inlet guide vane index i	2
Flow distorsion index l	1

Table 2.7: Fan noise parameters for noise prediction.

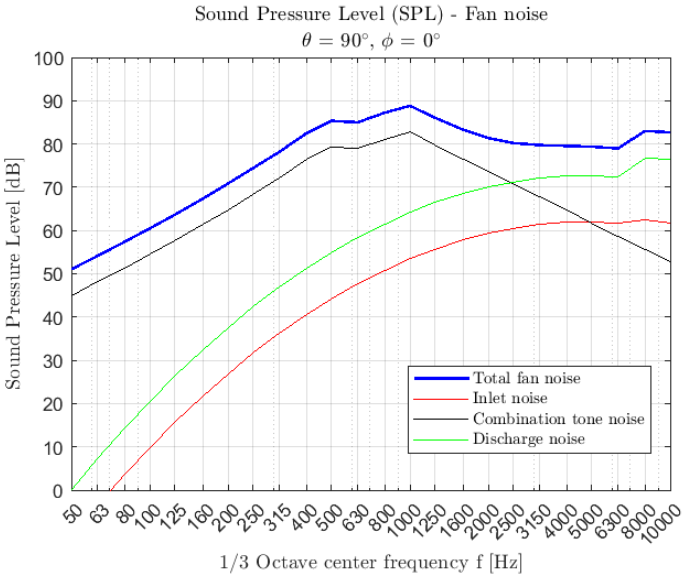

Figure 2.12: Fan noise SPL ($\theta = 90°$,$\phi = 0°$).

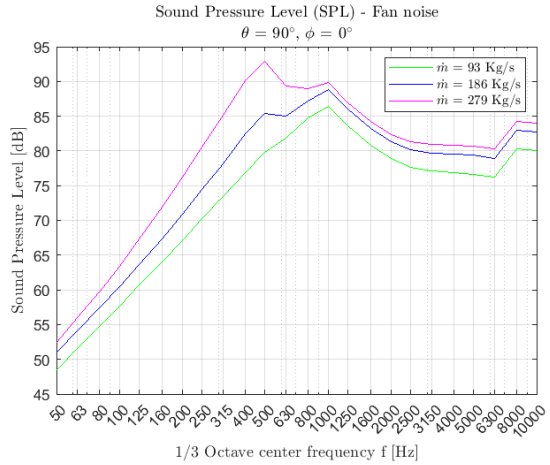

Figure 2.13: Fan noise SPL versus $\dot{m}$.

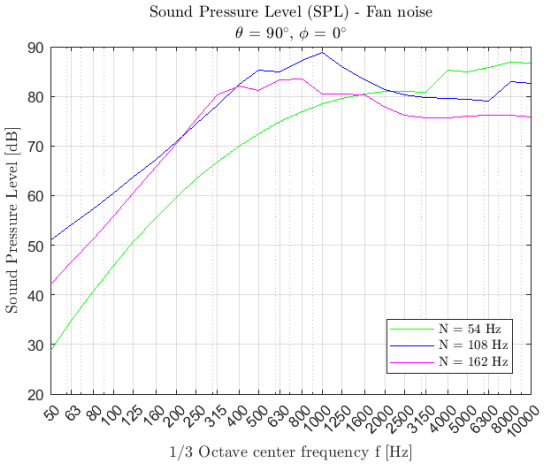

Figure 2.14: Fan noise SPL versus N.

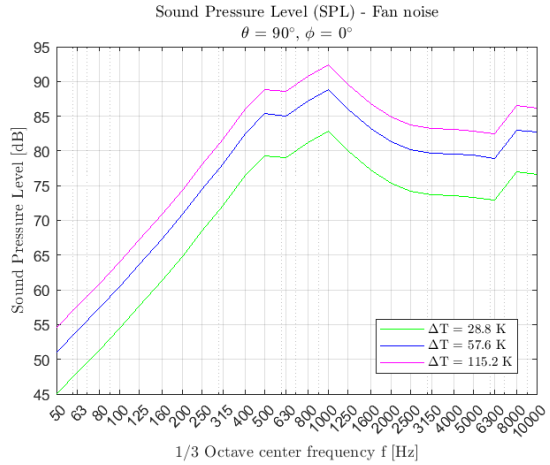

Figure 2.15: Fan noise SPL versus ΔT.

Overall noise Spetrically summing the mean-square acoutisc pressure of each component and computing the SPL, the overall aircraft noise is predicted. In the Figure 2.16 both cases for subsonic and supersonic jet are presented. Generally, airframe noise is not the lowest noise source in comparison with engine noise components. For a subsonic jet flow, jet and fan noise are comparable, whereas, as supersonic conditions occurs, the most dominant noise source is jet noise.

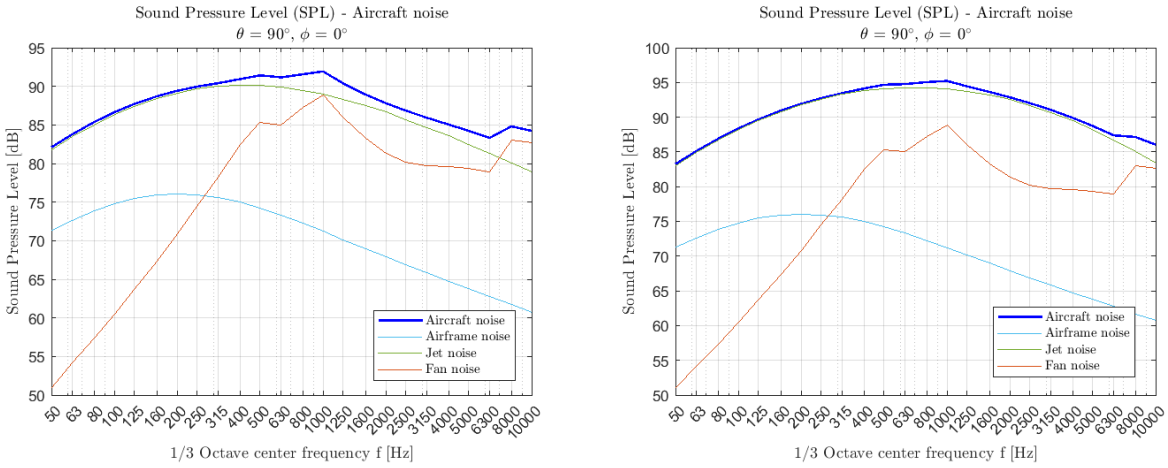

Figure 2.16: Overall aircraft noise SPL - subsonic and supersonic jet.

Chapter 3

Overall methodology

Once the noise model has been defined, it has been inegrated within the overall methodology in order to predict the ground-based noise level produced by an aircraft moving along an arbitrary flight path. Hereby, the main properties of the modules interfacing the noise model are discussed in this chapter. Despite the simple approach, the methodology includes some of the fundamental aspects for the development of a comprehensive method to predict aircraft noise level.

3.1 Framework

The overall methodology takes form from the fundamental aircraft noise prediction problem. The aircraft follows an arbitrary flight path in the presence of an observer on the ground, that in this case is represented by a microphone placed on the runaway. During this operation, noise sources on the aircraft emit radiation with defined power, directionality, and spectral distribution characteristics, all of which may depend on time. This source noise propagates through the atmosphere (being attenuated) to the vicinity of the observer. The observer receives signal from the direct ray plus a signal from a ray reflected by the local ground surface. Hereby, to develop a methodology aiming at predicting noise levels generated by an aircraft, different modules different modules are required to interface with each other. The way these modules exchange the information is described in the framework presented in Fig. 3.1.

The framework represents the modular strcuture that underlies the Matlab program built to employ the methodology. The main program calls other routines which load the input variables, perform calculations for the various aircraft modules or prepare the output. The main program ecompasses the following sequential steps:

- Definition of the coordinate reference system.
- Entering of data related to airframe/engine design, configuration and operating condition of the aircraft along the flight path.

- Selection of the desired trajectory to simulate by user (take-off, landing or simple flyover).
- Selection of the measurement point on ground where the user wants to predict aircraft noise levels.
- Computation of aircraft noise levels for each sub-components and for overall noise in terms of SPL.
- Processing of the SPL to get noise levels expressed as noise metrics used to quantify aircraft noise.

Excluding the first two steps, the others involve the calling for the routines employed to model the components needed to develop a first attempt of a comprehensive methology to predict aircraft noise levels.

The reference coordinate system is defined as represented in Fig. 3.2, where the reference point for aircraft noise prediction purposes are depicted:

- *Sideline noise measurement point*: the measurement point is along the line parallel to the axis of runaway centre line at a distance of 450 m, where the noise level is maximum during take-off. This single point refers to the lateral full-power reference noise measurement point, even though lateral noise level is typically measured considering a set of ground point along a line placed at a lateral distance of 450 m from the runaway centre line.
- *Flyover noise measurement point*: the measurement point is along the extended runaway centre line at a distance of 6500 m from the start to roll.
- *Approach noise measurement point*: the measurement point on the ground is along the extended runaway centre line at 2000 m from the threshold. This corresponds to a position 120 m vertically below the 3° descent path originating from a point 300 m beyond the threshold.
- *Approach threshold*: the beginning of approach procedure.
- *Start of take-off roll*: the beginning of take-off procedure.
- *ILS landing point and flight path*: the descent path defined for instrumental landing, with a descent angle of 3°.

Once the airspace, the aircraft and the performace along the flight path are defined, the execution of the program allows the user to set the desired trajectory, choosing between take-off, landing or flyover. Then, the simulation of the trajectory runs, calling the routines of the atmosphere and engine models. The evolution of aircraft configuration and operating paramters is continuously update and information about aircraft distance and noise sources directivity with respect to the microphones on ground are recorded with a sampling time of 0.5 s. When the simulation ends, the user is enabled

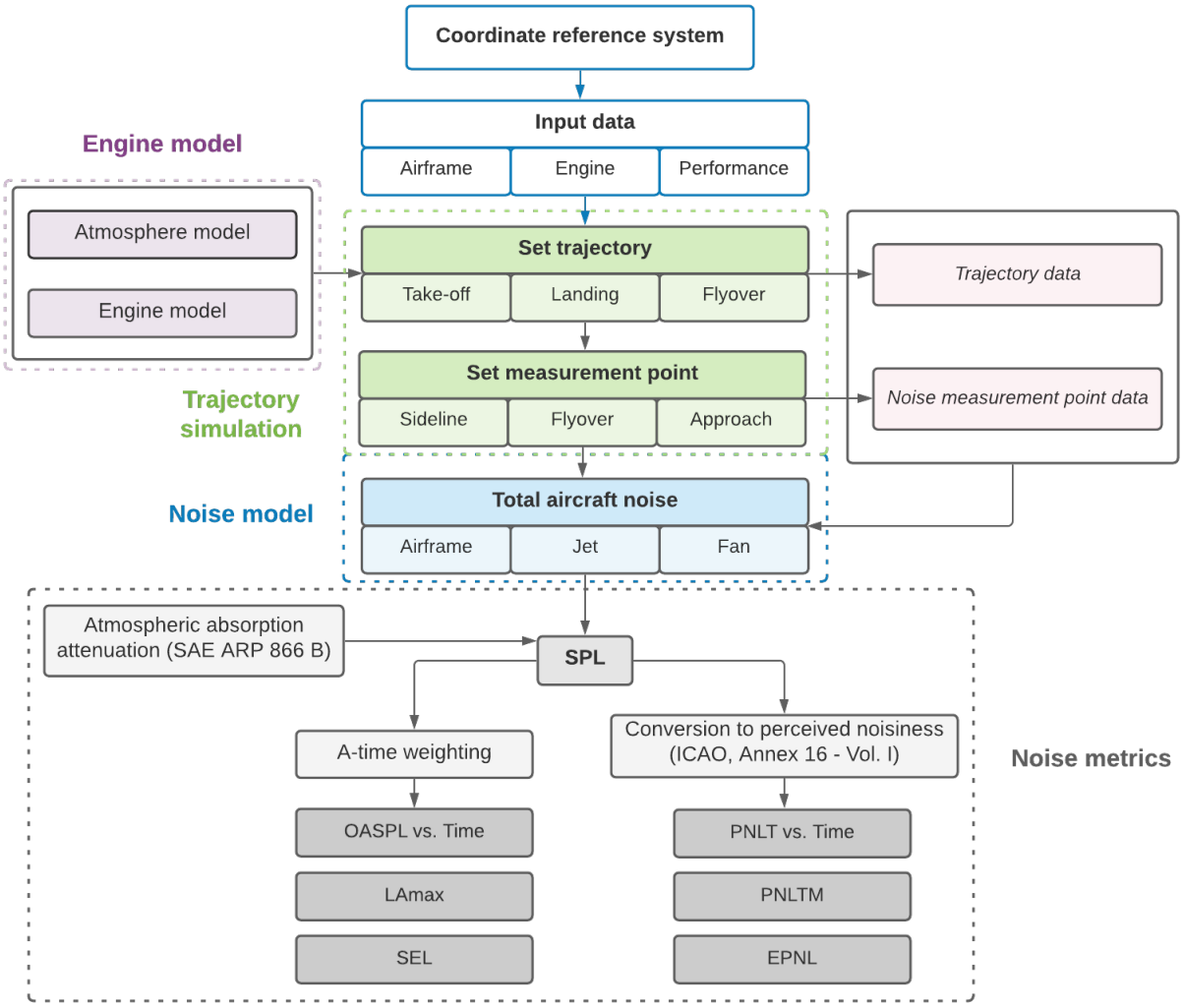

Figure 3.1: Overall methodology framework.

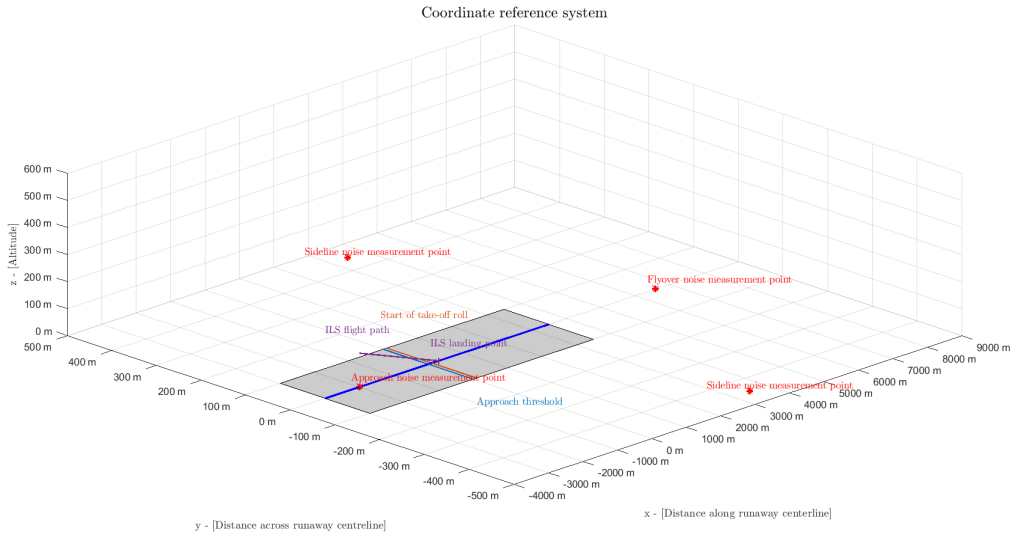

Figure 3.2: Coordinate reference system.

to extract the trajectory and the noise measurement point data. Afterwards, the rountines, employing the equations of the noise model, compute the mean-square acoustic pressure for each contribution and for overall noise for each time instant along the flight trajetory at which the microphone is turned on. Then, the mean-square acoustic pressure is converted in the SPL. Ultimatly, the SPL is concurrently processed to get the A-weighted SPL and the conversion to noisiness levels, to compute respectively the OASPL in dBA and the PNL in PNdB over the selected time interval for noise measurement. In this way, the LA_{max}, SEL, PNLTM and EPNL are given as output of the program.

3.2 Engine model

Engine noise prediction requires specific information about geometry and operational conditions, so an engine model is needed. Accordingly to the selected case study described in the paragraph 4.1, a two-spool turbojet engine with afterburner has been modelled taking as a reference the Olympus 593 MRK 610 (Fig. 3.3) data. Obviously, the type of the engine and the exhasut system affect the noise prediction, thus changing the case study requires modelling the specific engine under consideration. Furthermore, the equations implemented for the engine modelling must be thought as functional to the evaluation of the parameters of interest for noise asssessment at a conceptual design level. To verify that such a model can also be suitable for off-design studies and performance analysis is beyond the scope of this work.

The undertaken approach attaining a sufficiently reliable engine model comprises the on-design and off-design studies of engine core and the definition of the engine exhaust system. On design and off design conditions have been simulated on the basis

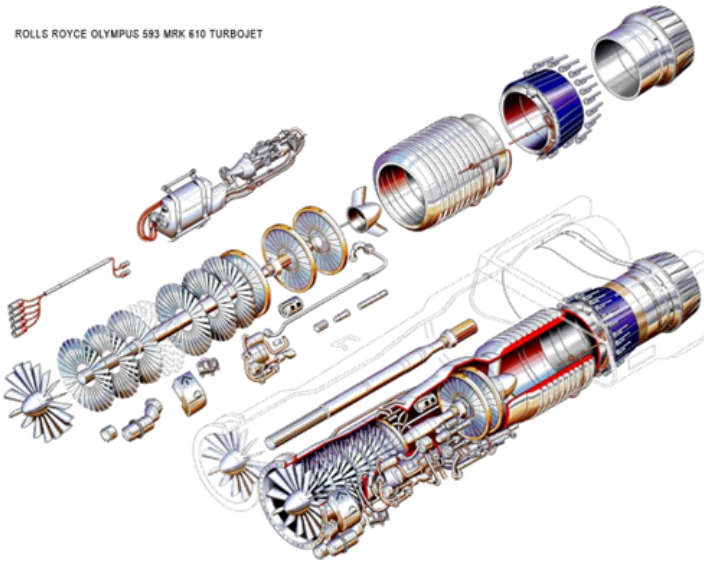

Figure 3.3: Rolls Royce Olympus 593 MRK 610.

of [41], a work that deals with the development and the employment of numerical simulation technique of stationary and transitional benefits of turbo engines.

Firstly, the engine has been defined without the afterburner, considering the on-design conditions in the Table 3.1.

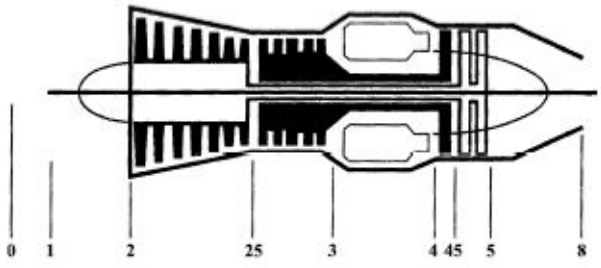

Figure 3.4: Engine station designation for a two-spool turbojet

The engine stations (Fig. 3.4) are listed below:

- Station 0: Area ahead of the inlet, where the airflow undisturbed.
- Station 1: Inlet diffuser.
- Station 2: Exit inlet diffuser, inlet low pressure compressor.
- Station 25: Exit low pressure compressor, inlet high pressure compressor.

- Station 3: Exit high pressure compressor, inlet combustor.
- Station 4: Exit combustor, inlet high pressure turbine.
- Station 45: Exit high pressure turbine, inlet low pressure turbine.
- Station 5: Exit low pressure turbine, nozzle duct.
- Station 8: Nozzle throat.
- Station 9: Exhaust nozzle.

On design

Flight conditions		
Mach	M_0	0.7
Altitude $[m]$	h	9936.48
Specific heat capacity (air) $[J/(KgK)]$	c_p	1004
Ideal gas constant (air) $[J/(KgK)]$	R	287
Intake		
Air mass flow $[Kg/s]$	$\dot{m}$	186
Ram efficiency	ϵ_d	0.98
Low pressure compressor		
Low compressor ratio	β_{cL}	3.237
Mechanical efficiency	η_{mcL}	1
Adiabatic efficiency	η_{cL}	0.87
High pressure compressor		
High compressor ratio	β_{cH}	4.788
Mechanical efficiency	η_{mcH}	1
Adiabatic efficiency	η_{cH}	0.87

Combustor		
Combusted gases specific heat $[J/(KgK)]$	$c_p^{'}$	1184
Combusted gases ideal constant $[J/(KgK)]$	$R^{'}$	293.77
Heat of reaction $[MJ/Kg]$	H_i	43.031
Combustor efficiency	η_b	0.98
Combustor pressure losses	ϵ_b	1
Turbine inlet temperature K	T_{4t}	1012.15
High pressure turbine		
Mechanical efficiency	η_{mtH}	0.95
Adiabatic efficiency	η_{tH}	0.93
Low pressure turbine		
Mechanical efficiency	η_{mtL}	0.95
Adiabatic efficiency	η_{tL}	0.93
Other parameters		
Rotational speed (low pressure spool) $[rpm]$	N_L	6500
Rotational speed (high pressure spool) $[rpm]$	N_H	8530

Table 3.1: On design condition - parameters definition. [41]

The on-design study has been conducted solving the engine cycle in a conventional way, whereas the off-design has been analyzed using the results reported in [41], obtained from the numerical resolution of the equilibrium equations of the engine varying the throttle, using the Newton-Raphson method. Precisely, the throttle has been defined as:

$$\tau = \frac{T_{4t}}{T_{4t}^*} \tag{3.1}$$

Where T_{4t}^* is the turbine inlet temperature on design. The throttle τ is assumed to vary from 1 to 0.5, that corresponds to the IDLE condition, where the thrust is:

$$S_{IDLE} = 0.05 S_{max} = 0.05 S^* = 4642.09N \tag{3.2}$$

The variations of β_{cH} β_{cL}, $\dot{m}$ and N_L with the throttle τ are reported in Fig. 3.5.

The data have been extrapolated from the maps using Get Data Analyzer and have been inserted in the routine implementing the engine model. In this way, once the throttle τ corresponding to the selected thrust has been set, the engine cycle is solved for a two-spool turbojet, updating the flight conditions at each point of the considered trajectory.

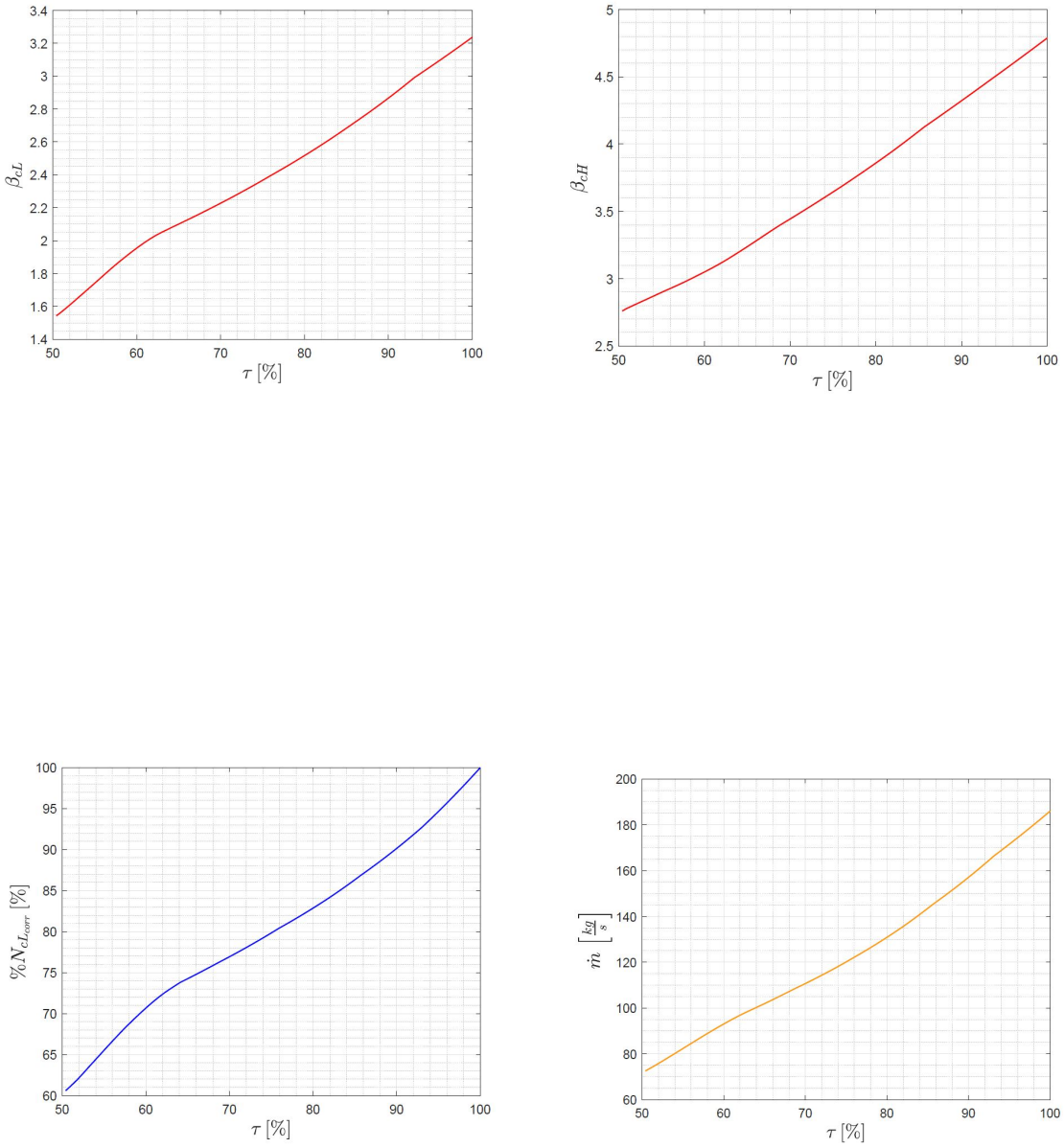

Figure 3.5: Engine parameters versus throttle τ at equilibrium.[41]

The afterburner has been modelled by the addition of another component after the low pressure turbine, that gives in exit a flow reaching a total temperature of 1700 K, considering an afterburner efficiency of 0.9. Precisely, since no data are available about aftererburners mounted on SST aircraft, the value of the afterburner exit total temperature has been selected from the General Electric J85, a one-spool turbojet eith afterburner [41]. At least, an exhaust system aiming at predicting the exhaust jet parameters as a function of thrust has been modelled. The Olympus 593 was equipped with an exhaust assembly comprises of a variable exhaust with a primary nozzle and a secondary nozzle. The primary nozzle sits at the end of the jet-pipe, and is a ring of petals operating in unison to vary the diameter, and therefore then the area of the jet pipe exit. The secondary nozzle assembly surrounds the primary nozzle; it was an arrangement of hinged *buckets*, whose position can be varied to control the exhaust in the most efficient way during all stages of flight Fig. 3.6. Together they make up another form of convergent/divergent duct.

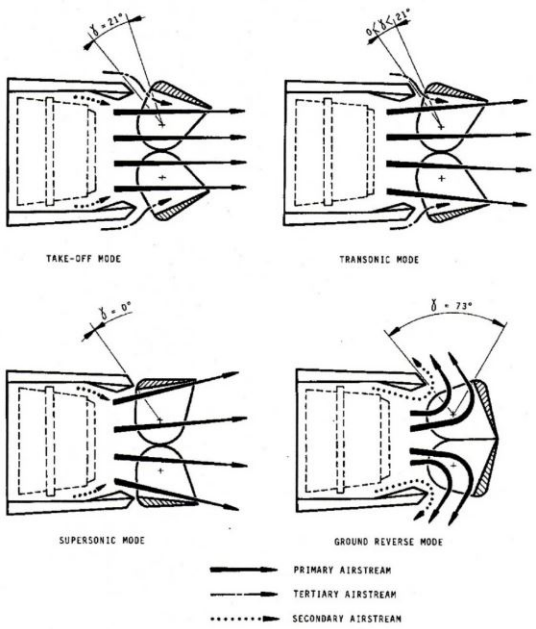

Figure 3.6: Modulation of twin secondary nozzle exhaust area.

For the applications of this work, the nozzle has been considered as a convergent nozzle with variable area, whereas the exhaust system has been assumed to be a divergent ejector nozzle, with an exhaust area (equal to fully expanded jet area) that is the 20 % larger than the throath area. Precisely, the ratio of the exit and throat area has been found in [42], between a range of typical values. Finally, the hypothesis made are:

- Isentropic and adiabatic flow, since no shock waves occur within the convergent/divergent duct.

- Critic condition at throat section ($M_t = 1$).
- The area ratio $\frac{A_e}{A_t}$ is fixed to 1.2.

The equations used are for nozzle inlet section:

$$\begin{cases} p_5^0 = \epsilon_n p_{45}^0 & \text{Nozzle inlet total pressure} \\ T_5^0 = T_{45}^0 & \text{Nozzle inlet total temperature} \end{cases} \tag{3.3}$$

At nozzle throat, as critic condition occurs:

$$\begin{cases} p_8 = \frac{p_5^0}{(\frac{\gamma'+1}{2})^{\frac{\gamma'}{\gamma'-1}}} & \text{Nozzle throat static pressure} \\ T_8 = \frac{T_5^0}{(\frac{\gamma'+1}{2})} & \text{Nozzle throat static temperature} \\ \rho_8 = \frac{p_8}{R' T_8} & \text{Nozzle throat static density} \end{cases} \tag{3.4}$$

Lastly, the exhaust jet parameters are computed as:

$$\begin{cases} p_j = \frac{p_5^0}{NPR} & \text{Exhaust jet static pressure} \\ T_j^0 = T_5^0 & \text{Exhaust jet total temperature (Adiabatic nozzle)} \\ M_j = \sqrt{\frac{2}{\gamma'-1}(NPR^{\frac{\gamma'-1}{\gamma'}} - 1)} & \text{Exhaust jet Mach number (Isentropic nozzle)} \\ V_j = \frac{1}{1+f}[u + (\frac{T - A_e(p_j - p_{amb})}{\dot{m}})] & \text{Exhaust jet speed} \\ a_j = \frac{V_j}{M_j} & \text{Exhaust jet speed of sound} \\ T_j = \frac{a_j^2}{\gamma' R'} & \text{Exhaust jet static temperature} \\ \rho_j = \frac{p_j}{R' T_j} & \text{Exhaust jet static density} \end{cases} \tag{3.5}$$

Where NPR is the Nozzle Pressure Ratio, that is the ratio of the nozzle total to static pressure, u is the aircraft speed and T is the thrust. If the afterburner is turned on, the throat area icreases to prevent the choking of the duct. The new area is computed in the following way:

$$A_{8,ab} = \frac{\dot{m}_{ab}}{\rho_{8,ab} a_{8,ab}} \tag{3.6}$$

Where $\dot{m}_{ab}$ is the sum of air and fuel mass flow, $\rho_{t,ab}$ is the density at the throat and $a_{t,ab}$ is the flow speed at the throat. These values take into account the increase of total temperature due to the afterburner:

$$\begin{cases} p_{8,ab} = \dfrac{p^0_{5,ab}}{(\frac{\gamma'+1}{2})^{\frac{\gamma'}{\gamma'-1}}} & \text{Nozzle throat static pressure} \\ T_{8,ab} = \dfrac{T^0_{5,ab}}{(\frac{\gamma'+1}{2})} & \text{Nozzle throat static temperature} \\ \rho_{8,ab} = \dfrac{p_{8,ab}}{R' T_{8,ab}} & \text{Nozzle throat static density} \\ \rho_{8,ab} = \dfrac{p_{8,ab}}{R' T_{8,ab}} & \text{Nozzle throat static density} \end{cases} \tag{3.7}$$

Where:

$$\begin{cases} p^0_{5,ab} = \epsilon_{ab} p^0_{45,ab} & \text{Afterburner exit total pressure} \\ T^0_{5,ab} = 1700K & \text{Afterburner exit total temperature} \end{cases} \tag{3.8}$$

Where ϵ_{ab} is equal to 0.9 and indicates the afterburner pressure losses.

3.3 Trajectory simulation

Usually, to predict ground noise immission along a flight path, the corresponding trajectory is assembled from straight flight segments with constant operational and configurational setting. Accordingly to this approach, the take-off and landing trajectory has been simulated as a flight path composed respectively by 5 and 3 flight segment constructed from fixed point data defining constant speed, thrust and altitude. However, an update of speed and thrust has been included, in order to gain a more accurate prediction of noise levels. Then, during the aircraft overflight, the measurement data are detected for a given interval of time at the three certification measurement points defined by ICAO. In the Figure Fig. 3.7 the input and the output of the routines implemented to simulate the LTO trajectories are reported.

Once the operational procedure data have been set and engine data have been defined, the routine updates aircraft position and performance data, including the computation of ambient conditions considering the standard atmosphere model. The outuput comprises of flight conditions, noise measurement point data for each noise measurement point, jet noise and fan noise data. These information are known for each point of the flight path and when the user select the point where he wants to predict aircraft noise level, the program extracts ambient conditions and noise measurement data relative to that point.

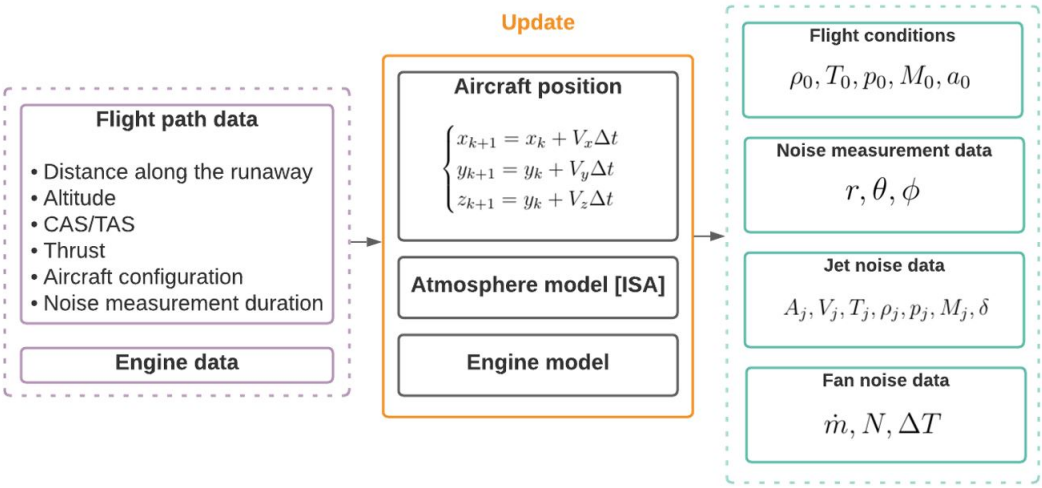

Figure 3.7

3.4 Noise metrics

Sound is the result of a sound source inducing vibration in the air. The movement of the particles causes fluctuations in the normal atmospheric pressure, that produces sound waves. These waves radiate in all directions from the source and may be reflected and scattered or may turn corners. When the source stops vibrating, the sound waves disappear almost instantaneously, and the sound ceases. This physical phenomena may be described in terms of frequency, amplitude and time pattern.

The rate at which a sound source vibrates, or makes the air vibrate, determines frequency, that is measured in Hz. In real-life situations, it is rare to found a sound characterized by a single frequency (a pure tone). Most of the sounds consist instead of a complex mixture of many frequencies. The frequency content of these sounds is characterized by a band of frequencies, usually an octave or 1/3 octave in width. Sound pressure is the amplitude or measure of the difference between atmospheric pressure (with no sound present) and the total pressure (with sound present) and its unit is the dB, that is expressed in a logarithmic scale, as in this way it is possible to encompass all the wide range of sound intensities. Such aspect means that the sound pressure levels of two separate sounds are not directly arithmetically additive. For example, if a sound is added to another sound of equal intensity, the total is only a 3 decibel increase or if the added sound is less to the higher of 10 dB or more, it does not affect the higher level.Lastly, the time pattern describes the temporal nature of the sound production, and it may be continuous, intermittent, impulsive or fluctuating.

Acoustic noise is classified as an unwanted sound considered unpleasant, loud or disruptive which is audible to the human ear. Such a particular sound can be quantify by a noise metric, that is an expression used to describe any measure of quantity of

noise at a receiver position. To assess the loudness or the annoyance of aircraft noise on human hearing system, a number of noise metrics are in using among different aviation organization, countries and airports [43]. However, aircraft noise metrics can be classified into three groups of measurement types [44]:

- *Single event (or instantaneous) metrics*: measurements taken to describe the noise occurring during one noise event, accounting only for sound amplitude. It is typically expressed as the maximum sound level reached during the event.
- *Exposure (or intergral) metrics*: used to provide a description of the type of noise exposure experienced over a given period of time. It is computed as a integral over a defined time interval.
- *Supplementary metrics*: measurements often used in conjunction with the above, to provide a more meaningful depiction of the potential impact of noise exposure.

The loudness of a noise emission is directly linked to the quantity of energy transferred throught the air causing changes in air pressure. The more energy put into making a sound, the louder it will be. Hence, the different noise metrics rely on different methods to evaluate the energy of a noise event, as previously described.

Aircarft noise metrics commonly in using are typically single event and exposure metrics. The instantaneous sound level metric can be frequency weighted or computed. The weighted sound level results from the correction of SPL, modified to de-emphasize the low frequency portion of sounds to approximate the human ear's response to sound. Once the frequency weighted Overall Sound Pressure Level (OASPL) evolution is known over a certain period of time, the instantaneous sound level corresponds to the maximum sound level recorded. There are several weightings (A, B, C, D) found on a sound level meter, but A-weighting is the most widely used by federal, state, and local agencies for environmental noise analyses to approximate the relative noisiness or annoyance of many commonly occurring steady state or intermittent sound. The noise metric associated with this A-weighted SPL is indicated as LA_{max} and is measured in dBA. Its graphical representation is given in Fig. 3.8.

The computed instantaneous noise metric used to measure aircraft noise is the Perceived Noise Level (PNL), that is a rating of the noisiness of a sound calculated from acoustic measurements. It is computed from sound pressure levels typically measured in one-third octave frequency bands and it is expressed in terms of PNdB. The PNL of a given sound is intended to be numerically equal to the level of an octave band of noise centered at 1000 Hz, which is judged equally noisy to the given sound [53]. The noise level associated with this metric is the Maximum Tone Corrected Percedived Noise Level PNLTM. The procedure used to derive the PNLTM from experimental measurements is standardized by ICAO in [12], and involves spectral analysis, with the conversion of SPL in noisiness levels by means of the correspondence with noy tables associated with each value of SPL for a given frequency and correction for spectral irregularities. Having the Tone Corrected Perceived Noise Level (PNLT) time evolution, the PNLTM is computed in the same manner as the LA_{max}, identifying the maximum sound level recorded.

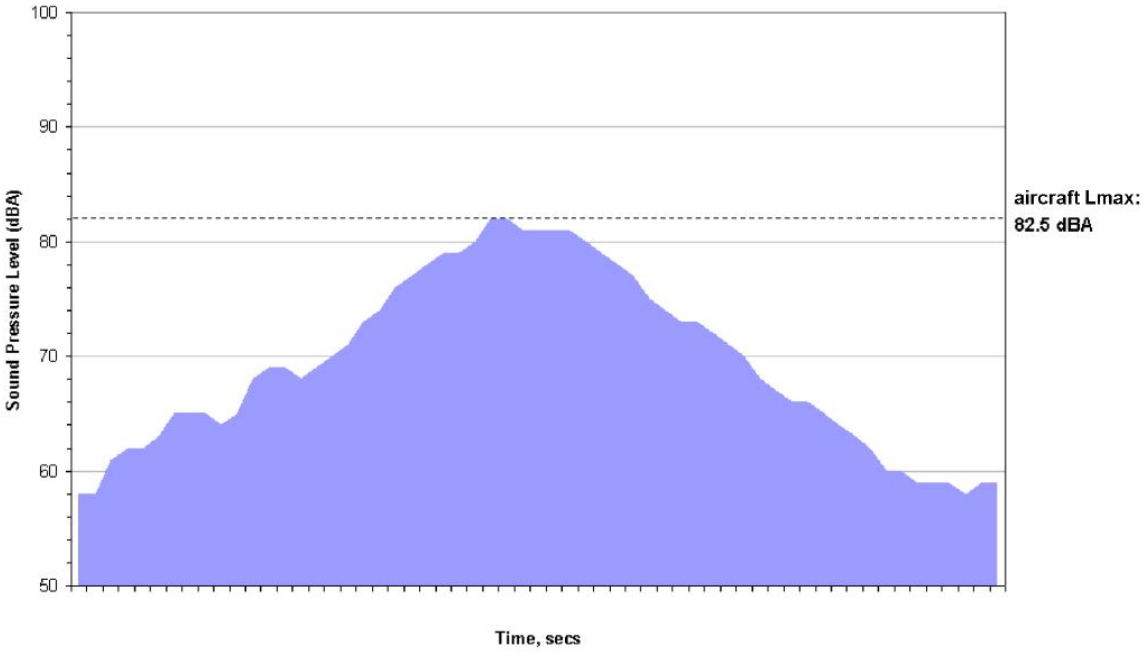

Figure 3.8: Graphical representation of LA_{max}. [44]

The integral noise metrics are duration corrected single event metrics. Hence, Sound Exposure Level (SEL) is energy averaged A-weighted sound level over a specified period of time or single event, with a reference duration of 1 second. On the other hand, Effective Perceived Noise Level (EPNL) consists of an integration over the noise duration of the PNLT, normalized to a reference duration of 10 s and measured in EPNdB. Both of these integral metrics require the definition of the time interval for integration, which is identify by the first and the last instant of time (kF and kL) when the sound level is 10 dBA or PNdB respectively lower than the maximum level. Graphical representation for SEL is presented in Fig. 3.9.

All the described metrics are used for aircraft noise certification. Precisely, LA_{max} and SEL are considered as loudness-based metrics, whereas PNLTM and EPNL are annoyance-based. It is also possible to find some approximated relationships bewteen both instantaneous and integral noise metrics. Altough the different ways of processing the frequency distribution of energy, in practice there is a fairly high correlation between the LA_{max} and PNLTM measures, that is $PNLTM \simeq LA_{max} + 13$. However the exact correction figure depends on factors such as aircraft type, operational characteristics, meteorological conditions and the distance from the aircraft flight path [44]. For exposure noise metrics, the rationale for normalising EPNL to 10 seconds is to penalise those aircraft that make a lot of noise for a relatively long time. As a consequence, the EPNL imparts greater subjective emphasis to energy at frequencies above 1 kHz and applies a tone correction, or 'penalty', in proportion to the protrusion of any discrete frequencies above the adjacent 1/3 octave band levels, whith resepct to

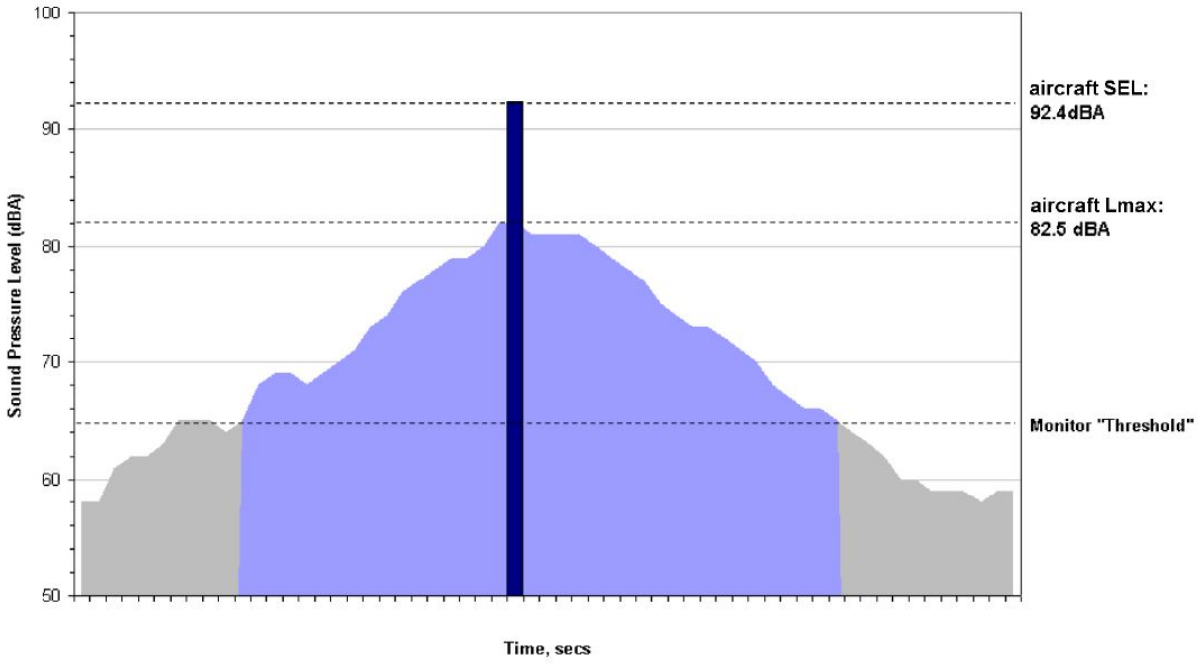

Figure 3.9: Graphical representation of SEL. [44]

SEL. Such tone correction in EPNL was originally introduced because early jet aircraft engines generated extremely high (and therefore annoying) fan and turbine tone levels. SEL were not thought to fully reflect these annoying tone levels. However, for modern engines, the corrections tend to be zero or small so that, although EPNL values remain numerically larger (about 3 or 5 dB) than SEL, the differences are fairly consistent across a wide range of current aircraft types [44].

Whitin the developed methodology, all the cited noise metrics have been computed from the SPL given in output by the routines dedicated to the noise source modelling. The procedure adopted is schematized in the diagram presented in Fig. 3.10.

First of all, it is needed to consider the attenuation of sound due to atmospheric absorption, since the distances between the noise source and the observer considered under the scope of this thesis are such that sound attenuation in the atmosphere is not a negligible phenomena. When a noise source emits sound waves, the observer on ground, placed at a certain distance from the source, receives a sound being attenuated for a number of factors which influence the propagation of noise. However, temperature and humidity are the parameters causing major reduction in sound as distance increasing. To determine the entity of these lossess, the mathematical procedure suggested in SAE ARP 866 B [54] has been adopted. The SARP considers only the classical and molecular absorption of sound energy by the atmosphere. The classical absorption results from energy dissipation through the effects of heat conduction and viscosity and is a function of frequency and temperature, whereas molecular absorption results principally from

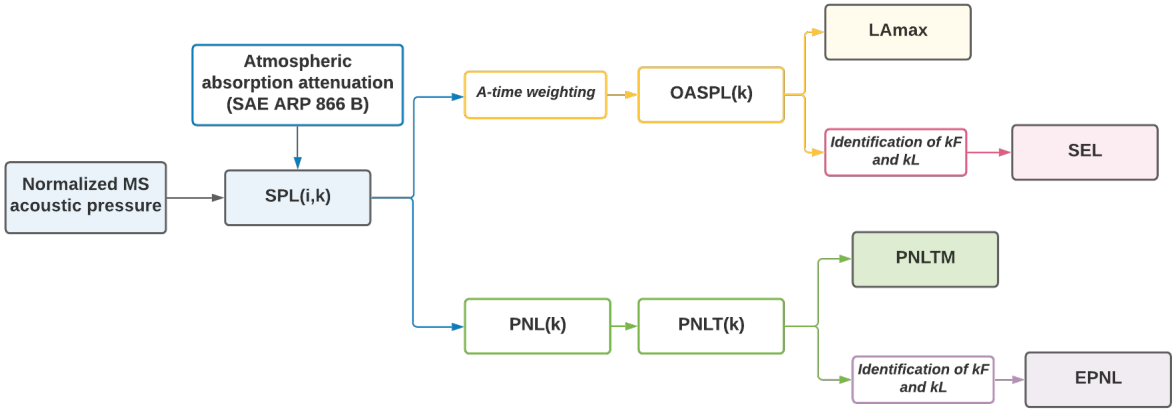

Figure 3.10: Procedure adopted in the overall methodology to compute noise metrics.

rotational and vibrational relaxion process of oxygen and nitrogen molecules and is a function of frequency, temperature and humidity. In particular, classical absorption is important only at higer frequencies and varies slightly with temperature; molecular absorption is the main contribution to sound attenuation, varying on a wide range of values, producing an higher sound reduction at highest frequencies. The SAE ARP 866 B reports a seven-step procedure that leads to the total atmospheric absorption coefficients as a sum of classical absorption component and a molecular absorption component. The total loss is expressed as the attenuation in db/100 m and is a function of frequency, temperature and relative humidity, defined as the amount of water vapour present in air expressed as a percentage of the amount needed for saturation at same air temperature. As a result, summing algebrically the lossess for each centre frequency in 1/3 octave band of the spcectrum, the SPL receveid on ground is obtained.

This SPL is a function of frequency and time. Another step is required before the calculation of the noise metrics. To get the LA_{max} and SEL, A-weighting of the frequency spectrum is needed. The new SPL is computed summing algebrically tabulated coefficients that de-emphasize the low frequency portion of sounds for each 1/3 octave centre frequency. Once the A-weighted SPL is given, it is possible to compute the OASPL, that is just a function of time, with the following formula:

$$OASPL(k) = 10log_{10} \sum_{i=1}^{24} 10^{(SPL_A(i,k)/10)} \tag{3.9}$$

Where i indicates the 1/3 frequency band considered between 50 Hz and 10000 Hz. Computing the OASPL for each time-instant k, the sound pressure level time evolution is known. Hence, the LA_{max} is simply obtained as:

$$LA_{max} = max(OASPL(k)) \tag{3.10}$$

The OASPL is defined over a certian time intervall with a sampling time of 0.5 s.

In order to obtain the information about the time instant kF and kL, when the sound level reaches the value $LA_{max} - 10$ dBA, the OASPL is interpolated and then kF and kL are determined with a tolerance of 0.1 dBA. At least, the SEL is computed as:

$$SEL = 10log_{10} \sum_{k=kF}^{kL} 10^{(OASPL(k)/10)} \tag{3.11}$$

The calculation of PNLTM and EPNL is quite similiar to the one just exposed. Firstly, PNL(k) is calculated from instantaneous 1/3 octave band sound levels, SPL(i,k), accordingly to the procedure described in [12]. Precisely, three steps have to be performed:

- Conversion of each 1/3 octave band SPL(i,k) from 50 to 10000 Hz to perceived noisiness n(i,k).
- Combine the perceived noisiness values n(i,k) in the following formula:

$$N(k) = 0.85n(k) + 0.15 \sum_{i=1}^{24} n(i,k) \tag{3.12}$$

  Where n(k) is the largest of the 24 values of n(i,k) and N(k) is the total perceived noisiness.

- Convert the total perceived noisiness, N(k), into PNL(k), by the following formula:

$$PNL(k) = 40 + \frac{10}{log_{10}2} log_{10} N(k) \tag{3.13}$$

After that, spectral irregularities are adjusted by the correction factor C(k), calculted on the basis of the evaluation of the slopes in SPL spectrum. Finally, the PNLT is computed as:

$$PNLT(k) = PNL(k) + C(k) \tag{3.14}$$

Therefore, the PNLTM is defined as:

$$PNLTM = max(PNLT(k)) \tag{3.15}$$

Once the time instant kF and kL are determined, the EPNL can be calculated considering a sampling time of 0.5 s and a reference noise duration of 10 s:

$$EPNL = 10log_{10} \sum_{k=kF}^{kL} 10^{(PNLT(k)/10)} - 13 \tag{3.16}$$

Where 13 dB is a constant relating the one-half second values of PNLT(k) to the 10 s reference duration.

Chapter 4

Validation

After a description of the selected case study and the reference database, the Chapter provides the results derived from the matching between the experimental NPD curves and the predicted NPD curves. Thus, the accuracy of the developed methodology in predicting the overall aircraft noise level has been estimated for flyover trajectories at different altitudes and thrust ratings.

4.1 Case study

Concorde was a supersonic civil transport category aircraft capable of carrying aproximatly 100 to 125 passengers over extended routes at a cruising speed that is 2.5 times greater than that of subsonic aircraft.

Although the intention of this work is turned towards the next generation of SST aircraft, it is conceivable to assume the Concorde design as an initial reference, as it includes the main characteristics of an SST aircraft (Fig. 4.1).

Concorde has an ogival delta planform wing, with thickness/chord ratio 3% at root, 2.15% from nacelle outboard. Longitudinal and lateral control was provided through three elevons on trailing-edge of each wing, of aluminium alloy honeycomb construction. Each elevon is independently operated by a tandem jack, each half supplied from an independent hydraulic source and controlled by a separate electrical system; there were not higli-lift devices, while leading-edges ahead of air intakes are electrically de-iced. Directional control was provide through vertical fin and rudder only; two-section alluminium rudder controlled in same way as elevons. Another typical feature of the Concorde was the droop nose: precisely, nose was drooped hydraulically to improve forward view during take-off, initial climb, approach and landing. Retractable visor was raised hydraulically to fair in windscreen in cruising flight. Landing gear was hydraulically-retractable tricycle type; twin-wheel steerable nose unit retracts forward and our-wheel bogie main units retract inward. It was provided with oleo-pneumatic shock-absorbers and retractable tail bumper. About the powerplant, Concorde was a four-jet supersonic transport. The engine was the Rolls-Royce/Snecma Olympus 593, a two-spool turbojet with afterburner, initially designed for military aircraft and

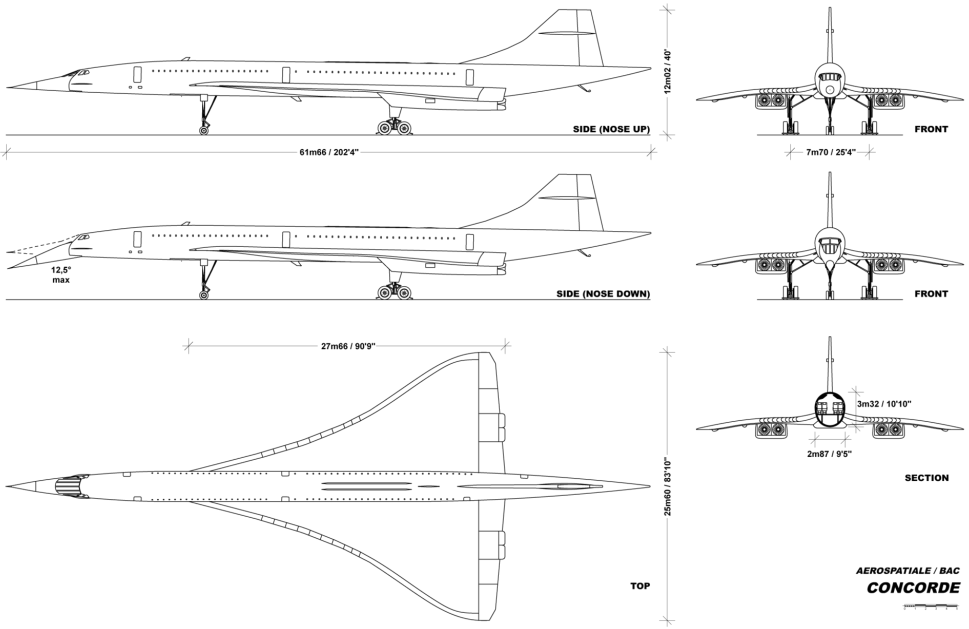

Figure 4.1: Concorde views.

later adapted for civil applications. Each engine consisted of hydraulically controlled variable-area (by ramp) air intake, engine bay and nozzle support structure. Fuel system was used also as heat sink and to maintain aircraft trim. Indeed, all tanks were of integral construction and were in two groups, with total usable capacity of about 117285 litres. In particular, main group included five tanks in each wing and four tanks in fuselage and maintains CG automatically in cruising flight, maintaining correct relationship between CG and aerodynamic centre of pressure by transferring fuel rearward during acceleration and forward during return to subsonic flight.

Finally, another peculiarity of the Concorde and in general of the SST aircrafts is the mission profile. Concorde flew on fixed and dedicated east-west ocean routes over the North Atlantic Ocean. These routes and the relative heights were defined in such a way as to avoid interference with subsonic air traffic. The cruising altitude is between FL500 and FL600, as at that altitude changes in weather conditions have such a low influence that no change of route is necessary. The take-off took place with the afterburner on in order to reach the speed required for rotation and lift off. The afterburner was also used to reach the supersonic phase of the cruise. During the flight phases over continental areas supersonic flight was not allowed for aero-acoustic reasons, so the aircraft was forced to maintain a Mach of 0.93-0.95. Until supersonic flight was allowed, the Concorde was forced to maintain a constant flight altitude; for example, New York Air Control directed the aircraft toward the ocean at an altitude of FL300 before authorizing acceleration to cruising speed. The phases of ascent and acceleration from subsonic to supersonic were the most critical from the point of view of the aircraft wall temperature. Given the criticality of the acceleration phase, the

Concorde needed a free corridor from the point where the afterburners were turned on to the point where they were turned off (phase no longer than 15 minutes). The fact that the cruising altitude is defined between FL500 and FL600 is due to the fact that the aircraft was on a parabolic trajectory and not at a fixed altitude to minimize skin temperatures. When the temperature reached 127 °C the autopilot performed a temperature-dependent trajectory and no longer Mach-dependent. The descent phase, in analogy to the climb phase, starts with a supersonic descent to FL410, until the subsonic transition, another critical phase that can generate shock waves, therefore it must not take place near populated areas. The choice of FL410 is given by the fact of not wanting to have excessive losses in terms of performance and fuel consumption. When landing, once the touchdown has been made, the minimum runway length had to be 1830 m [49].

In the Tables A.2, 4.2, 4.3, 4.4 and 4.5 are listed the reference data collected from [47] and [48]. The data refer to the initial production version Concorde Series 200, of which the first two examples were flown on 6 December 1973 at Toulouse (F-WTSB) and 13 February 1974 at Filton (G-BBDG).

In conclusion, the Concorde and SST aircraft feautures that affect LTO noise generation are:

- For the airframe noise: the wing planform, the control surfaces and the landing gear. In particular, due to a limited effectiveness of the horizontal tail plane, the architecture with elevons is preferred for controlling supersonic aircrafts, which will be devoid of the horizontal tail plane. On the other hand, the landing gear typically has a tricycle architecture with longer legs than those of supersonic aircraft, to allow take off at high angles of attack. Precisely for the latter reason, the Concorde has not the secondary control surfaces, which would therefore have been aerodianamically inefficient.

- For the engine noise: the type of engine and its operational parameters. Typically today supersonic aircrafts are propelled with turbofan engines with afterburner. Such a powerplant manly contributes to the noise generation during take-off and is the reason why the noise level of a supersonic aircraft is greater with respect to subsonic one.

Airframe		
Delta wing	Wing span b_w $[m]$	25.56
	Surface S_w $[m^2]$	358.25
	Aspect Ratio AR	1.7
	Root chord c_r $[m]$	27.66
	Sweep angle Λ $[°]$	55
	Elevons area S_{elev} $[m^2]$	32
Vertical tail	Height b_v $[m]$	11.32
	Surface S_v $[m^2]$	33.91
	Root chord c_v $[m]$	10.59
	Rudder area S_{rudd} $[m^2]$	10.40
Landing gear	N structure (main)	2
	N wheels (main)	4
	Tyre diameter (main) d_{tyre_m} $[m]$	1.2
	Structure length (main) l_{struct_m} $[m]$	2.5
	N structure (forward)	1
	N wheels (forward)	2
	Tyre diameter (forward) d_{tyre_f} $[m]$	0.787
	Structure length (forward) l_{struct_f} $[m]$	3
Fuselage	Length (overall) l_f $[m]$	61.66
	Width (max) d_{max} $[m]$	2.88
	Heigt (max) h_{max} $[m]$	3.32

Table 4.1: Concorde reference airframe data

Engine		
General characteristics	Number	4
	Type	Turbojet (Rolls-Royce/Snecma Olympus 593)
	Length l_{eng} $[m]$	4.039
	Diameter d_{eng} $[m]$	1.212
Components	Compressor	Axial-flow (7 stages high-pressure, 7 stages low-pressure)
	Combustors	Nickel alloy construction annular chamber
	Turbine	2 stages (1 stage high-pressure, 1 stage low-pressure)
	Fuel type	Jet A-1
Performance	Max Thrust $[kN]$	wet: 169.2, dry: 139.4
	Overall pressure ratio	15.5
	Air mass flow $[Kg/s]$	186
	SFC (cruise) $[g/(kN * s)]$	33.8

Table 4.2: Concorde reference engine data

Weights and loadings		
	Operating Empty Weight OEW $[Kg]$	78015
	Maximum Take-off Weight $MTOW$ $[Kg]$	176445
	Max Zero-Fuel Weight $MZFW$ $[Kg]$	92080
	Max Landing weight MLW $[Kg]$	78015
	Max Wing Loading W/S $[Kg/m^2]$	488
	Thrust - to - Weight ratio T/W	0.373

Table 4.3: Concorde reference weights and loadings

Performance	
Max Cruising Speed (15635 m) V_{cruise} $[m/s]$	272.656
	$M = 2.05$
Rate of climb at S/L V_v $[m/min]$	1.525
Service ceiling h $[m]$	18290
Take-off distance $[m]$	3124
Landing distance $[m]$	2444
Range with max fuel and 5352 Kg payload $[m]$	7215
Range with max payload at M = 2.05 $[m]$	6380

Table 4.4: Concorde reference performance

Operational noise characteristics	
Sideline reference $EPNL_L$ $[EPNdB]$	111
Cutback reference $EPNL_F$ $[EPNdB]$	114
Approach reference $EPNL_A$ $[EPNdB]$	115

Table 4.5: Concorde reference operational noise characteristics

4.2 ANP database

The ANP database is an online data resource makes available by Eurocontrol Experimental Cente to accompain the ECAC Doc 29 and ICAO Doc 9911 guidance documents on airport noise contour modelling [50]. The collected data are related to engine and aerodynamic coefficients and weights for take-off and landing at reference ambient conditions (mean sea level elevation and $15°C$ for air temperature) and provide also default *procedural steps* to enable the construction of flight profiles. To support the computation of noise contours around airports, the database comprises also Noise Power Distance (NPD) and Spectral classes data. Having this set of information, the procedure described in [51] enables the evaluation of ground-noise around the airport.

For noise modelling purposes, the three-dimensional flight path has to be constructed through the synthesis of different segments or *procedural steps* that describe the pilot's selections of engine power, flap angle, and acceleration/vertical speed. The different kinds of segments reported in ANP are take-off ground roll, climb at constant speed, power cutback, accelerating climb and flap retraction, accelerating climb after flap retraction, descent and deceleration and final landing approach.

Once aircraft movements are identified throught the *segmentation* of the trajectory, the geometrical aspects of sound radiation and propagation between aircraft and observer are determined. This process allows the computation of noise levels, both maximum and time integrated, from NPD data, that define noise from aircraft traversing idealised horizontal flight paths of infinite length at constant speed and power at reference ambient conditions. The noise contributions from each of these segments are subsequently summed at the observer position.

NPD curves NPD relatonships are noise event levels tabulated as a function of distance below an aeroplane in steady level flight at a reference speed ($V = 160\ knots$), in a reference atmosphere, for each of a number of engine power settings. The data account for the effects of sound attenuation due to spherical wave spreading (inverse-square law) and atmospheric absorption. The distance is defined perpendicular to the aeroplane flight path and the aircraft wing-axis (i.e. vertically below the aircraft in non-banked flight) [51]. Noise levels are typically expressed in terms of LA_{max} and SEL and depends on specific aircraft types, variants, flight configurations (approach, departure, flap settings) and power settings.

Maximum noise level and time integrated (applicable to an infinite flight path) are generaly estimated by an interpolation, unless values happen to be tabulated for power-setting and/or distance exactly. A linear interpolation is used between tabulated power-settings, whereas a logarithmic interpolation is used between tabulated distances (Fig. 4.2). If P_i and P_{i+1} are engine power values for which noise level versus distance data are tabulated, the noise level $L(P)$ at a given distance for intermediate power P, between P_i and P_{i+1}, is given by:

$$L(P) = L(P_i) + \frac{L(P_{i+1}) - L(P_i)}{P_{i+1} - P_i}(P - P_i) \tag{4.1}$$

If, at any power setting, d_i and d_{i+1} are distances for which noise data are tabulated, the noise level $L(d)$ for an intermediate distance d, between d_i and d_{i+1} is given by:

$$L(d) = L(d_i) + \frac{L(d_{i+1}) - L(d_i)}{log(d_{i+1}) - log(d_i)}(log(d) - log(d_i)) \tag{4.2}$$

By using these equations a noise level $L(P, d))$ can be obtained for any power setting P and any distance d that is within the envelope of the NPD data base, where the envelope is defined by air temperature less than 30°, product of air temperature and relative humidity greater than 500 and wind speed less than 8 m/s.

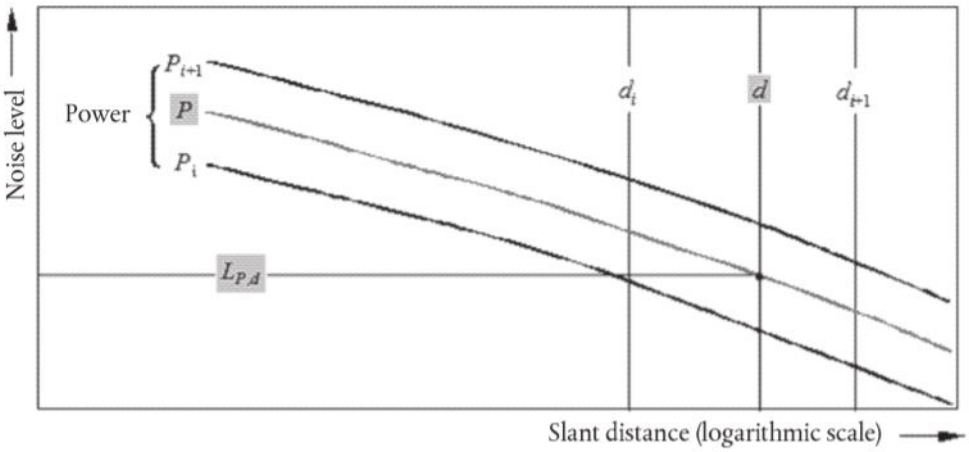

Figure 4.2: Interpolation in NPD curves [51].

For distance d outside the envelope, data are extrapolated on the basis of the same linear interpolation equations, with a lower limit of 30 m be imposed on d, as, at short distances, noise levels increase very rapidly with decreasing propagation distance.

4.3 Results

The Matlab routines have been employed to get the NPD curves for the selected case study. Once the input data have been fixed, a series of flyover trajectories at different altitudes and power settings with constant aircraft speed has been simulated within a reference airspace, considering a distance on ground long 10 Km and a time interval for noise measurement of 120 s ((Fig. 4.3)). In this way, using a linear interpolation for the results obtained for each pair of altitude and thrust, it was possible to obtain the NPD curves for the considered aircraft for each power setting.

Hence, the accuracy of the developed methodology has been evaluated by the comparison of the NPD curves from ANP database and the predicted NPD curves, for both single event and time integrated noise metric, i.e. LA_{max} and SEL.

Input data for simulation are reported in the Tables 4.6, 4.7 and 4.8.

Aircraft speed V	82 m/s
Ambient temperature T	$15°C$
Relative humidity HR	0.7

Table 4.6: Aircraft speed and ambient conditions.

Altitude	
$[ft]$	$[m]$
630	192
1000	305
2000	610
4000	1219
6300	1920
10000	3048

Table 4.7: Altitude variations.

Thrust	
$[lb]$	$[N]$
10000	44480
20000	88960
28000	124550
32000	142340

Table 4.8: Thrust variations.

The aircraft speed has been fixed at $V = 80\ m/s$ in accordance with the reference airspeed used to derive the NPD curves from experimental measurements, whereas the ambient conditions have been set to the reference conditions suggested in [51] for noise contours modelling around the airports.

The NPD curves reported in the ANP database are defined for a range of altitudes that varies from 200 ft (61 m) to 25000 ft (7620 m). Since the noise levels cannot be measured experimentally, the values at higher altitudes are typically obtained by the extrapolation of the measured data and may be less accurate. Therefore, accounting also for the limitations of the semi-empirical methods for lowest and highest altitudes, it was considered conceivable to exclude them and perform the validation for altitudes that varies from 630 ft (192 m) to 10000 ft (3048 m) for each power setting.

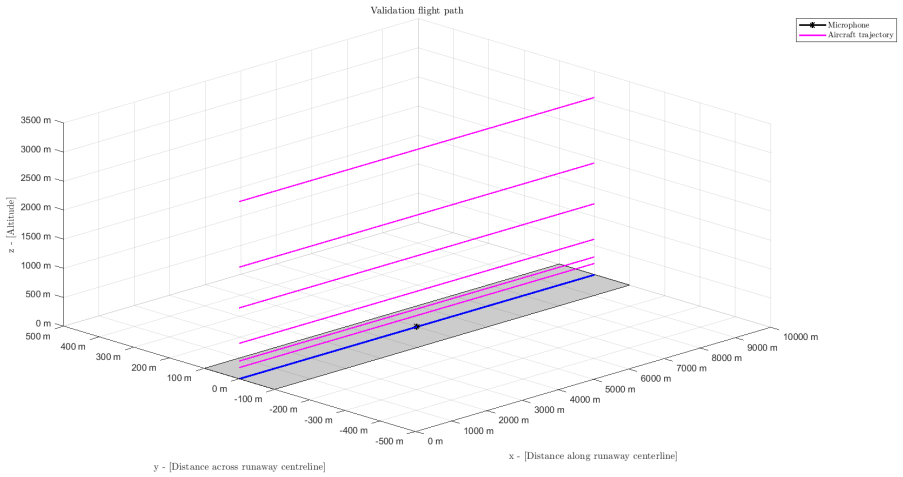

Figure 4.3: Airspace for validation.

The airspace has been defined to correctly predict the SEL, as a time integrated noise metric calculation need the identification of the two time instants in which the OASPL is 10 dBA less than the maximum. If the time interval for noise measurement is too shorter, the microphone will not detect the noise levels at 10 dBA less than maximum. So, a reasonable time interval of 120 s has been fixed. Consequently the distance on ground, that follows the x-axis track of the aircraft, has to be at least of 9840 Km, that is the distance that an aircraft runs at 82 m/s in 120 s. The microphone is placed at the middle of the runaway and turned on for the fixed time interval, detecting the aircraft movements paramaters that are necessary to compute the noise levels. The LA_{max} is the maximum A-weighted sound level recorded during the over-flight of the aircraft, considering each time instant in which the microphone is turned on. The SEL represents the entire noise event uniformly compressed into a reference time of one second, hence it is computed as the sum of sound pressure contained within the time interval between kF and kL, that are the two time instants at which the OASPL is 10 dBA less than the maximum. As the time interval defined to record the sound is not enough to detect the SEL at higher altitudes, if kF and kL are not identified, SEL

is computed with the empirical formula contained in INM Handbook [52], used as a standard procedure to derivate NPD curves by the extrapolation of measured data:

$$SEL = LA_{max} + 7.19 + 7.73log_{10}(D/1000) \tag{4.3}$$

Where D is the distance from ground in ft.

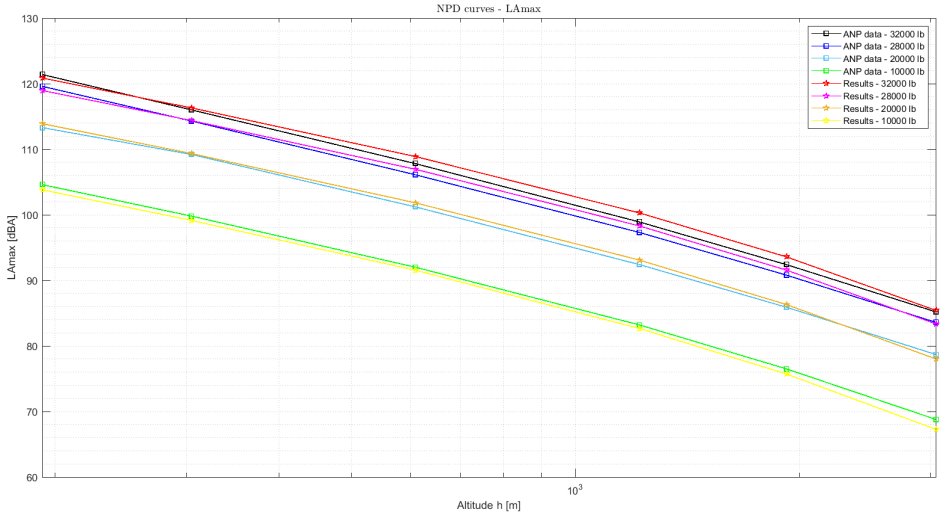

Figure 4.4: Matching with NPD curves - LA_{max}

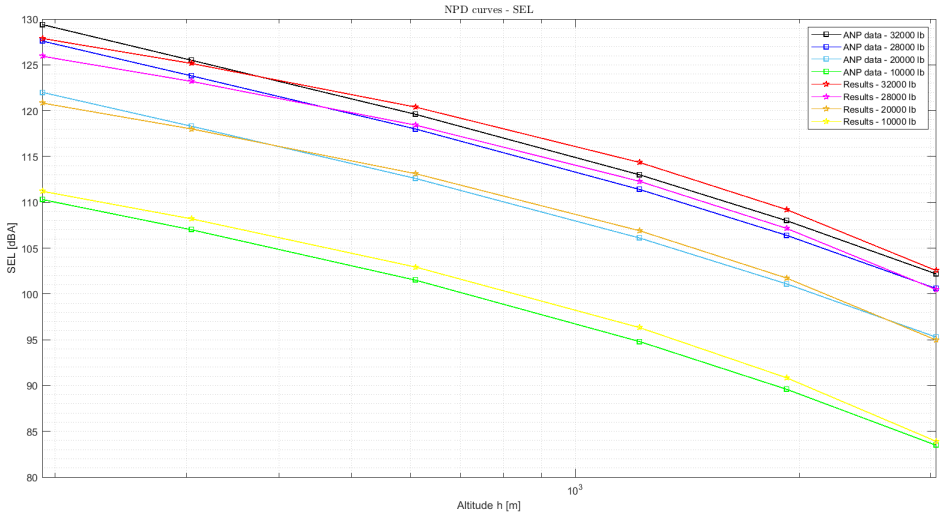

Figure 4.5: Matching with NPD curves - SEL

The prediction error has been calculated in absolute terms respectively for LA_{max} and SEL as:

$$E_{LAmax} = LA_{max_p} - LA_{max_{ANP}} \tag{4.4}$$

$$E_{SEL} = SEL_p - SEL_{ANP} \tag{4.5}$$

Where LA_{max_p} and SEL_p are the predicted noise levels. Ultimatly, the RMSE has been computed as:

$$RMSE_{LA_{max}} = \sum_{i=1}^{i=N} \sqrt{\frac{(LA_{max_p}(i) - LA_{max_{ANP}}(i))^2}{N}} \tag{4.6}$$

$$RMSE_{SEL} = \sum_{i=1}^{i=N} \sqrt{\frac{(SEL_p(i) - SEL_{ANP}(i))^2}{N}} \tag{4.7}$$

Where N is the number of noise levels considered for each thrust rating varying the altitude. The matchings between the predicted and the experimental values for the noise metrics under consideration are presented in Fig. 4.4 and Fig. 4.5 and the results are tabulated in 4.9 and 4.10. Analyzing the results for LA_{max}, the prediction error is between -1.51 dBA and 1.38 dBA, whereas for SEL is between -1.55 dBA and 1.52 dBA. Looking at LA_{max}, the method seems to underpredict the maximum noise level at the lowest thrust rating. On the contrary, the SEL is overpredicted by the method for the lowest thrust rating. However, looking at the resultas for all power settings, some correlation cannot be found between the accuracy of the method and the thrust ratings.

Error [dBA] - LA_{max}	$T = 44480\ N$	$T = 88960\ N$	$T = 124550\ N$	$T = 142340\ N$
$h = 192\ m$	-0.78	0.60	-0.64	-0.54
$h = 305\ m$	-0.65	0.14	0.07	0.31
$h = 610\ m$	-0.46	0.62	0.83	1.08
$h = 1219\ m$	-0.54	0.69	0.99	1.38
$h = 1920\ m$	-0.78	0.41	0.77	1.18
$h = 3048\ m$	-1.51	-0.67	-0.23	0.23
Error [dBA] - SEL	$T = 44480\ N$	$T = 88960\ N$	$T = 124550\ N$	$T = 142340\ N$
$h = 192\ m$	0.90	-1.17	-1.55	-1.51
$h = 305\ m$	1.19	-0.29	-0.60	-0.35
$h = 610\ m$	1.43	0.53	0.42	0.79
$h = 1219\ m$	1.52	0.79	0.89	1.35
$h = 1920\ m$	1.25	0.64	0.76	1.21
$h = 3048\ m$	0.43	-0.31	-0.10	0.36

Table 4.9: Prediction error - LA_{max} and SEL.

RMSE [dBA] - LA_{max}			
$T = 44480\ N$	$T = 88960\ N$	$T = 124550\ N$	$T = 142340\ N$
0.86	0.55	0.67	0.90
RMSE [dBA] - SEL			
$T = 44480\ N$	$T = 88960\ N$	$T = 124550\ N$	$T = 142340\ N$
1.18	0.69	0.88	1.03

Table 4.10: RMSE - LA_{max} and SEL.

Rather it is possible to ascertain that the prediction error become greater at lowest altitudes, and has been verified that this situation occurs also for altitudes higher than the ones considered. These discrepancies are discussed also in [53], where the motivation is attributed to the sound attenuation for atmospheric absorption based on distance, temperature and relative humidity. Precisely, the document deals with an investigation about significant anomalies with measured and theoretical results in deriving NPD curves to be used in INM. To determine the NPD curve, one needs to extract the atmospheric and distance attenuation components to provide a source level, move the aircraft to a new position and then apply the distance attenuation and atmospheric attenuation for a reference atmosphere of $25°C$, 101325 Pa and relative humidity of 70%. By that method one could validate the NPD curve for any position and any atmospheric conditions. However, when seeking to verify the results with the field measurements, agreement could not be obtained between the field measurements and the predicted levels for smaller and larger distances, as depicted in the Fig. 4.6.

The INM is based on the algorithm and framework from the SAE AIR 1845 standard, which considers SAE ARP 866 B for atmospheric absorption coefficient calculation. Since in this validation a temperature of $15°C$ has been considered, typically an overstimation of noise levels occurs for altitude between 300 m and 1920 m, rather than an undestimation that could occur with a temperature of $25°C$. However, the trend is similalr to NPD curve derived following the SAE AIR 1845 standard.

Ultimatly, the prediction error falls within [-1.55, 1.52] dBA for both the noise metrics considered, with a more accurate prediction for single event metric. The NPD curve trend typically undestimate the noise level for lowest and highest altitude, and slightly overstimate the middle altitudes. Probably, changing the reference ambient conditions, the method could gain an higher accuracy for the middle altitudes. Considering that the tolerance suggested in ECAC Document 29 is ± 1.5 dBA [53], it is assumed that the developed methodology has sufficient accuracy for conceptual design applications to predict noise levels generated during the LTO cyle.

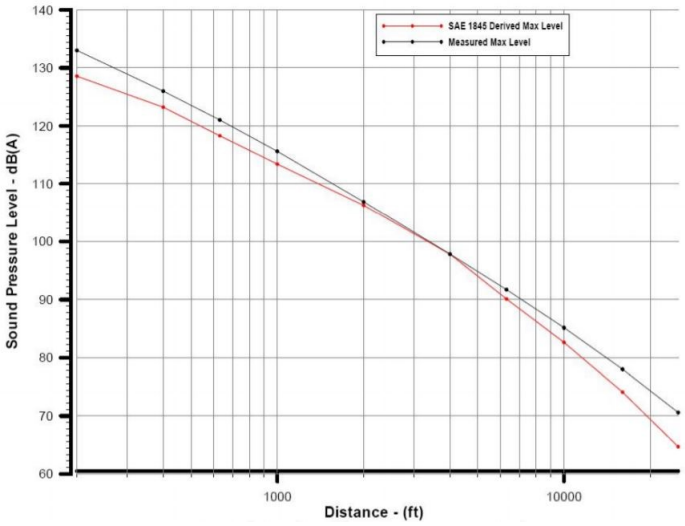

Figure 4.6: Discrepancies between measured and predicted noise max level. [53]

Afterburner In order to obtain a preliminary estimation of the noise impact resulting from the use of the afterburner, the NPD curves have been derived setting a thrust level equal to 176380 N, as it is the maximum thrust value reported in the ANP database for the Concorde take-off procedure. The increase in jet exhasut speed and Mach number has been derived from the engine model described in the Chapter 3, considering the higher total temperature resulting from reheating and the adaptation of the throat section of the nozzle to avoid choking. The assessment has been evaluated with respect to the noise levels reached at the maximum dry thrust level with the following formulas, respectively for LA_{max} and SEL:

$$\Delta L_{max,wet} = \frac{L_{max,wet} - L_{max,dry}}{L_{max,dry}} \tag{4.8}$$

$$\Delta SEL_{max,wet} = \frac{SEL_{wet} - SEL_{dry}}{SEL_{dry}} \tag{4.9}$$

Where $\Delta L_{max,wet}$ and $\Delta SEL_{max,wet}$ represents the increment in noise levels when the afterburner is turned on. This parameter has been calculated for each point of the NPD curve and then an arithmetic has been calculated for both LA_{max} and SEL. NPD curves are reported in the Figures 4.6 and 4.6 and the results express as percentage shows that the afterburner produces an addition of 4.24 % in instantaneous noise level an 3.52 % in integrated noise level. Although this is a preliminary estimate, it confirms that the use of the afterburner, typically used for the take-off phase and for the transition to the supersonic flight regime, is strongly discouraged due to the generation of high noise levels.

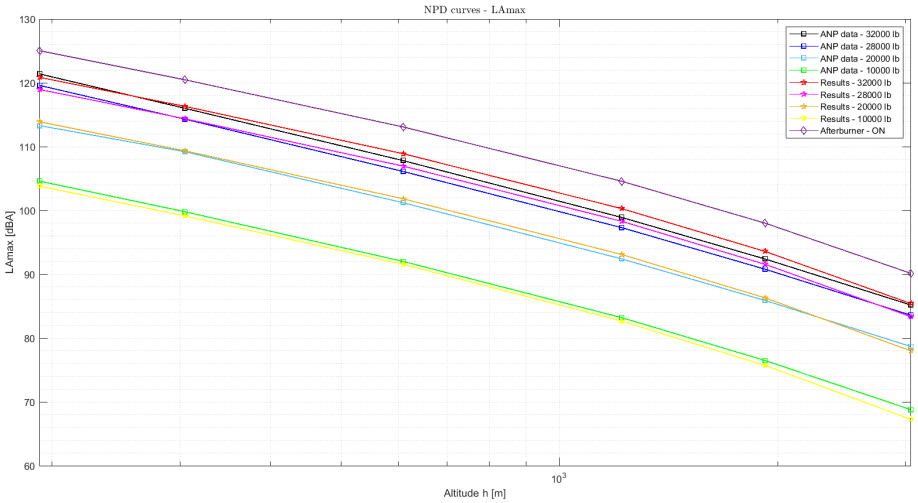

Figure 4.7: Estimation of NPD curve when the afterburner is turned on - LA_{max}

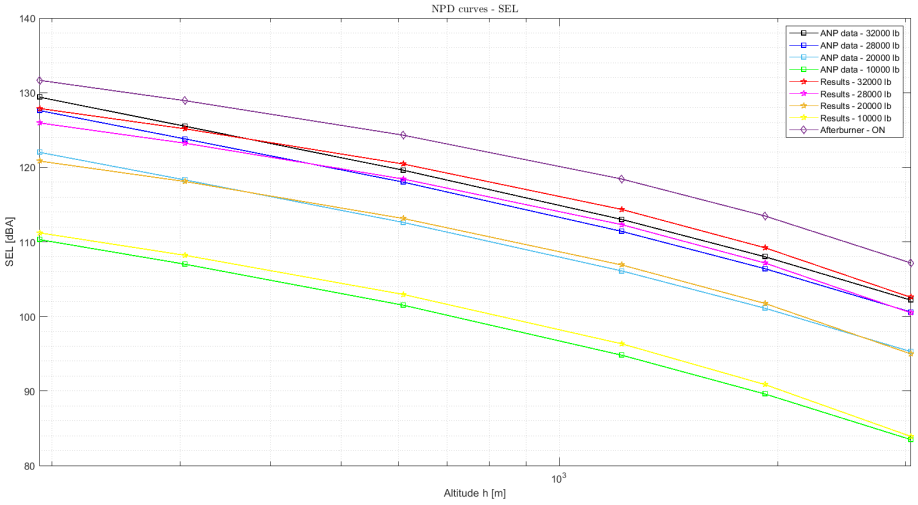

Figure 4.8: Estimation of NPD curve when the afterburner is turned on - SEL

Chapter 5

Application

Departure and approach procedures have been simulated on the basis of ANP departure fixed-point data (distance on ground, altitude, thrust, TAS/CAS). Hence, this Chapter contains the results of noise prediction for those trajectories at sideline, flyover and approach measurement point, in terms of LA_{max}, SEL, PNLTM and EPNL. In addition, noise contributions have been reported for each measurement point in terms of LA_{max}. Such results have been briefly commented to provide an example of how the developed methodology can be useful for carrying out design and performance evaluations aimed at minimizing LTO noise. The results are in agreement with the information found in literature. Therefore, it has been demonstrated that the methodology could be applied for LTO noise prediction purposes to attain a preliminary estimation of aircraft noise levels and information about the most relevant contributions.

5.1 Departure

The departure procedure has been defined by 5 consecutive flight segments and the flight path data are reported in the Table 5.1. After take-off, the first segment with a 5° climb angle is initiated up to an altitude of 100 m. This climb segment is simulated with extracted gear and the afterburner turned on for about 30 s, starting with the full wet thrust setting. Subsequently, the climb angle decreasea and at an altitude of 200 m the landing gear is retracted and the thrust gradually decreases. The simulation ends when the aircraft reaches a thrust rating of 60 % at an altitude of 914 m. The resulting flight path is presented in Figure 5.1.

Noise levels has been predicted at sideline and flyover certification measurement points over a 60 s noise duration. The results obtained consist of OASPL and PNLTM time evolution and relative noise levels for overall aircraft noise, both instantaneous and integral. Furthermore, noise levels for each contribution has been also predicted in terms of LA_{max}, in order to assess the most dominant noise source.

The Figure 5.1 shows the results for sideline measurement point, which corresponds to maximum power condition. During the aircraft overflight over this point, the afterburner is turned on and, as it can see, the noise level start with high values of sound

Departure			
Distance on ground [m]	Altitude [m]	TAS [m/s]	Thrust [N]
0	0	18	176380
2124	0	101	148540
3847	122	129	142340
4653	305	130	141600
4957	324	131	81400
14176	914	134	81400

Table 5.1: Fixed point data for departure procedure.

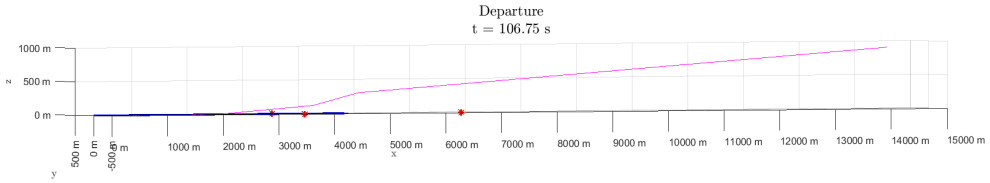

Figure 5.1: Selected departure flight path.

pressure level. After the pass-by, the thrust rapidaly decreases and the noise levels follow the same trend. Since the thrust greatly influences noise generation at this point, the most domanint noise source is the jet noise, and in particular shock cells noise, as supersonic conditions occur with high values of exhaust flow Mach number. However, noise levels of each contribution indicate that also fan noise and airframe noise cannot be overlooked. Indeed, airframe noise is affected by aircraft speed, whereas fan noise depends on engine operating conditions. Noise levels are reported in the Table 5.2.

The Figure 5.3 reports the noise data for flyover measurement point, that is associated with an intermediate power condition. It can be observed that for the first 20 s is elevated although the plane is still distant from the measurement point, and has a peak. This occurs beacause the thrust level is the maximum in dry conditions over that time period, and as it rapidly decreases the sound pressure level goes down and subsequently it increases again as the aircraft approaches the microphone. Also at this point the most dominant noise source is jet noise, whereas airframe and fan noise are reduced, as they are more affected by the increase in altitude and the lower thrust (fan noise). Noise levels are reported in the Table 5.3.

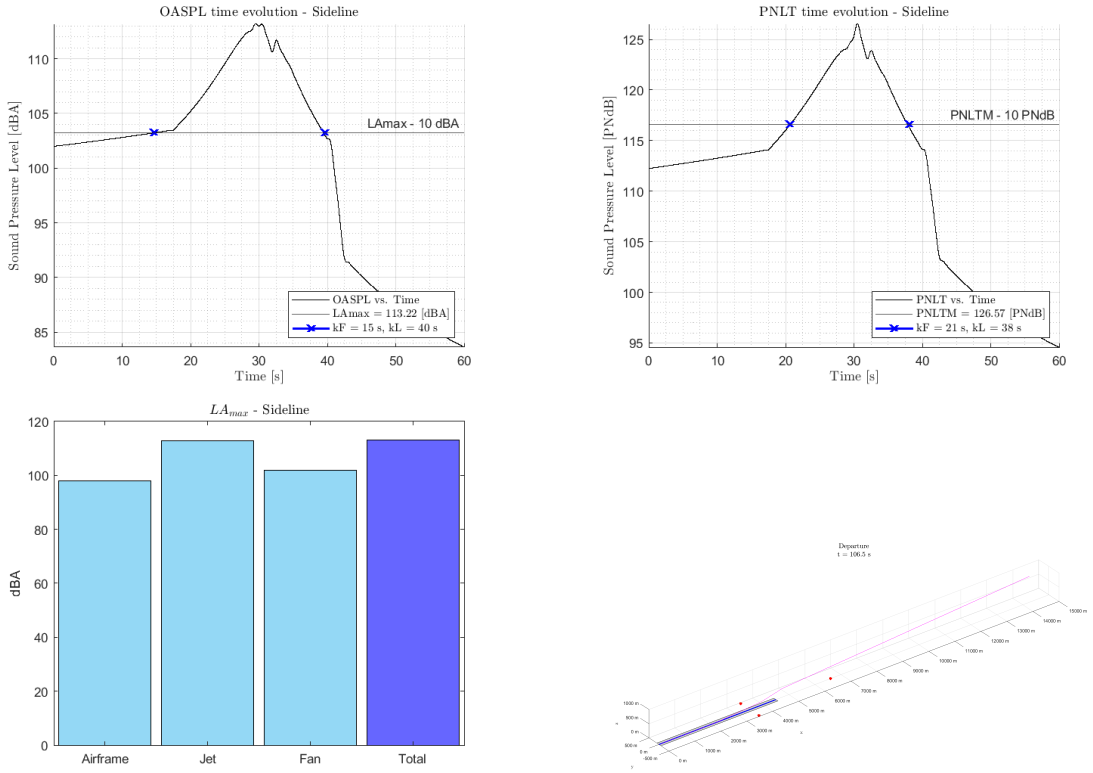

Figure 5.2: Sideline measurement point - noise data.

Noise levels - sideline		
LA_{max} - Airframe	LA_{max} - Jet	LA_{max} - Fan
98.02 dBA	112.94 dBA	101.78 dBA

LA_{max}	SEL	$PNLTM$	$EPNL$
113.22 dBA	123.16	126.57 PNdB	124.53 EPNdB

Table 5.2: Noise levels for each contribution and overall aircraft noise - Sideline

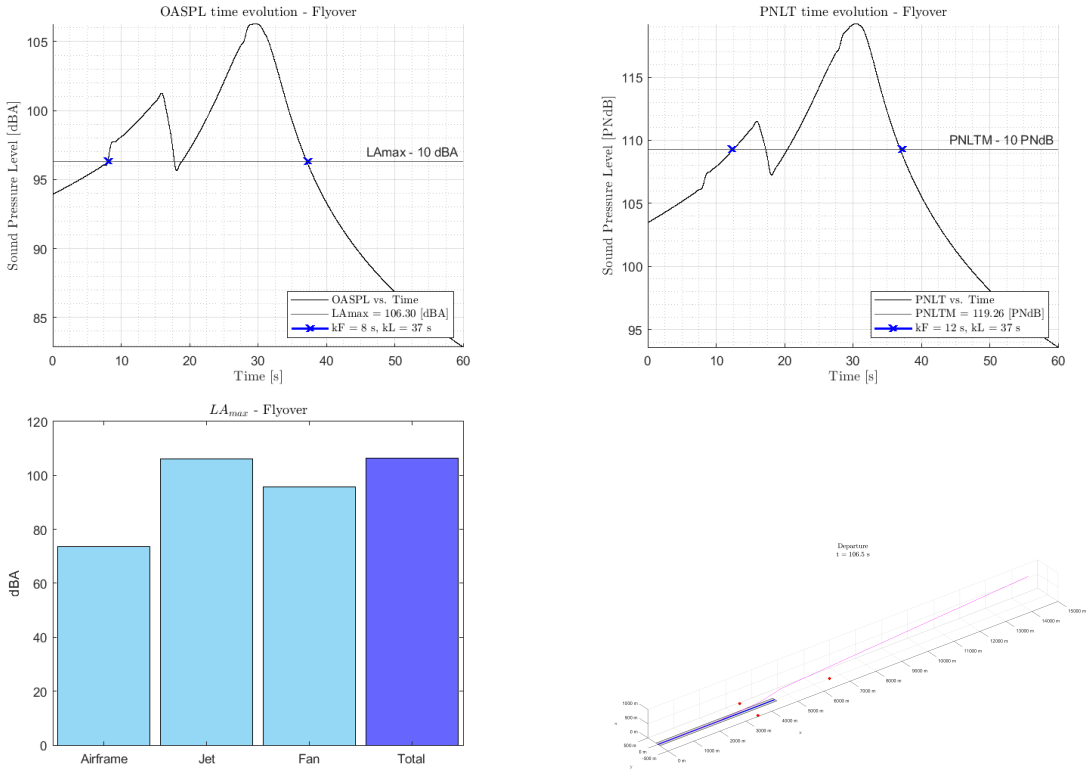

Figure 5.3: Flyover measurement point - noise data.

Noise levels - flyover		
LA_{max} - Airframe	LA_{max} - Jet	LA_{max} - Fan
73.65 dBA	106.20 dBA	95.68 dBA

LA_{max}	SEL	$PNLTM$	$EPNL$
106.30 dBA	116.31	119.26 PNdB	118.45 EPNdB

Table 5.3: Noise levels for each contribution and overall aircraft noise - Flyover

5.2 Approach

The approach procedure has been defined by 3 consecutive flight segments and the flight path data are reported in the Table 5.4. The simulation starts at 5816 m from the ILS landing point and at an altitude of 305 m. The flight segments hold a $-3°$ descent down to the touch down point. Along the last segment, the aircraft holds the the glide slope and speed settings, following the ILS flight path. The landing gear is extracted over the duration of noise measurement and the thrust rating varies from 40% to 10%. The resulting flight path is presented in Figure 5.4.

Approach			
Distance on ground [m]	Altitude [m]	CAS [m/s]	Thrust [N]
5816	305	84.36	56960
4993	261	79.99	42720
23553	0	15.43	28480
0	0	0	14240

Table 5.4: Fixed point data for approach procedure.

The OASPL and PNLT time evolution and noise contributions are reported in the Figure 5.5. As it can see, jet noise is no longer the major source of noise, which instead becomes fan noise. However, while jet noise and fan noise can be compared to each other, the airframe produces a very low noise level, likely due to the low aircraft speed.

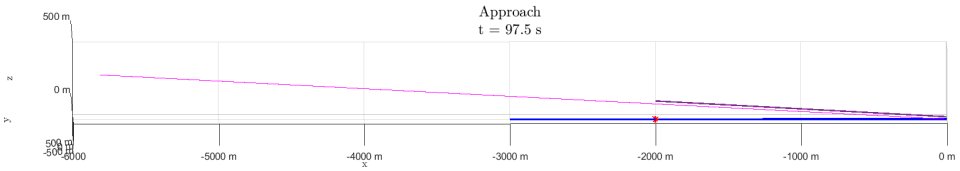

Figure 5.4: Selected approach flight path.

Ultimatly, noise levels are presente in the Table 5.5. As it can see, noise generated during approach produces sound levels definitely lower in comparison with noise generated during landing. Indeed, approach noise measurement point corresponds to a low power condition.

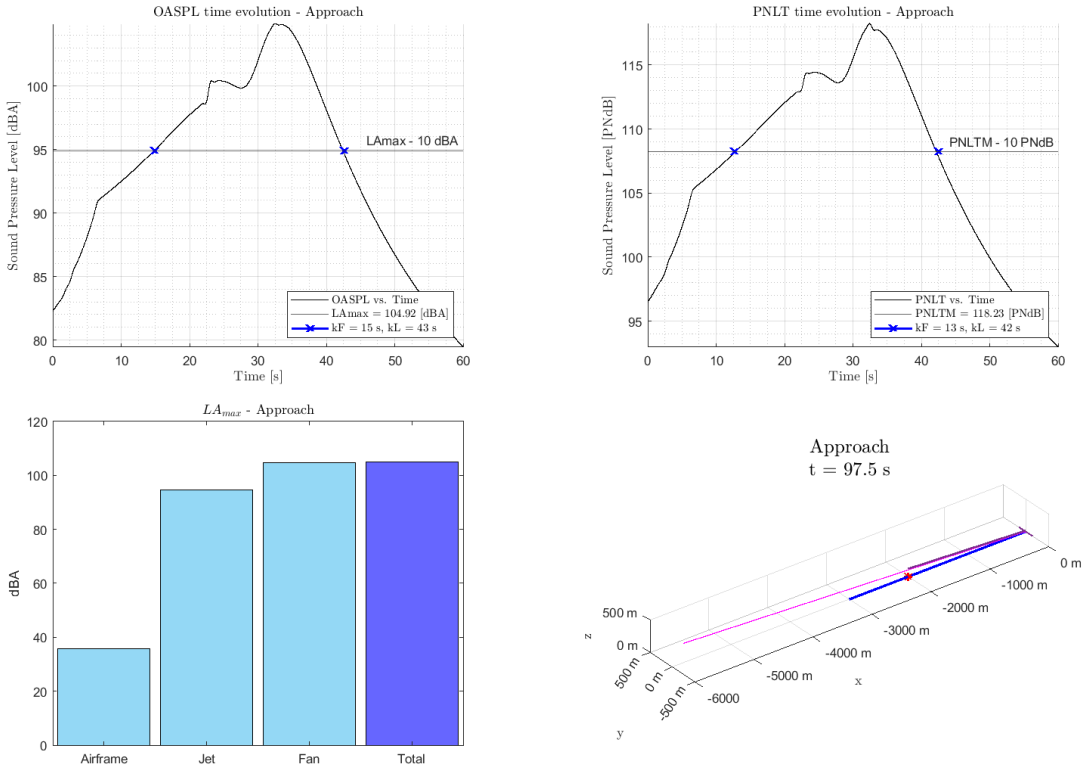

Figure 5.5: Approach measurement point - noise data.

Noise levels - approach		
LA_{max} - Airframe	LA_{max} - Jet	LA_{max} - Fan
35.69 dBA	94.71 dBA	104.83 dBA

LA_{max}	SEL	$PNLTM$	$EPNL$
104.92 dBA	115.34	118.23 PNdB	118.85 EPNdB

Table 5.5: Noise levels for each contribution and overall aircraft noise - Approach

Chapter 6

Conclusions and further developments

The main motivation for the presented thesis is the development af a methodology able to introduce noise emission estimation at conceptual design level for a SST aircraft.

Focusing on noise generated during take-off and landing, a first attempt towards the development of SST aircraft noise prediction routines aiming at predicting several noise metrics along flyover, departure and approach flight path has been realized. To achieve this objective, a general understanding of the main properties of a comprehensive noise prediction model has been gained, semi-empirical equations for noise source modelling relying on aircraft design and operational parameters have been identified and the most influencial parameters amog these have been recognized.

Furhtermore, the overall methodology framework has been described, highlighting the main components necessary to obtain an estimate of ground-based noise levels from an aircraft moving along a flight path.

At least, a dedicated validation has been performed for LA_{max} and SEL, using the methodology to get the NPD curves along flyover trajectories and comparing the results with the data of the ANP database. Thus, it has been demonstated that the prediction error falls within the interval [-1.55,1.52] dBA. Moreover, a noise level increment due to the afterburner has been determined through the evaluation of NPD curves for the maximum wet thrust.

Afterwards, an application of the methodology to the take-off and landing procedures defined in the ANP database has been performed. Builing the flight paths from segments identified by fixed point data, the trajectories have been simulated and noise levels at the certification points have been predicted. The results show up that the most dominant noise source during take-off is jet noise, and that the use of the afterburner greatly affects lateral noise level. In addition, approach conditions are the less critical for noise generation. However, it has been found that jet and fan noise become comparable at this noise and power condition.

Ultimatly, the outcome of this research proved the feasibility of introducing a preliminary noise assessment at a conceptual design level for SST aircraft and, as a consequence, the possibility to support decision-making process in the early stages of the design process in order to mitigate noise generation in the vicinity of airports.

Therefore, with appropriate improvements in noise source and engine modelling, the methodology can be useful to provide guidelines for the design of future low-noise SST together with operational procedures able to mitigate the LTO noise.

In particular, some examples to improve the noise model, gaining an high-fidelity level and extending its capability in the identification of low-noise designs, could include the modelling of more complex nozzles, such as plug and/or chevron nozzle, or the evaluation of the impact in noise reduction of jet noise suppression measures.

At least, to reach a complete assessment of the acoustic impact of SST aircraft, as a possible future development it could be thought of including within the developed framework additional modules dedicated to the evaluation of the sonic boom, through appropriate models and definition of the entire profile mission of the aircraft.

Appendix A

Main noise sources

Noise sources	Noise generating mechanism	Relevant parameters
Landing gear	Broadband noise due to turbolent flow on various element of landing gear and tonal noise due to cavities	- Length and number of strut - Diameter and number of wheels - Number of gears and gears doors - Inflow speed
Flaps	Broadband noise due to turbolence around side edges and gaps	- Flaps deflection angle - Local inflow velocity - Chord length - Angle of attack - Slat deflection angle - Sweep angle
Slats	Broadband noise due to turbolence in gaps	- Local inflow velocity - Chord length - Sweep angle - Geometry between slat - and wing, e.g. gap - height and overlap
Lift and control surfaces	Broadband noise due to turbolence at trailing edge	- Turbolent intensity at the trailing edge - Sweep angle - Geometry/shape of the trailing edge
Spoilers and speed brakes	Detached flow turbolence at trailing edge	- Spoiler geometry - Flight velocity
Krueger (leading edge device)	Not understood	- Geometry - Inflow velocity - Sweep angle

Table A.1: Overview of airframe noise sources [33]

Noise sources	Noise generating mechanism	Relevant parameters
Fan	- Thickness and loading noise - Interaction rotor-stator - Stator vane - Struts - Fan-intake interaction e.g. engine inlet or pylons - Tonal noise due to shock cells on blades (harmonic) - Shock cell interaction with nacelle (not harmonic sequence)	- Inlet geometry - Number of blades - Number of vanes - Fan pressure ratio - Relative tip Mach number - Inlet flow distortion, e.g. due to an angle of attack or due to a pylon in front of the engine
Jet	- Turbolent mixing - Shock noise (only in cruise condition)	- Velocity differences between the streams, i.e. free, core and bypass stream - Temperature - Nozzle diameter - Nozzle type
Combustion	-Mainly broadband noise - Direct contribution due to the expansion of the gas mixture in the combustion chamber - Indirect noise contribution due to the convection of non-uniformities through pressure gradients in the turbine	- Temperature - Pressure ratio - Sweep angle - Combustion type (lean, rich)
Turbine	Tonal and broadband noise (due to same mechanism as fan noise generation)	- Number of blades - Number of vanes - Mach number - Shaft speed - Axial stage spacing - Number of stages - Exit area - Shaft power
Compressor	Tonal and broadband noise similar to fan	- Same as fan

Table A.2: Overview of engine noise sources [33]

Appendix B

Airframe noise directivity

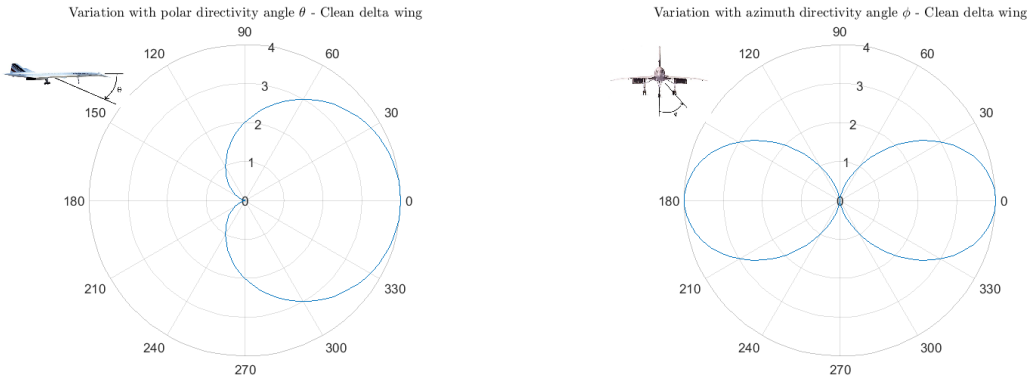

Figure B.1: Clean delta wing directivity

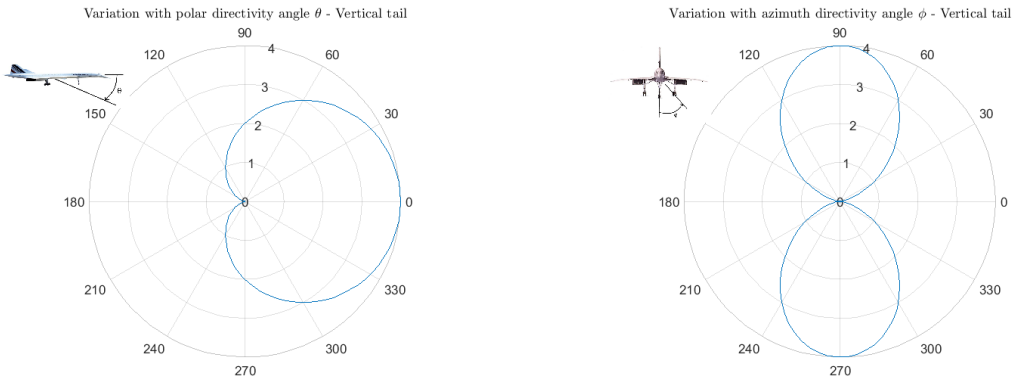

Figure B.2: Vertical tail directivity.

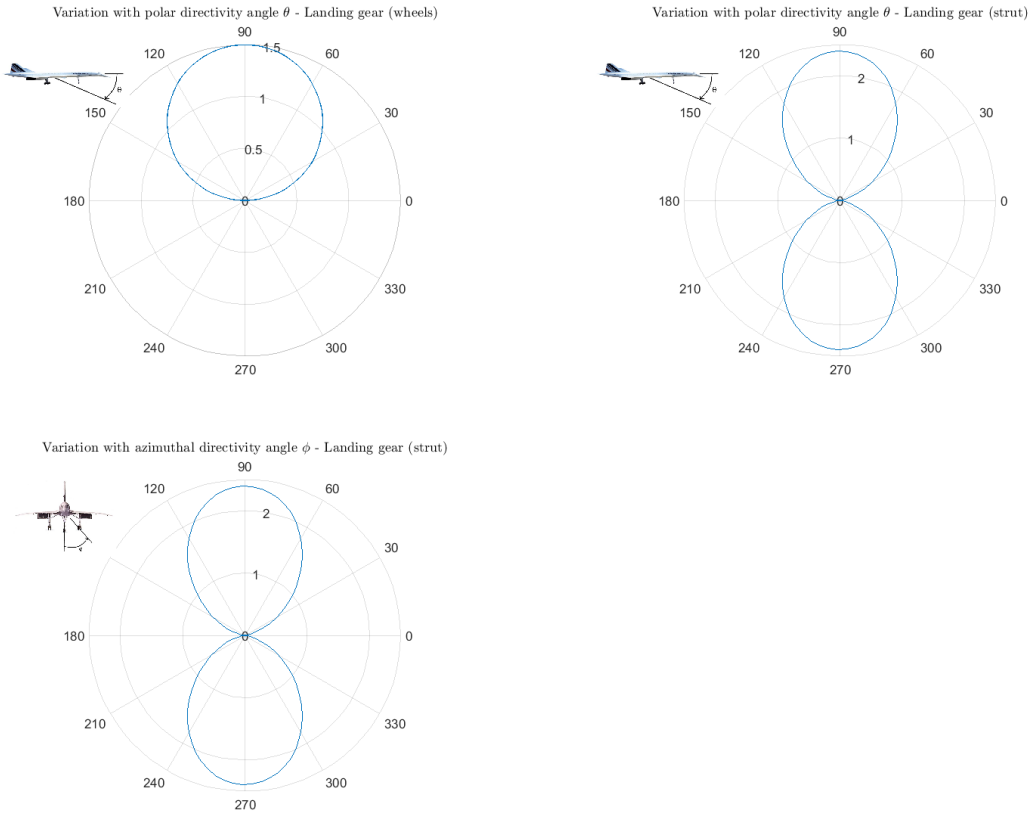

Figure B.3: Landing gear directivity.

Appendix C

Engine noise directivity

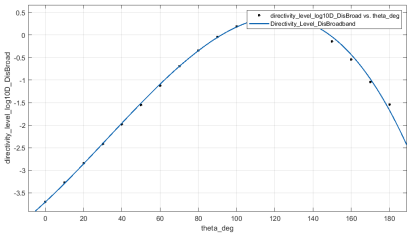

Figure C.1: Jet mixing noise directivity.

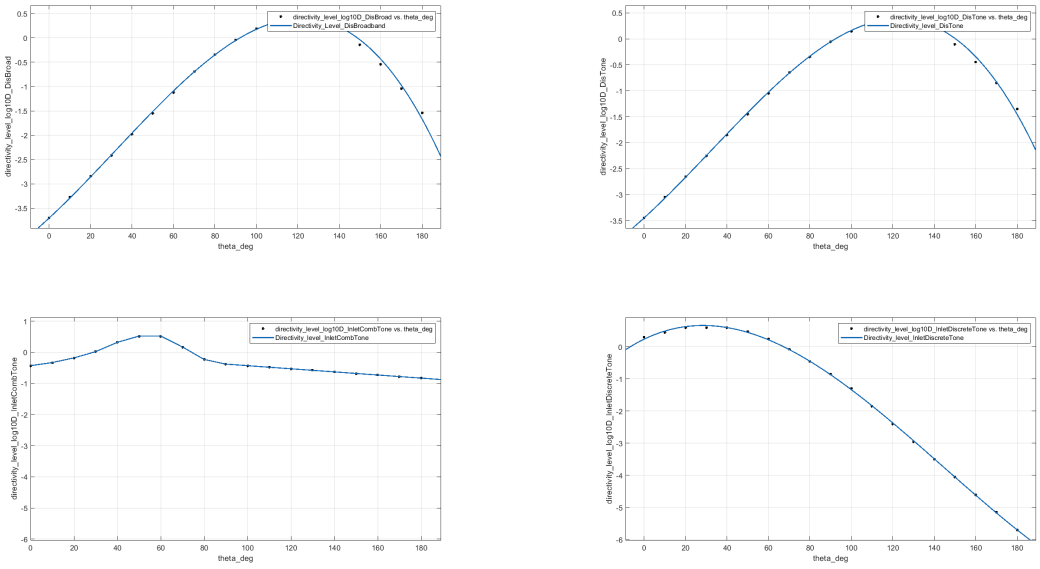

Figure C.2: Fan noise directivity.

Bibliography

[1] IATA: *Outlook for the global airline industry*, Report, 2019.

[2] Boeing: *Commericial Market Outlook*, Report, 2020-2039.

[3] EASA, EEA, Eurocontrol: *European Aviation Environmental Report*, 2019.

[4] ICAO: *Environmental Report*, 2019.

[5] `https://hub.united.com`

[6] Congressional Research Service: *Supersonic Passenger Flights*, November 2018.

[7] M.J.T. Smith: *Aircraft Noise*, Cambridge Aerospace Series, Cambridge University Press, `ISBN 0-521-61699-9, 2004`

[8] Schultz TJ: *Synthesis of social surveys on noise annoyance* J Acoust Soc Am. 1978 Aug;64(2):377-405. `doi: 10.1121/1.382013. PMID: 361792.`

[9] Deborah A. Black, John A. Black, Tharit Issarayangyun, Stephen E. Samuels: *Aircraft noise exposure and resident's stress and hypertension: A public health perspective for airport environmental management*

[10] Franssen EA, van Wiechen CM, Nagelkerke NJ, Lebret E.: *Aircraft noise around a large international airport and its impact on general health and medication use*, Occupational and Environmental Medicine. 2004 May;61(5):405-413. `doi: 10.1136/oem.2002.005488.`

[11] J.I. Nijsse: *Design and Noise Acceptability of Future Supersonic Transport Aircraft*, MSc. Thesis, TU Delft, December 18, 2020.

[12] ICAO: *ANNEX 16 to the Convention on International Civil Aviation, Environmental Protection.* ,Tech. rep., Vol. I (8th edition), ICAO, July 2017.

[13] `https://www.icao.int`

[14] `https://rumble-project.eu`

[15] D. G. Crighton 1991: *Aeroacoustics of Flight Vehicles: Theory and Practice: Noise Sources*, NASA Reference Publication 1258, RDC Technical Report 90-3052 (H. H. Hubbard, editor).

[16] ICAO: *Guidance on the balanced approach to aircraft noise management*, October, 2010.

[17] Nicolas E. Antoine, Ilan M. Kroo: *Aircraft Optimization for Minimal Environmental Impact*, Journal Article, Journal of Aircraft July 41 (4): 790, 2004.

[18] Nicolas E. Antoine, Ilan M. Kroo: *Framework for Aircraft Conceptual Design and Environmental Performance Studies*, Journal Article, AIAA Journal October 43 (10): 2100, 2005.

[19] Andrew March, Ian Waitz and Karen Willcox: *A Methodology for Integrated Conceptual Design of Aircraft Configuration and Operation to Reduce Environmental Impact*, Book Chapter, 9th AIAA Aviation Technology, Integration, and Operations Conference (ATIO) 21-23 September 2009, Hilton Head, South Carolina © 2009 by Massachusetts Institute of Technology.

[20] Filippone, Antonio: *Aircraft noise prediction*, Progress in Aerospace Sciences, Volume 68, Pages 27-63, ISSN 0376-0421, 2014.

[21] Farassat, F. and Casper, J. H.: *Towards an Airframe Noise Prediction Methodology: Survey of Current Approaches.*, in 44th AIAA Aerospace Sciences Meeting and Exhibit, 2006. doi:10.2514/6.2006210.

[22] Dobrzynski, Werner: *Almost 40 Years of Airframe Noise Research: What Did We Achieve?*, Journal of Aircraft, vol. 47, n.2, pages 353-367, doi:10.2514/1.44457.

[23] Raney, John P., S. L. Padula, and W. E. Zorumski: *NASA progress in aircraft noise prediction*, Vol. 81915. National Aeronautics and Space Administration, Scientific and Technical Information Branch, 1981.

[24] Leonard Lopes and Casey Burley: *Design of the Next Generation Aircraft Noise Prediction Program: ANOPP2*, 17th AIAA/CEAS Aeroacoustics Conference (32nd AIAA Aeroacoustics Conference), `https://arc.aiaa.org/doi/abs/`.

[25] Bertsch, Lothar and Isermann, Ullrich: *Tool Development for Low-Noise Aircraft Design*, Journal of Aircraft, vol. 47, n. 2, pages 694-699, `doi: 10.2514/1.43188, 2010`.

[26] Filippone, Antonio and Bertsch, Lothar and Pott-Pollenske, Michael: *Validation strategies for comprehensive aircraft noise prediction methods*, 2012.

[27] J.R. Olmstead, G.G. Fleming, J.M. Gulding, C.J. Roof, P.J. Gerbi, and A.S. Rapoza: *Integrated Noise Model (INM) Version 6.0 Technical Manual, U.S. Department of Transportation Federal Aviation Administration*, Report No. FAA-AEE-02-01, January 2002,Washington, D.C., USA

[28] ECAC.CEAC Doc 29: *Report on Standard Method of Computing Noise Contours around Civil Airports*, Volume 3, Part 1 - Reference Cases and Verification Framework, 7 December, 2016.

[29] Bertsch, Lothar and Isermann, Ullrich: *Noise prediction toolbox used by the DLR aircraft noise working group*, INTER-NOISE and NOISE-CON Congress and Conference Proceedings, 2013.

[30] Bertsch L., *Noise Prediction within Conceptual Aircraft Design*, PhD thesis, Institute of Aerodynamics and Flow Technology, DLR, Braunschweig, 2013.

[31] Wilson, M.: *An introduction to high speed aircraft noise prediction.*, 1992.

[32] R.E. Gillian: *Aircraft Noise Prediction Program User's Manual*, NASA Langley Research Center, 1982.

[33] Bertsch, L., Simons, D., Snellen, M.: *Aircraft Noise: The major sources, modelling capabilities, and reduction possibilities*, (IB 224-2015 A 110 ed.) DLR, 2015.

[34] Fink, Martin R.,*Noise Component Method for Airframe Noise*, Journal of Aircraft, vol. 16, n. 10, pages 656-665,1979, `doi:10.2514/3.58586`.

[35] M.R. Fink: *Airframe Noise Prediction Method*, FAA Research Report, FAA-RD-77-29, March 1977.

[36] Stone, James R., and Frances J. Montegani: *An improved prediction method for the noise generated in flight by circular jets*, 1980.
[37] Stone, James R.: *Interim prediction method for jet noise*, 1974.
[38] Barbosa, Joao and Dezan, Daniel: *Single-Stream Jet Noise Prediction Using Empirical Methodology for a Newly Designed Turbojet Engine*, Proceedings of the ASME Turbo Expo, doi: 10.1115/GT2013-95199, 2013.
[39] Almeida, Odenir: *Semi-Empirical Methods for Coaxial Jet Noise Prediction*, 2008.
[40] Heidmann, M.: *Interim prediction method for fan and compressor source noise*, 1975.
[41] Gregorio Stiuso: *Tecnica di simulazione numerica delle prestazioni stazionarie e transitorie di turbomotori.*, Rel. Michele Ferlauto. Politecnico di Torino, Corso di laurea magistrale in Ingegneria Aerospaziale, 2019.URI:http://webthesis.biblio.polito.it/id/eprint/11258.
[42] Stitt, L. E.:*Exhaust Nozzles for Propulsion Systems with Emphasis on Supersonic Cruise Aircraft.*, 1990.
[43] Vasov, Ljubiša and Stojiljkovic, Branimir and Cokorilo, Olja and Mirosavljevic, Petar and Gvozdenovic, Slobodan: *Aircraft noise metrics*, Journal Safety Engineering, vol. 4, December, 2014, doi: 10.7562/SE2014.4.02.04.
[44] ERCD Report 0904: *Metrics for Aircraft Noise*,January 20, 2009.
[45] Bennett, R. L., Pearsons, K. S: *Handbook of aircraft noise metrics*, Contractor Report (CR), March 1, 1981
[46] A-21 Aircraft Noise Measurement Aviation Emission Modeling: *Standard Values of Atmospheric Absorption as a Function of Temperature and Humidity*, ARP 866B, December, 2021, doi: https://doi.org/10.4271/ARP866B.
[47] *Jane's All the world's aircraft*, 1965-66.
[48] *Jane's All the world's aircraft*, 1974-75.
[49] Underwood, Matthew C: *Concept of operations for integrating commercial supersonic transport aircraft into the national airspace system*, 2017.
[50] www.aircraftnoisemodel.org
[51] Directive 2002/49/EC of the European Parliament and of the Council, 25 June 2002.
[52] Cooper, Steven:*Problems with the INM: Part 3 - Derivation of NPD Curves*, Cooper2006ProblemsWT, 2006.
[53] Cooper, Steven and Maung, John:*Problems with the INM: Part 2 – Atmospheric Attenuation*, Cooper2006ProblemsWT, 2006.
[54] ECAC.CEAC Doc 29, 4th ed.:*Report on Standard Method of Computing Noise Contours Around Civil Airports*, proceedings of the European Civil Aviation Conference, European Civil Aviation Conference (ECAC) Document 29, Paris, https://www.ecac-ceac.org/ecac-docs [retrieved 7 Dec. 2016].